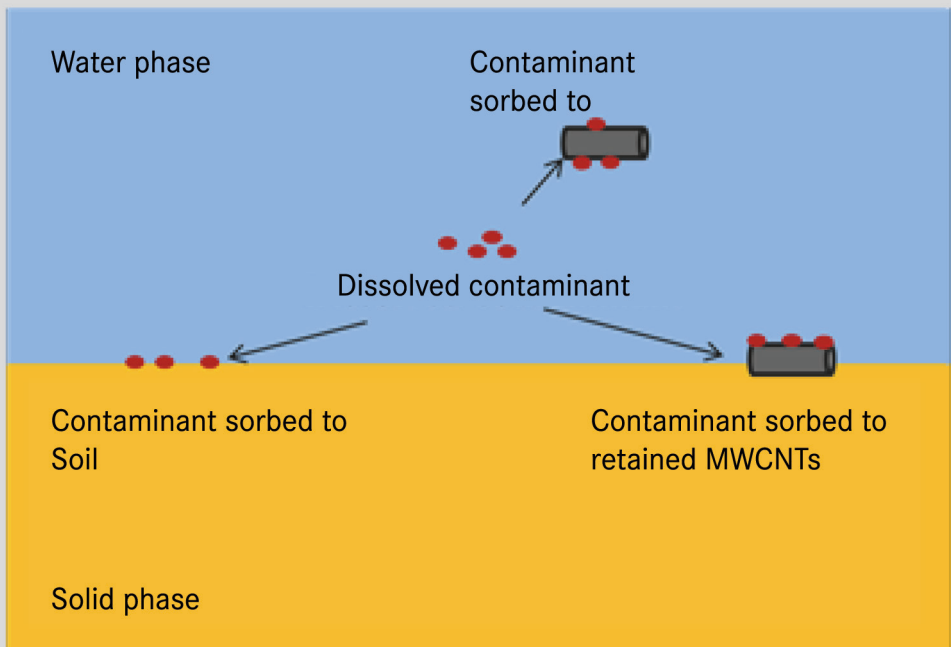


Transport, co-transport, and retention of functionalized multi-walled carbon nanotubes in porous media

Miaoyue Zhang

The interactions between MWCNTs and contaminants in saturated soil



Forschungszentrum Jülich GmbH
Institute of Bio- and Geosciences
Agrosphere (IBG-3)

Transport, co-transport, and retention of functionalized multi-walled carbon nanotubes in porous media

Miaoyue Zhang

Schriften des Forschungszentrums Jülich
Reihe Energie & Umwelt / Energy & Environment

Band / Volume 352

ISSN 1866-1793

ISBN 978-3-95806-198-9

Bibliographic information published by the Deutsche Nationalbibliothek.
The Deutsche Nationalbibliothek lists this publication in the Deutsche
Nationalbibliografie; detailed bibliographic data are available in the
Internet at <http://dnb.d-nb.de>.

Publisher and
Distributor: Forschungszentrum Jülich GmbH
Zentralbibliothek
52425 Jülich
Tel: +49 2461 61-5368
Fax: +49 2461 61-6103
Email: zb-publikation@fz-juelich.de
www.fz-juelich.de/zb

Cover Design: Grafische Medien, Forschungszentrum Jülich GmbH

Printer: Grafische Medien, Forschungszentrum Jülich GmbH

Copyright: Forschungszentrum Jülich 2016

Schriften des Forschungszentrums Jülich
Reihe Energie & Umwelt / Energy & Environment, Band / Volume 352

D 82 (Diss. RWTH Aachen University, 2016)

ISSN 1866-1793
ISBN 978-3-95806-198-9

The complete volume is freely available on the Internet on the Jülicher Open Access Server (JuSER)
at www.fz-juelich.de/zb/openaccess.



This is an Open Access publication distributed under the terms of the [Creative Commons Attribution License 4.0](https://creativecommons.org/licenses/by/4.0/),
which permits unrestricted use, distribution, and reproduction in any medium, provided the original work is properly cited.

Abstract

The information on transport and retention behavior of functionalized multi-walled carbon nanotubes (MWCNTs) in porous media is essential for environmental protection and remediation due to the wide applications of MWCNTs and lack of disposal regulations. The aim of this study is therefore to investigate: i) the attachment, transport, retention and remobilization of ^{14}C -labeled functionalized MWCNTs in different porous media (quartz sand (QS), goethite-coated quartz sand (GQS), and soil), ii) co-transport of pollutants (chlordecone (CLD) and sulfadiazine (SDZ)) by MWCNTs, and iii) the role of surfactant on MWCNTs transport as a modeled soil remediation process, based on column and batch experiments at the environmentally relevant concentrations under various physiochemical conditions. The breakthrough curves (BTCs) and retention profiles (RPs) were determined and simulated based on advective- dispersive equation by using different numerical models that considered both time- and depth- dependent blocking functions.

The effect of goethite coating on MWCNTs transport was conducted in mixtures of negatively charged QS and positively charged GQS. The linear equilibrium sorption model provided a good description of batch results, and the distribution coefficients (K_D) drastically increased with the GQS fraction that was electrostatically favorable for retention. Similarly, retention of MWCNTs increased with the GQS fraction in packed column experiments. However, calculated values of K_D on GQS were around two orders of magnitude smaller in batch than packed column experiments due to differences in lever arms associated with hydrodynamic and adhesive torques at microscopic roughness locations. Furthermore, the fraction of the chemically heterogeneous sand surface area that was favorable for retention was much smaller than the GQS fraction, presumably because nanoscale roughness produced shallow interactions that were susceptible to removal. These observations indicated that only a minor fraction of the GQS was favorable for MWCNT retention. These same observations held for several different sand sizes.

In the saturated soil column experiments, BTCs for MWCNTs exhibited greater amounts of retardation and retention with increasing solution ionic strength (IS) or in the presence of Ca^{2+} in comparison to K^+ , and RPs for MWCNTs were hyper-exponential in shape. Fitted values of the retention rate coefficient and the maximum retained concentration of MWCNTs were higher with increasing IS and in

the presence of Ca^{2+} in comparison to K^+ . Significant amounts of MWCNTs and soil colloids release was observed with a reduction of IS due to expansion of the electrical double layer, especially following cation exchange (when K^+ displaced Ca^{2+}) that reduced the zeta potential of MWCNTs and the soil. Analysis of MWCNTs concentrations in different soil size fractions revealed that >23% of the retained MWCNTs mass was associated with water-dispersible colloids (WDCs), even though this fraction was only a minor portion of the total soil mass (around 2.4%). More MWCNTs were retained on the WDC fraction in the presence of Ca^{2+} than K^+ . These findings indicated that some of the released MWCNTs by IS reduction and cation exchange were associated with the released clay fraction, suggesting the potential for facilitated transport of MWCNTs by WDCs.

The sorption and mobility of two ^{14}C -labeled contaminants, the hydrophobic CLD and the readily water-soluble SDZ, in the absence or presence of MWCNTs were investigated by applying in the column studies at different injected times. The experimental results indicated that the presence of mobile MWCNTs facilitated remobilization of previously deposited CLD and its co-transport into deeper soil layers, while retained MWCNTs enhanced SDZ deposition in the topsoil layers due to the increased adsorption capacity of the soil. The modeling results then demonstrated that the mobility of MWCNTs in the soil and the high affinity and entrapment of contaminants to MWCNTs were the main reasons for MWCNT-facilitated contaminant transport. On the other hand, immobile MWCNTs had a less significant impact on the contaminant transport, even though they were still able to enhance the adsorption capacity of the soil.

An outlook study about the effect of surfactant on the transport of MWCNTs in QS and GQS was conducted in the presence of the sodium dodecylbenzenesulfonate (SDBS, anionic surfactant) or Triton[®] X-100 (TX100, nonionic surfactant). The adsorption of TX100 and SDBS on QS and GQS followed the order $\text{GQS} > \text{QS}$ due to the higher surface area and surface charge of GQS. High-affinity type adsorption isotherms of TX100 and SDBS on MWCNTs were found. Transport results indicated that the mobility of MWCNTs was highly sensitive to the type of surfactant, the input concentration of surfactant, and the properties of porous media.

In conclusion, all results mentioned above provided important insight into MWCNTs mobility in the subsurface environment.

Zusammenfassung

Aufgrund des breiten Anwendungsbereiches von funktionalisierten mehrwandigen Kohlenstoffnanoröhrchen (MWCNTs), sowie Lücken in der Regulierung in der Entsorgung ist es für den Umweltschutz und die Sanierung von essentieller Bedeutung, Erkenntnisse über den Transport und die Retention von MWCNTs in porösen Medien zu gewinnen. Ziel dieser Arbeit ist es i) die Anlagerung, Transport, Retention und Remobilisierung von ^{14}C radioaktiv-markierten MWCNTs in unterschiedlichen porösen Medien (Quarzsand (QS), goethit-beschichteten Quarzsand (GQS) und Boden), ii) den Kotransport von Schadstoffen (Chlordecon (CLD) und Sulfadiazin (SDZ)) durch MWCNTs und iii) den Einfluss von Tensiden auf den Transport von MWCNTs in einem Modell-Bodensanierungsprozess zu untersuchen. Hierfür wurden Säulen- und Batchexperimente mit umweltrelevanten MWCNTs-Konzentrationen bei verschiedenen physikochemischen Bedingungen durchgeführt. Die experimentellen Durchbruchkurven (DBK) und Retentionsprofile (RP) wurden basierend auf der Advektions-Dispersionsgleichung durch Anwendung von verschiedenen numerischen Modellen, welche die zeit- als auch tiefenabhängige „Blocking“- Funktion berücksichtigen, simuliert.

Der Einfluss von Goethit auf den Transport von MWCNTs wurde in einer Mischung aus negativ geladenen QS und positiv geladenen GQS durchgeführt. Die Batchergebnisse konnten mit dem verwendeten linearen Gleichgewichts-Sorptionsmodell gut beschrieben werden. Mit zunehmender GQS- Fraktion, welche elektrostatisch günstig für Retention war nahm der Verteilungskoeffizient (K_D) drastisch zu. Auch in gepackten Säulen nahm die MWCNTs- Retention in mit steigender Goethit- Fraktion zu. Jedoch waren in Batchversuchen verglichen mit den Säulenversuchen die berechneten Werte von K_D bei GQS um zwei Größenordnungen kleiner, basierend auf unterschiedlichen hydrodynamischen und adhäsiven Drehmomenten an mikroskopisch rauen Stellen der Kollektoroberfläche. Zudem war im gemischten porösen Medium die Oberfläche, welche günstig für Retention war viel kleiner als die Goethit- Fraktion. Vermutlich löst die nano- skalige Rauigkeit der Sandoberfläche Interaktionen aus, welche die Retention von MWCTs kontrollieren. Diese Beobachtungen liefern Hinweise, dass nur eine geringe Fraktion des GQS für die Retention von MWCNTs günstig war. Gleiches konnte für verschiedene Sand-Korngrößen beobachtet werden.

DBKs von MWCNTs zeigten in gesättigten Bodensäulenversuchen größere Retardation und Retention mit zunehmender Ionenstärke (IS) oder in der Anwesenheit von Ca^{2+} im Vergleich zu K^+ . RPs von MWCNTs zeigten ein hyper-exponentielles Tiefenprofil. Die simulierten Werte des Retentionsrate Koeffizienten und die maximale zurückgehaltene Konzentration an MWCNTs waren mit zunehmender IS und in Anwesenheit von Ca^{2+} im Vergleich zu K^+ höher. Eine signifikante Menge an freigesetzten MWCNTs und Bodenkolloiden wurde bei der Reduzierung der IS und die dadurch verursachte Erweiterung der elektrischen Doppelschicht beobachtet, besonders nach einem Kationenaustausch (K^+ ersetzte Ca^{2+}), welches das Zetapotential von MWCNTs und dem Boden reduzierte. Analysen der MWCNTs-Konzentrationen in verschiedenen Bodengrößen-Fractionen ergaben, dass >23% der zurückgehaltenen MWCNTs mit wasser- dispergierbaren Kolloiden (WDCs) assoziiert waren, obwohl diese Fraktion nur einen geringen Anteil des Bodens ausmachte (ca. 2.4%). Mehr MWCNTs wurden an der WDC Fraktion zurückgehalten in Anwesenheit von Ca^{2+} als in Anwesenheit von K^+ . Diese Ergebnisse zeigen, dass ein Teil der durch IS Reduzierung und Kationenaustausch freigesetzten MWCNTs mit der freisetzten Tonfraktion assoziiert waren und so ein Potential für den erleichterten Transport von MWCNTs durch WDC vermuten lassen.

Die Sorption und Mobilität von zwei ^{14}C -markierten Schadstoffen (das hydrophobe CLD und das wasserlösliche SDZ) wurden in An- und Abwesenheit von MWCNTs in Säulenversuchen bei verschiedenen Injektionsreihenfolgen untersucht. Die experimentellen Ergebnisse zeigten, dass die Anwesenheit von mobilen MWCNTs die Remobilisierung von zuvor angelagerten CLD fördern und dessen Kotransport in tiefere Bodenschichten aufgrund der zunehmenden Adsorptionskapazität des Bodens erleichtern. Dagegen verstärken die verbleibenden MWCNTs die Deposition von SDZ in den oberen Bodenschichten aufgrund der zunehmenden Adsorptionskapazität des Bodens. Die modellierten Ergebnisse demonstrieren, dass die Mobilität von MWCNTs im Boden und die hohe Affinität von Schadstoffen zu MWCNTs sowie deren Einschluss durch MWCNTs der Hauptgrund für den durch MWCNTs erleichterten Schadstoff-Kotransport war. Andererseits hatten immobile MWCNTs weniger signifikanten Einfluss auf den Schadstofftransport, obwohl sie in der Lage sind die Adsorptionskapazität des Bodens zu verstärken.

Vorversuche mit Natriumdodecylbenzolsulfonat (SDBS, anionisches Tensid) und Triton[®] X-100 (TX100, nicht ionisches Tensid) in QS und GQS wurden durchgeführt, um den Effekt von Tensiden auf den MWCNTs Transport zu untersuchen. Die Adsorption von TX100 und SDBS an QS und GQS folgte der Reihe GQS > QS > aufgrund der größeren Oberfläche und Oberflächenladung von GQS. Für TX100 und SDBS an MWCNTs wurde eine Hochaffinitäts-Adsorptionsisotherme gefunden. Die Transportergebnisse wiesen darauf hin, dass die Mobilität von MWCNTs stark sensitiv bezogen auf den Tensidtyp und -konzentration, sowie die Eigenschaften des porösen Mediums war.

Zusammenfassend zeigen alle oben genannten Ergebnisse einen wichtigen Einblick auf die Mobilität von MWCNTs in der Umwelt.

Table of contents

Abstract	I
Zusammenfassung	III
Table of contents	VI
1. Introduction	1
1.1 Carbon nanotubes and their applications	1
1.2 Transport of engineered nanoparticles especially carbon nanotubes in porous media	5
1.3 Co-transport of chemicals by engineered nanoparticles in porous media	7
1.4 The role of soil colloids for engineered nanoparticles transport.....	8
1.5 Chlordecone and sulfadiazine	9
1.6 Objectives of the thesis	11
2. Theoretical background	13
2.1 Transport of engineered nanoparticles in saturated porous media...13	
2.1.1 Stability and aggregation of engineered nanoparticles.....	13
2.1.2 Colloid filtration theory	15
2.1.3 Extension of colloid filtration theory	17
2.2 Colloid-facilitated contaminant transport in saturated porous media	18
3. Materials and methods.....	21
3.1 Carbon nanotubes.....	21
3.2 Chlordecone and sulfadiazine	22
3.3 Surfactants.....	23
3.4 Quartz sand and goethite coated quartz sand	25
3.5 Soil	25
3.6 Batch and dialysis adsorption experiments.....	26
3.7 Water-saturated column setup.....	28
3.8 Soil fractionation.....	31
3.9 Numerical modeling.....	32
4. Results and discussion.....	35
4.1 Transport and retention of carbon nanotubes in goethite coated quartz sand.....	35
4.1.1 Characterization of goethite coated sand.....	35
4.1.2 Batch results	36
4.1.3 Effect of mass ratio of goethite in porous media.....	37
4.1.4 Effect of grain size	43

4.2	Transport and retention of carbon nanotubes in soil.....	45
4.2.1	MWCNT suspension stability	45
4.2.2	Zeta potential	45
4.2.3	Transport and Retention of MWCNTs	46
4.2.4	Release of MWCNTs	51
4.2.5	Soil size fractionation	55
4.3	Co-transport of chlordecone and sulfadiazine in the presence of carbon nanotubes in soils	58
4.3.1	Sorption results.....	58
4.3.2	Single-species transport in soil.....	60
4.3.3	Co-transport.....	63
4.4	Outlook: Influence of surfactant on carbon nanotubes transport in porous media	69
4.4.1	Adsorption of surfactants on QS, GQS and MWCNTs.....	69
4.4.2	Transport of surfactant-MWCNTs in quartz sand.....	71
4.4.3	Transport of surfactant-MWCNTs in goethite-coated quartz sand ..	74
5.	Summary and conclusions.....	78
	References	81
	List of Figures	98
	List of Tables	101
	List of Abbreviations	102
	List of Symbols	104
	Curriculum vitae	107
	Publications.....	109
	Acknowledgements.....	111

1. Introduction¹

In nanotechnology, manufactured or engineered nanoparticles (ENPs), which are generally sized between 1 and 100 nanometers, had dramatically increasing applications in the last decade. Due to the unique electronic, chemical, and physical properties by their fine size, ENPs are widely used in various applications such as cosmetics, medical devices, environmental remediation, electronics and plastics (Åkerman et al. 2002, Harris et al. 2006, Lowry and Casman 2009, Nowack and Bucheli 2007). Considering their wide use and lack of disposal regulations, ENPs are expected to ultimately lead to the release into the environment (Boxall et al. 2007, Gottschalk et al. 2009). Thus, understanding their fate, mobility, toxicity and bioavailability is needed. In this study, transport, co-transport and retention of functionalized multi-walled carbon nanotubes (MWCNTs) in different porous media were conducted to assess their fate in the environment.

1.1 Carbon nanotubes and their applications

Carbon nanotubes (CNTs) are allotropes of carbon with a needle-shaped nanostructure (Iijima 1991, Mauter and Elimelech 2008). CNTs are members of the fullerene structural family and are categorized as single-walled CNTs (SWCNTs), which are individual graphene tubes, and multi-walled CNTs (MWCNTs), which consist of more than two graphene tubes. The schematic illustrations of SWCNT (Figure 1.1a) and MWCNT (Figure 1.1b) are shown in Figure 1.1.

¹ Contains parts from “Resubmitted to Environmental Pollution, Miaoyue Zhang, Irina Engelhardt, Jirka Šimůnek, Scott A. Bradford, Daniela Kasel, Anne E. Berns, Harry Vereecken, Erwin Klumpp, Co-transport of chlordecone and sulfadiazine in the presence of functionalized multi-walled carbon nanotubes in soils, 2016”, “In press in Environmental Science & Technology, Miaoyue Zhang, Scott A. Bradford, Jirka Šimůnek, Harry Vereecken, and Erwin Klumpp, Do Goethite Surfaces Really Control the Transport and Retention of Multi-Walled Carbon Nanotubes in Chemically Heterogeneous Porous Media?, 2016”, and “Under revision in Water Research, Miaoyue Zhang, Scott A. Bradford, Jirka Šimůnek, Harry Vereecken and Erwin Klumpp, Roles of Cation Valance and Exchange on the Retention and Colloid-Facilitated Transport of Functionalized Multi-walled Carbon Nanotubes in a Natural Soil, 2016 ”.

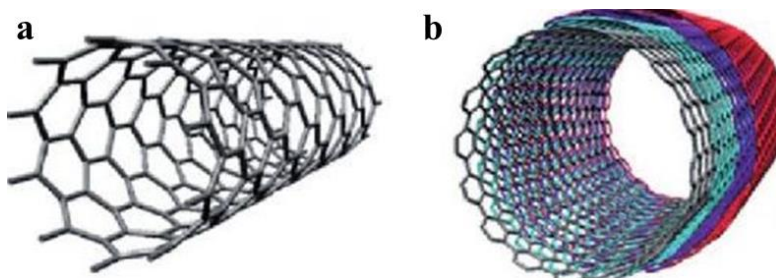


Figure 1.1 Schematic illustrations of a single-walled carbon nanotube (a) and a multi-walled carbon nanotube (b). Reprinted from Tan et al. (2011).

Structures, properties and applications

Unlike most spherical ENPs, CNTs have the cylindrical nanostructure, and exhibit high surface areas and a high aspect ratio even up to 132,000,000:1 (Jaisi et al. 2008, Wang et al. 2009). Similar to the graphite, CNTs are composed entirely of sp^2 bonds, which provide their unique and high specific strength up to $48,000 \text{ kN}\cdot\text{m}\cdot\text{kg}^{-1}$ (Das 2013, Eatemadi et al. 2014, Maynard 2007). CNTs have been utilized in numerous commercial applications due to their unique properties (Gannon et al. 2007, Gohardani et al. 2014, Liu et al. 2009b). The low weight of CNTs can result in significantly improved mechanical properties and electrical conductivity in biodegradable polymer composites (Chahine et al. 2014, Lalwani et al. 2013, Newman et al. 2013, Penza et al. 2004). Due to the extraordinary thermal conductivity and electrical properties, CNTs can form carbon nanotube field-effect transistors, electrical cables and wires (Janas et al. 2014, Postma et al. 2001). CNTs have also been used for other promising applications in batteries due to their exciting electronic properties (de las Casas and Li 2012), solar cells because of strong UV/Vis-NIR absorption characteristics (Guldi et al. 2005), hydrogen storage (Jones and Bekkedahl 1997) and radar absorption (Lin et al. 2008, Liu et al. 2007). Except that, CNTs exhibit strong sorption capacities of heavy metals, radionuclides, and organic compounds. Therefore they can be considered as absorbents for environmental remediation and water treatment (Camilli et al. 2014, Mauter and Elimelech 2008, Pan and Xing 2012, Zhang et al. 2010).

Surface modification

For the increasing applications of CNTs, stable CNT suspensions are required. However, CNTs are generally with hydrophobic surface, which undoubtedly hinder their dispersion in solvents. Thus, surface modification/functionalization of CNTs by oxidation with strong acids (e.g., HNO_3 , $\text{HNO}_3/\text{H}_2\text{SO}_4$, or H_2O_2), adsorbing surfactant, or adding polymers (Liu 2005, Moore et al. 2003, Smith et al. 2009, Sun et al. 2002) is generally applied for facilitating the formation of well-dispersed CNT suspensions. The surface oxidation with strong acids was also used for purification of CNTs to remove amorphous carbon and metal impurities (Peng and Liu 2006, Xing et al. 2005).

After functionalization/oxidation with strong acid, more oxygen-containing functional groups onto CNTs were observed. This process is summarized in Figure 1.2. The oxidation process does not significantly change the physical/structural characteristics of CNTs (Cho et al. 2008), but result in a few effects on the chemical composition of CNTs. Consequently, the zeta potential, water solubility, and aggregation state of CNTs in water change (Chen et al. 2004, Saltiel et al. 2005, Wu et al. 2013). In addition, oxidized CNTs have lower sorption capacity of hydrophobic organic substances such as naphthalene and natural organic matter which are determined by hydrophobic π - π interactions (Cho et al. 2008, Smith et al. 2012) and stronger sorption capacity of divalent cations such as Zn^{2+} and Cd^{2+} due to the interaction with the negatively charged surface oxides (Cho et al. 2010). Thus, surface oxidation of CNTs will undoubtedly influence the transport and retention behavior of CNTs in porous media.

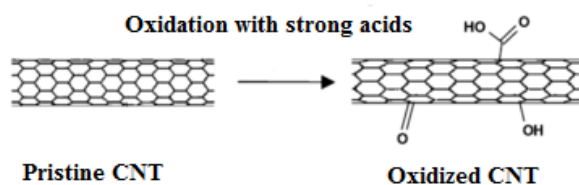


Figure 1.2 Oxidation of carbon nanotubes (CNTs). Modified from Grassian (2008).

Another method for surface modification of CNTs is addition of surfactants or polymers. Moore et al. (2003) used a series of anionic, cationic, and nonionic surfactants and polymers to test the ability of suspending CNTs. The results showed

that sodium dodecylbenzenesulfonate (SDBS) had the most well resolved spectral features for the ionic surfactant especially for anionic surfactants, and the size of the hydrophilic group and molecular weight of nonionic surfactants or polymers determined the CNTs suspended. In addition, surfactants also influence the transport behavior of CNTs in porous media, and the interactions between clay minerals and CNTs (Han et al. 2008, Lu et al. 2013, Lu et al. 2014).

Toxicity and risk management

The toxicity and risk management of ENPs like CNTs have been an important issue for nanotechnology applications due to the widespread use and lack of disposal regulations. Available literature indicates that CNTs are biologically non-degradable, and they are therefore expected to be very persistent in the environment (Lam et al. 2004). Several potential health risks of CNTs in environmental ecosystems have been identified (Farré et al. 2009, Lam et al. 2006). An understanding of factors that influence the transport and fate of CNTs in soils and groundwater is needed to assess the potential risks that CNTs pose to humans and ecosystems.

Current studies indicated that parameters such as structure, size distribution, surface area, surface charge and aggregation state as well as the purity of CNTs have considerably affected the ecotoxicity of CNTs. Generally, the cellular uptake mechanism used for the toxic studies of CNTs is affected by physicochemical properties (e.g., structure, size, surface area and aggregation). Kam et al. (2006) found that short SWCNTs with various functionalizations can easily transport proteins and oligonucleotides into living cells. Wick et al. (2007) suggested that the cytotoxicity of CNTs were affected by the degree and kind of agglomeration of CNTs. Cheng and Cheng (2012) found that the length of CNTs and sonication time for CNTs dispersed influenced their toxicity in zebrafish embryos. Kang et al. (2008) demonstrated that the diameter of CNTs influenced the cytotoxicity of CNTs, and SWCNTs were more toxic to bacteria than MWCNTs. Surface charge of CNTs can affect their size distribution, aggregation state and the adsorption capacity of ions (Chi et al. 2016, Simon-Deckers et al. 2009). For example, acid-functionalized SWCNTs exhibited greater toxicity and cytotoxicity to embryo than pristine SWCNTs (Saxena et al. 2007). Mouchet et al. (2016) indicated that the toxicity of different aquatic organisms may be due to physiological effects in relation to the ingestion of CNTs. Based on the cellular uptake mechanism, the environmental exposure of CNTs may

result in toxic effects to animals and plants (Grubek-Jaworska et al. 2006, Schwab et al. 2011, Smith et al. 2007).

1.2 Transport of engineered nanoparticles especially carbon nanotubes in porous media

ENPs may release into the environment like subsurface by via injection wells, leaking, and landfills during their manufacture, transport, application, and disposal (Grassian 2008). To date, numerous studies investigated the fate and transport behavior of ENPs in different porous media, indicating that the transport and retention of ENPs was sensitive to the structure of ENPs (O'Carroll et al. 2013, Wang et al. 2012d), ionic strength (IS) (Han et al. 2014, Tian et al. 2012c), Darcy velocity (Liang et al. 2013b, O'Carroll et al. 2013), grain size of the porous media (Kasel et al. 2013a, Mattison et al. 2011), in the presence of surfactant (Lu et al. 2013, Lu et al. 2014), organic matter (Wang et al. 2012b, Yang et al. 2013), and/or clay particles (Cai et al. 2014, Liang et al. 2013a). However, investigations on CNTs transport in chemically heterogeneous porous media (goethite coated quartz sand or soil), remobilization of retained CNTs, and the association with soil colloids still have limited attention.

The stability and aggregation of CNTs plays an important role in their fate and transport behavior in the subsurface. The stabilization of CNTs could be affected by the solution chemistry, surface oxidation, in the presence of surfactant, organic matter, and clay minerals, which could alter the surface charge of CNTs and influence electrostatic repulsive forces (Han et al. 2008, Jaisi and Elimelech 2009, Jaisi et al. 2008, Lu et al. 2013, Smith et al. 2009, Smith et al. 2012, Tian et al. 2012b). Tian et al. (2012a) found that SWCNTs exhibited high mobility in the saturated and unsaturated porous media by all three surface modified (oxidation, surfactant coating, and humic acid coating). Jiasi et al. (2008) showed that SWCNTs retention was sensitive to the IS, cation valence, and the retention of SWCNTs increased as IS increased or by addition of calcium ions. Lu et al. (2013, 2014) demonstrated that the CNTs stabilized by different surfactants such as SDBS, octyl-phenolethoxylate (TX100) and cetylpyridinium chloride (CPC) exhibited different mobility. Enhanced mobility of CNTs was also observed when the CNTs suspension was in the presence of humic acid (Jaisi et al. 2008, Wang et al. 2008). Han et al. (2008) found that clay minerals

(kaolinite and montmorillonite) could influence the stability of surfactant stabilized MWCNTs suspensions, but this effect also depended on the type of surfactant.

In general, the structure, morphology and size of CNTs would influence their physicochemical properties such as surface area, adsorption affinity, and straining process in porous media. Wang et al. (2012d) investigated MWCNTs with the same diameter and different lengths, and found that the retention of MWCNTs was increased as the length of MWCNTs increased. O' Carroll et al. (2013) suggested that smaller diameter of MWCNTs were less mobile in comparison to the larger ones, which was likely due to the enhanced Brownian motion leading to more collisions between the MWCNTs and the porous media. The properties of porous media also influence the mobility and retention of CNTs. CNTs exhibited higher retention in the finer textured sand due to a greater number of retention sites (Kasel et al. 2013a, Mattison et al. 2011).

The flow rate during the colloid transport behavior also plays an important role, which influence the hydrodynamic conditions and mass transfer rate between solid phase and liquid phase during the transport (Bradford et al. 2011a, Bradford et al. 2011b). Liu et al. (2009a) found the mobility of CNTs increased significantly as the flow rate increased.

To date, most studies on CNTs transport mentioned above were performed in model soil systems such as quartz sand or glass beads, which do not reflect the full complexity and heterogeneity of natural soils (e.g. complex grain size distribution and pore structure, surface roughness, and chemical heterogeneity). Kasel et al. (2013b) found limited transport of functionalized MWCNTs in undisturbed and unsaturated soils. Fang et al. (2013) showed that the mobility of CNTs suspended in a nonionic surfactant solution varied with the size of soil particles and the soil's sand content, and was negatively correlated to the soil's clay content. However, the number of investigations on CNTs transport in soil is still limited. No research studies have systematically examined the influence of soil chemical heterogeneities on the transport and fate of functionalized CNTs. Furthermore, the detachment or release of retained engineered nanoparticles (ENPs) like CNTs from the solid phase is also important for predicting the ultimate fate and transport of ENPs in the subsurface, but has received little research attention. There are even fewer studies on the effects of CNTs on the mobility of other solutes and compounds, such as organic and inorganic contaminants, and surfactant in porous media. In addition, most of studies on CNTs

transport only determine the breakthrough curves (BTCs). The information on retention profiles (RPs) in the solid phase is scarce. RP also provides important information on the transport and retention mechanisms for ENPs transport (Bradford and Bettahar 2005). More research is needed for a better understanding on the transport and retention of CNTs in different porous media under various conditions.

1.3 Co-transport of chemicals by engineered nanoparticles in porous media

In general, colloids (e.g., suspended nanoparticles, clay particles, and metal oxides) in the subsurface can act as carriers for contaminants or other chemicals because of their mobility and large sorption capacity. This process is often defined as “colloid-facilitated contaminant transport” (co-transport) (Bradford and Kim 2010, Šimůnek et al. 2006, Šimůnek et al. 2012). Many studies have demonstrated that contaminants were transported not only in the dissolved form, but also as sorbed to the mobile colloids (Grolimund et al. 1996, Mansfeldt et al. 2004, Šimůnek et al. 2006, Thiele-Bruhn 2003, Von Gunten et al. 1988). This information is important for environmental protection and risk assessment for both contaminants and colloids.

However, only very few studies have investigated the co-transport between ENPs and contaminants (Hofmann and Von der Kammer 2009, Zhang et al. 2011). These studies reported that ENPs affect the contaminant transport if nanoparticles have a strong mobility in porous media, a high adsorption capability, or if they are present in high concentrations. These studies used a mixture of ENPs and contaminants or assumed that the sorption equilibrium was reached. However, it is relatively unlikely that ENPs and contaminants are simultaneously released into the environment or are in sorption equilibrium before being released. Recent studies have additionally reported that various organic or inorganic contaminants such as pesticides, antibiotics, and heavy metals can sorb to and be transported by CNTs (Joško et al. 2013, Kim et al. 2014, Luo et al. 2013, Ren et al. 2011). An important implication of the CNTs presence in the environment is that they may significantly affect the fate of various contaminants and that they may potentially be used for their remediation. To the best of our knowledge, there has been no soil columns experimental and numerical analysis concerning the fate and transport of CNTs and contaminants that were not released simultaneously. Such studies could simulate a possible soil remediation

scenario when CNTs are released, either on purpose or accidentally, into an initially contaminated soil.

Surfactants are often used for CNTs stabilization. Lu et al. (2013, 2014) demonstrated that surfactant could significantly influence the transport of CNTs in porous media, which also can be seen as a co-transport process. However, these studies were performed at a higher input concentration of CNTs with a lower concentration of surfactant. The total concentration of surfactants that discharges in municipal sewer is about 20-70 mg L⁻¹ (Matthijs et al. 1999), which is much greater than the discharged concentration of MWCNTs as predicted (Gottschalk et al. 2009). Surfactants at these concentrations could be efficient enough to stabilize CNT suspension when both surfactant and CNT release into environment due to their applications. The effect of surfactant with a higher input concentration than CNTs on CNTs transport has limited attention.

1.4 The role of soil colloids for engineered nanoparticles transport

Soil colloids play an important role for ENPs transport, retention, and remobilization. Liang et al. (2013a) suggested the potential for soil colloids to facilitate silver nanoparticles transport in undisturbed and unsaturated soil due to the IS reduction and cation exchange. Cai et al. (2014) found the clay particles (bentonite and kaolinite) could enhance the titanium dioxide nanoparticles (nTiO₂) breakthrough in quartz sand in both NaCl and CaCl₂ solutions, and the attachment of nTiO₂ onto clay particles were observed under all experimental conditions. Han et al. (2008) also found that the clay minerals could affect the stability of the CNTs suspension modified by surfactants. Water-dispersible colloids (WDCs) are indicators for mobile soil colloids (de Jonge et al. 2004); e.g., WDCs are particles from the soil clay fraction that are less than 2 µm in size that are easily dispersible from soil with aqueous solution (Jiang et al. 2012, Jiang et al. 2014). Knowledge of the interaction and association between ENPs and WDCs is therefore important for better understanding the fate of ENPs in soil. However, the effects of perturbations in solution chemistry on the release and colloid-facilitated transport of MWCNTs in soil have not yet been studied; let alone the association between MWCNTs and soil colloids.

Clay particles also play an important role on ENPs retention in porous media (Wang et al. 2012a, Wang et al. 2013). Iron (Fe) and aluminum (Al) oxyhydroxides are the most common source of surface charge heterogeneity in natural aquatic environments. Both Fe and Al oxyhydroxides are amphoteric minerals that have relatively high points of zero charge. The zero point of charge for Fe and Al oxyhydroxides is reported to be 7.5 and 9 (Parks 1965), respectively. These minerals adsorb protons and acquire a net positive surface charge in aquatic environments that are below their zero point of charge. In contrast, common silica minerals exhibit a net negative surface charge at ambient pH values because of their lower zero point of charge (Alvarez-Silva et al. 2010). Natural porous media therefore often exhibit surface charge heterogeneity. An electrostatic interaction of functionalized CNTs is expected to be “favorable” on positively charged Fe and Al hydroxyoxides and “unfavorable” on negatively charged silica minerals under neutral pH conditions. In addition, a number of experimental and theoretical studies have demonstrated the important role of roughness on colloid and nanoparticle retention (Bradford and Torkzaban 2015, Torkzaban and Bradford 2016). Nanoscale roughness on macroscopically “unfavorable” surfaces locally reduces the energy barrier height to create regions where particle interaction in a primary minimum is “favorable” (Bradford and Torkzaban 2013, Bradford and Torkzaban 2015). The combination of nanoscale roughness and Born repulsion on a macroscopically “favorable” surface also creates a shallow primary minimum where interacting particles are susceptible to diffusive or hydrodynamic removal (Bradford and Torkzaban 2013, Bradford et al. 2015). Consequently, the question arises whether iron oxide coated surfaces are truly favorable to CNT retention. No research studies have systematically examined the influence of soil chemical heterogeneities on the transport and fate of functionalized CNTs.

1.5 Chlordecone and sulfadiazine

Chlordecone (CLD, $C_{10}Cl_{10}O$), which is also known as kepone, is a highly chlorinated pesticide. Although almost 20 years after the prohibition, the residual CLD still contaminate soils, fresh and coastal waters, aquatic biota, and crops due to its long-term application (Cabidoche and Lesueur-Jannoyer 2012). CLD, is a known persistent organic pollutants (POP) related to Mirex and

dichlorodiphenyltrichloroethane (DDT) (Metcalf 2000). The molecular structure of CLD is shown in Figure 1.3.

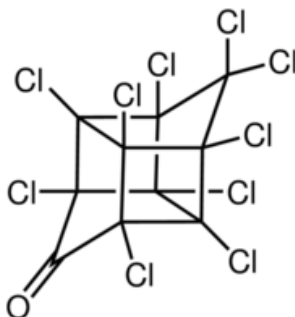


Figure 1.3 Structural formula of chlordecone.

Antibiotics widely used in animal and human medicine lead to their release into the environment (Pailler et al. 2009, Sun et al. 2014, Tamtam et al. 2008). The major risk of antibiotics in environment is the development and spreading of resistant pathogens that can reach the food chain via drinking water or the root uptake by plants (Dolliver et al. 2007, Kemper 2008). Sulfadiazine (SDZ, 4-amino-N-pyrimidin-2-yl-benzenesulfonamide) is a widely used sulfonamide antibiotic (Sittig et al. 2014, Unold et al. 2009, Wehrhan et al. 2007). The molecular structure of sulfadiazine is shown in Figure 1.4.

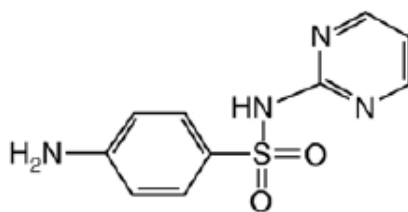


Figure 1.4 Molecular structure of sulfadiazine. Reprinted from Wehrhan et al. (2007).

1.6 Objectives of the thesis

This study aims to gain important insights into the transport and co-transport behavior of functionalized MWCNTs at environmentally relevant concentrations in different porous media. Both breakthrough curves (BTCs) and retention profiles (RPs) were determined and simulated. The objectives of the thesis included:

Transport and retention of carbon nanotubes in goethite coated quartz sand - In order to understand the mechanism of MWCNTs transport in heterogeneous porous media, the attachment, transport, and retention of MWCNT at low concentration in both batch and column experiments in a chemically heterogeneous porous medium with different mass ratios of quartz sand (QS) and goethite coated quartz sand (GQS) were investigated (Chapter 4.1). Several different sand grain sizes were applied in these experiments. Measured and simulated BTCs and RPs provided an improved understanding of MWCNT retention in chemically heterogeneous porous media, especially on the role of electrostatically “favorable” surfaces.

Transport and retention of carbon nanotubes in soil - To better understand roles of soil colloids, solution IS, and cation type on the transport, retention and release behavior of functionalized MWCNTs (1 mg L^{-1}) in a natural soil, both BTCs and RPs for MWCNTs were determined in column experiments, and a numerical model was employed to simulate their fate in soil (Chapter 4.2). The retained concentration of MWCNTs was subsequently determined for different soil size fractions (e.g., sand, silt, and water dispersible colloids (WDCs)) in order to investigate the interaction or association between soil colloids and MWCNTs. Furthermore, experiments were conducted to study the release of soil colloids and MWCNTs due to perturbations in solution chemistry (e.g., IS reductions and cation exchange).

Co-transport of chlordecone and sulfadiazine in soils in the presence of carbon nanotubes – In order to investigate the sorption and mobility of both contaminants in the absence and presence of functionalized MWCNTs, the transport behavior of MWCNTs in combination with the contaminants was studied by analyzing adsorption isotherms, as well as BTCs and RPs (Chapter 4.3). The column data were analyzed using the C-Ride module (Šimůnek et al. 2012) of HYDRUS-1D (Šimůnek et al. 2016), which accounts for advective-dispersive transport of both colloids and contaminants, attachment, detachment and straining of colloids, and kinetic sorption of contaminants to both soil and colloids.

Influence of surfactant on carbon nanotubes transport in porous media – To better understand the role of surfactant for MWCNTs transport in porous media, the adsorption isotherms of sodium dodecylbenzenesulfonate (SDBS, anionic surfactant) and Triton[®] X-100 (TX100, nonionic surfactant) on QS, GQS, and MWCNTs were determined (Chapter 4.4). The transport behavior of MWCNTs in QS or GQS was investigated determining BTCs of MWCNT, TX100, and SDBS. The results provided important insights into the potential of surfactants to facilitate the transport of MWCNTs in the subsurface environment.

2. Theoretical background²

2.1 Transport of engineered nanoparticles in saturated porous media

The mass transfer process of colloids/ENPs from water phase to solid phase involves two major mechanisms: solid-water interface attachment and pore straining (Grassian 2008). The solid-water interface attachment includes particle-solid (particle-surface) interactions such as electrostatic, van der Waals, and hydrophobic interactions, and colloidal movement by Brownian diffusion, sedimentation, and interception (Grassian 2008).

2.1.1 Stability and aggregation of engineered nanoparticles

Similar to colloids, the transport behavior of ENPs also strongly depends on their stability and aggregation behavior. This stability and aggregation behavior of ENPs is controlled by the electrostatic interactions including particle-particle and particle-surface interactions. Generally, both colloids/ENPs and porous media have charged surface in water and therefore attract the counter ions, resulting in an electric double layer (Stern layer and diffuse layer) and creating the potential for solid-water interface attachment (Grassian 2008). Zeta potential is the electric potential at the boundary between the Stern and diffuse layers in colloidal suspensions, which has a strong impact on the stability and mobility of ENPs in porous media (Grassian 2008).

Derjaguin-Landau-Verwey-Overbeek (DLVO) theory (Grassian 2008, Petosa et al. 2010) can be used to describe the stability of colloids/ENPs suspension by calculating the total potential energy. The total potential energy (W_{tpe}) is described as the sum of the electrical double layer repulsion energy (W_{edl} , repulsion potential) and the van der Waals attraction energy (W_{vdw} , attraction potential). The schematic depiction of DLVO theory is presented in Figure 2.1, which shows the total potential energy as a function of distance of particle-particle or particle-surface. The primary

² Contains parts from “Resubmitted to Environmental Pollution, Miaoyue Zhang, Irina Engelhardt, Jirka Šimůnek, Scott A. Bradford, Daniela Kasel, Anne E. Berns, Harry Vereecken, Erwin Klumpp, Co-transport of chlordecone and sulfadiazine in the presence of functionalized multi-walled carbon nanotubes in soils, 2016”, “In press in Environmental Science & Technology, Miaoyue Zhang, Scott A. Bradford, Jirka Šimůnek, Harry Vereecken, and Erwin Klumpp, Do Goethite Surfaces Really Control the Transport and Retention of Multi-Walled Carbon Nanotubes in Chemically Heterogeneous Porous Media?, 2016”, and “Under revision in Water Research, Miaoyue Zhang, Scott A. Bradford, Jirka Šimůnek, Harry Vereecken and Erwin Klumpp, Roles of Cation Valance and Exchange on the Retention and Colloid-Facilitated Transport of Functionalized Multi-walled Carbon Nanotubes in a Natural Soil, 2016 ”.

minimum happens when the attractive forces overpower the repulsive forces at lower molecular distances, resulting in coagulating and irreversible aggregation for particles. The second minimum happens at greater molecular distances in comparison to the primary minimum, but the attractive forces still can induce particle flocculation. The energy barrier is the repulsive region between the primary and secondary minima.

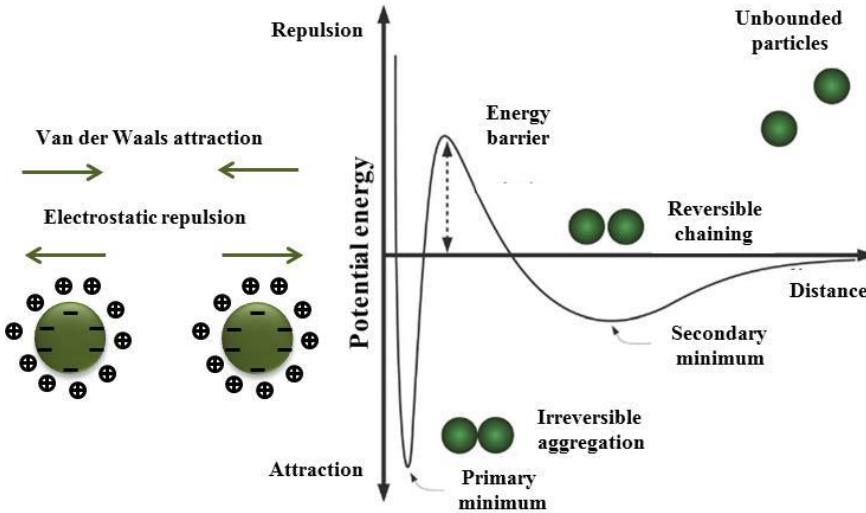


Figure 2.1 Schematic depiction of the classical DLVO theory. Adapted from Faraudo et al. (2013).

As mentioned above, both zeta potential and the total potential energy are influenced by the chemical conditions of transport system such as IS, pH, and in the presence of surfactant or humic acid. The increasing IS will increase the adhesive force for ENPs on collector surface due to compression of the double layer thickness and zeta potential decreasing (Jaisi et al. 2008, Tian et al. 2012c). However, the classical DLVO theory sometimes is weak to evaluate the experimental observations (Salerno et al. 2006). For example, the extended DLVO could explain other impacts on ENPs deposition such as surface roughness due to IS effect or in the presence of organic matter, which is neglected in the classical DLVO theory (Tong and Johnson 2007). In addition, the DLVO theory is developed for spherical colloids. For non-spherical colloids such as CNTs, the DLVO theory is therefore used to describe

semiquantitatively the stability and interactions between functionalized CNTs and collector surface (Derjaguin 1941, Liao et al. 2008).

2.1.2 Colloid filtration theory

The processes of colloid/ENP transport in porous media are shown in Figure 2.2, the colloidal movement by Brownian diffusion, sedimentation, and interception brings the colloids/ENPs into contact with the solid-water interface. As shown in Figure 2.2, Brownian diffusion (a) is the dominant mechanism for the movement of smaller colloids due to thermal effects. Interception (b) and gravitational sedimentation (c) are the mainly mechanism for the larger colloids movement. The contact between the colloids suspended in fluid streamlines and the solid surface results in interception. If the density of the colloids/ENPs is greater than the density of water, colloids/ENPs could transport vertically out of the fluid streamlines and move toward the solid surface (gravitational sedimentation) (Grassian 2008). The classical colloid filtration theory (CFT) that bases on the one-dimensional advection-dispersion equation (ADE) is generally used to help understanding the transport mechanism, which can be written as (Tufenkji and Elimelech 2004, Tufenkji et al. 2003):

$$\theta \frac{\partial C}{\partial t} + \rho \frac{\partial S}{\partial t} = \theta D \frac{\partial^2 C}{\partial x^2} - q \frac{\partial C}{\partial x} \quad (2.1)$$

$$\rho \frac{\partial S}{\partial t} = \theta k_{att} C \quad (2.2)$$

where θ is volumetric water content [$L^3 L^{-3}$; where L denotes units of length], C is colloid/ENPs concentration in liquid phase [$N L^{-3}$; where N denotes number], t is the time [T; where T denotes units of time], S is the total solid phase concentration ($N M^{-1}$), ρ is the bulk density of the porous matrix [$M L^{-3}$; where M denotes units of mass], x is the spatial coordinate [L], D is the hydrodynamic dispersion coefficient for colloids/ENPs [$L^2 T^{-1}$], q is the Darcy velocity [$L T^{-1}$], k_{att} is the first-order particle attachment rate coefficient [-], which can be given as:

$$k_{att} = \frac{3(1-\theta)q}{2d_{50}} \eta \quad (2.3)$$

where d_{50} is the median diameter of the porous media [L], η is the single collector efficiency [-, porous medium], is commonly related to the theoretical (maximum) collector efficiency, η_0 , such as $\eta = \alpha\eta_0$, α is the attachment or collision efficiency. The theoretical collector efficiency (η_0) is the sum of the contributions by diffusion, interception, and sedimentation.

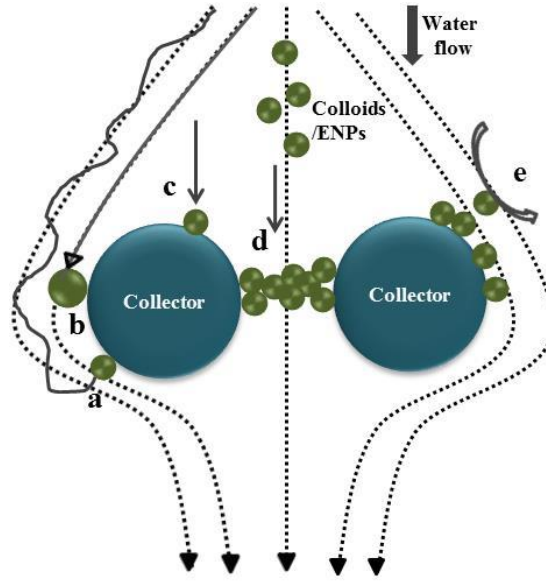


Figure 2.2 Schematic depictions of colloid/engineered nanoparticle (ENP) transport in porous media by Brownian diffusion (a), interception (b), gravitational sedimentation (c), straining (d), and blocking (e). The dotted lines and solid lines represent the fluid streamlines and colloid/ENP paths, respectively. Adapted from Lin et al. (2010) and Grassian (2008).

However, CFT could not fully predict all the observed transport behavior of colloids/ENPs in porous media. CFT assumes an exponential RP as a function of depth of colloids/ENPs retained in the solid phase, which is consistent with the favorable attachment conditions for colloids/ENPs (Tufenkji and Elimelech 2005a), whereas other RPs with a hyper-exponential or nonmonotonic shape have been found (Bradford et al. 2006b, Bradford et al. 2011a, Kasel et al. 2013a, Kasel et al. 2013b, Liang et al. 2013b). In addition, CFT also assumes to predict the spherical colloids in

spherical collector, which is therefore limited to predict non-spherical colloids such as CNTs or bacteria.

2.1.3 Extension of colloid filtration theory

As mentioned above, CFT are available for favorable attachment conditions. In order to describe other mechanism during colloids/ENPs transport especially for unfavorable attachment conditions, additional numerical model should be involved, which summarized as follows (Gargiulo et al. 2007),

$$\rho \frac{\partial S}{\partial t} = \theta \psi k_{sw} C - \rho k_{rs} S \quad (2.4)$$

where $k_{sw} [T^{-1}]$ is the first-order retention rate coefficients (including all the retention mechanism), $k_{rs} [T^{-1}]$ is the first-order release rate coefficients, and ψ is dimensionless functions that account for time or depth-dependent retention. When $\psi = 1$, Equation (2.4) is the CFT that assumes only attachment and detachment during the colloids/ENPs transport.

Site-blocking (Figure 2.2) is the mechanism that accounts for time-dependent retention, which describes the breakthrough of colloids/ENPs increases with injection over time due to the available retention locations filled over time. The time-dependent Langmuirian blocking by setting ψ of Equation (2.4) equal to:

$$\psi_1 = 1 - \frac{S}{S_{max}} \quad (2.5)$$

where $S_{max} [NM^{-1}]$ is the maximum solid phase concentration.

For unfavorable attachment condition, pore straining is additional dominant mechanism for colloids/ENPs attachment during transport in porous media (Grassian 2008, Šimůnek et al. 2008). Pore straining (Figure 2.2) is the process of fine particles. When particles transport in down-gradient by fluid, they are trapped or constricted in the pore space that are too small to admit them to pass, which depends on both particle size and pore size distributions (Bradford et al. 2004, Bradford et al. 2003, Bradford et al. 2006b).

In this case, the value of ψ of Equation (2.4) was defined as:

$$\psi_2 = \left(\frac{d_{50}+x}{d_{50}}\right)^{-\beta} \quad (2.6)$$

where β [-] is a fitting parameter which controls the shape of the RP, which helps to describe the hyper-exponential RP (Bradford and Bettahar 2006).

2.2 Colloid-facilitated contaminant transport in saturated porous media

The co-transport process includes contaminant transport, colloid transport, and the interactions among colloids and contaminants. All of these complex processes result in more flexible transport models for co-transport description than regular solute or colloid transport. Numerical models simulating co-transport are generally based on the mass balance equations for both colloids and contaminants and account for various interactions between the colloids, contaminants, and soil. They consider various equilibrium and kinetic models such as the first-order sorption of contaminants to soil, the first-order kinetic attachment of colloids (Corapcioglu and Jiang 1993, Jiang and Corapcioglu 1993), irreversible nonlinear kinetic attachment of colloids (Saier and Hornberger 1996), and competitive Langmuir kinetic sorption of contaminants on colloids (van de Weerd and Leijnse 1997).

In this study, i) only two phases (water phase and solid phase) are considered for the saturated system, ii) only one type of colloids exist in the system, and iii) colloids/ENPs are stable in the liquid phase. Based on the colloid transport mentioned above, the time- dependent blocking function and depth-dependent retention of colloids/ENPs during transport are also considered in the following model (Šimůnek et al. 2012). The schematic process of co-transport is shown in Figure 2.3. As shown in Figure 2.3, colloids can exist in water phase as mobile colloids, the rest are immobile colloids that retain in water-solid interface by straining or other attachment process. This process has been introduced in Chapter 2.1. The process for contaminants including: i) dissolved in water phase, ii) sorbed to soil by instantaneous and kinetical sorption process, iii) sorbed to mobile colloids, and iv) sorbed to immobile colloids. These processes are reversible.

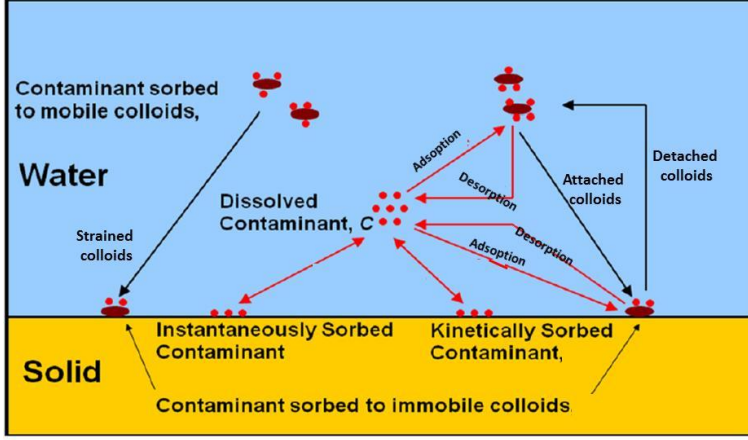


Figure 2.3 Schematic of colloids-facilitated solute transport in saturated porous media. Adapted from Šimůnek et al. (2012).

Contaminant transport in porous media is described using the advection-dispersion equation, which is given as:

$$\theta \frac{\partial C_c}{\partial t} + \rho \frac{\partial S_c}{\partial t} = \theta D_c \frac{\partial^2 C_c}{\partial x^2} - q \frac{\partial C_c}{\partial x} \quad (2.7)$$

where C_c is the contaminant concentration in the liquid phase [ML^{-3}], D_c is the hydrodynamic dispersion coefficient for contaminant [L^2T^{-1}], S_c is the contaminant concentration sorbed to the solid phase [MM^{-1}]. Sorption of contaminant was described using a two-site adsorption-desorption model as follows (van Genuchten and Wagenet 1989):

$$S_c = S_e + S_k \quad (2.8)$$

$$\frac{\partial S_e}{\partial t} = f K_d \frac{\partial C_c}{\partial t} \quad (2.9)$$

$$\frac{\partial S_k}{\partial t} = \omega [(1 - f) K_d C_c - S_k] \quad (2.10)$$

where S_e [MM^{-1}] is the contaminant concentration on one fraction of the sorption sites (type-1 sites), on which sorption is assumed to be instantaneous, S_k [MM^{-1}] is the

contaminant concentration on the remaining sorption sites (type-2 sites), on which sorption is considered to be a first-order kinetic rate process, f [-] is the fraction of exchange sites assumed to be in equilibrium with the solution phase, K_d is the partition coefficient of contaminant for linear adsorption [L^3M^{-1}], ω is the first-order rate constant [T^{-1}].

The interactions between the contaminant and mobile or immobile colloids during coupled colloids/ENPs and contaminant transport are described as follows (Pang and Šimůnek 2006, Šimůnek et al. 2006, Šimůnek et al. 2012), the degradation of contaminant is not considered:

$$\begin{aligned} \theta \frac{\partial C_c}{\partial t} + \rho \frac{\partial S_e}{\partial t} + \rho \frac{\partial S_k}{\partial t} + \theta \frac{\partial CS_{mM}}{\partial t} + \rho \frac{\partial SS_{iM}}{\partial t} = \theta D_c \frac{\partial^2 C_c}{\partial x^2} - q \frac{\partial C_c}{\partial x} + \\ + \theta D_c \frac{\partial^2 CS_{mM}}{\partial x^2} - q \frac{\partial CS_{mM}}{\partial x} \end{aligned} \quad (2.11)$$

where S_{mM} and S_{iM} [MM^{-1}] are the contaminant concentrations sorbed to mobile and immobile colloids/ENPs, respectively. Concentrations of contaminant sorbed to immobile and mobile colloids can be written as follows:

$$\begin{aligned} \theta \frac{\partial CS_{mM}}{\partial t} = \theta D_c \frac{\partial^2 S_{mM} C}{\partial x^2} - q \frac{\partial CS_{mM}}{\partial x} + \\ \theta \psi_m k_{amM} C_c - \theta k_{dmM} CS_{mM} - \theta k_{sw} CS_{mM} + \rho k_{rs} SS_{iM} \end{aligned} \quad (2.12)$$

$$\rho \frac{\partial SS_{iM}}{\partial t} = \theta \psi_{im} k_{aiM} C_c - \rho k_{diM} SS_{iM} + \theta k_{sw} CS_{mM} - \rho k_{rs} SS_{iM} \quad (2.13)$$

where k_{aiM} and k_{diM} are the rate coefficients for contaminant sorption to and desorption from immobile colloids/ENPs [T^{-1}], respectively; and ψ_m and ψ_{im} are dimensionless variables that adjust the sorption rate to a number of mobile and immobile colloids/ENPs present, respectively. Detailed list of all transport and reaction equations involved in colloid-facilitated solute transport are described in detail in the manual of C-Ride (Šimůnek et al. 2012).

3. Materials and methods³

3.1 Carbon nanotubes

Radioactively (^{14}C) labeled and unlabeled MWCNTs that prepared by catalytic chemical vapor deposition using ^{14}C -benzene as feedstock gas were applied for all experiments (Bayer Technology Services GmbH, Germany). The specific radioactivity was about 3.2 MBq mg^{-1} . MWCNTs were boiled with 70% nitric acid (Sigma-Aldrich Chemie GmbH, Germany) for 4 h, resulting in additional oxygen-containing functional groups (e.g., carboxylic groups) on their surfaces (Figure 1.2). Therefore, the MWCNT suspensions were prepared at desired input concentration with desired electrolyte solutions (KCl or CaCl_2) and ultrasonicated for 15 min at 65 W by a cup horn sonicator as stock suspension, and then ultrasonicated again for 10 min before injection, leading to better-dispersed MWCNTs during the experiments.

The characterization and aggregation behavior of functionalized MWCNTs is given in Kasel et al. (2013a, 2013b). In brief, after acid treatment, the amount of Mg, Mn, Co, and Al were less than 0.07 wt% and the intensity of the binding energy of the O 1s spectra was significantly higher. The median diameter of MWCNTs is 10-15 nm and the median length is 200-1000 nm (Pauluhn 2010). The transmission electron microscopy (TEM) images of MWCNTs are shown in Figure 3.1. The electrophoretic mobility of MWCNTs with desired electrolyte solutions was measured using a Zetasizer Nano (Malvern Instruments GmbH, Herrenberg, USA). The hydrodynamic radius measured by dynamic light scattering (DLS, Zetasizer Nano, Malvern Instruments GmbH, Herrenberg, USA) cannot reflect the real geometric particle diameter (Hassellöv et al. 2008, Pecora 2000) for non-spherical particles like MWCNTs. Nevertheless, it can be used for comparison of the stability of MWCNTs suspensions due to the effect of IS and surfactant. The hydrodynamic radius of unlabeled functionalized MWCNTs: i) suspended in KCl and CaCl_2 at IS=10 mM were measured 0, 1, and 4 h after suspension preparation, and ii) in 1 mM KCl at

³ Contains parts from “Resubmitted to Environmental Pollution, Miaoyue Zhang, Irina Engelhardt, Jirka Šimůnek, Scott A. Bradford, Daniela Kasel, Anne E. Berns, Harry Vereecken, Erwin Klumpp, Co-transport of chlordecone and sulfadiazine in the presence of functionalized multi-walled carbon nanotubes in soils, 2016”, “In press in Environmental Science & Technology, Miaoyue Zhang, Scott A. Bradford, Jirka Šimůnek, Harry Vereecken, and Erwin Klumpp, Do Goethite Surfaces Really Control the Transport and Retention of Multi-Walled Carbon Nanotubes in Chemically Heterogeneous Porous Media?, 2016”, and “Under revision in Water Research, Miaoyue Zhang, Scott A. Bradford, Jirka Šimůnek, Harry Vereecken and Erwin Klumpp, Roles of Cation Valance and Exchange on the Retention and Colloid-Facilitated Transport of Functionalized Multi-walled Carbon Nanotubes in a Natural Soil, 2016 ”.

different surfactant concentrations (0, 10, and 50 mg L⁻¹) were measured after suspension preparation and 1 h. The pH values of MWCNTs suspensions at different surfactant concentrations (0, 10, and 50 mg L⁻¹, 1 mM KCl) or in the effluent from column experiments were measured by pH meter (Mettler Toledo MP230 pH meter).

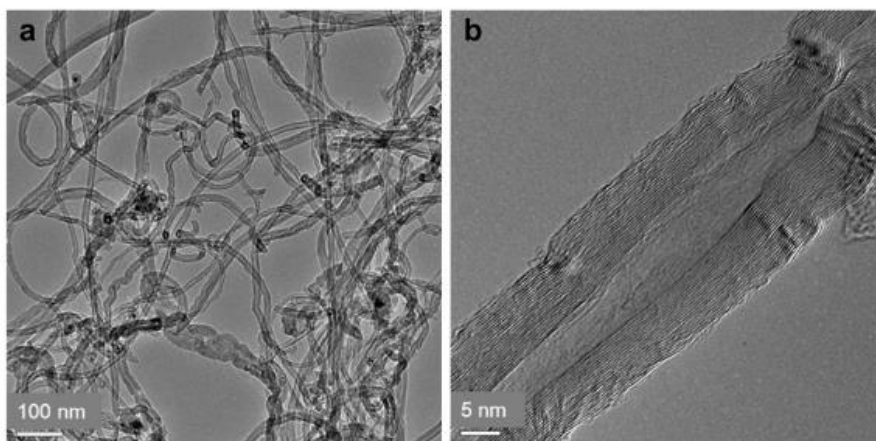


Figure 3.1 Transmission electron microscopy images of multi-walled carbon nanotubes at different magnifications: (a) 100 nm and (b) 5 nm. Reprinted from Kasel et al. (2013a).

3.2 Chlordecone and sulfadiazine

Radioactively (¹⁴C) labeled chlordecone (CLD) dissolved in acetone was purchased from Moravек Biochemicals (Brea, CA, USA). The specific radioactivity of ¹⁴C-labeled CLD was 2.94 MBq mg⁻¹. For preparation of the desired CLD solution concentration, the ¹⁴C-labeled CLD was mixed with non-labeled CLD (Sigma-Aldrich Chemie GmbH, Steinheim, Germany). After the acetone had evaporated, the flasks were filled to the required volume with 1 mM KCl.

Radioactively (¹⁴C) pyrimidine-ring-labeled sulfadiazine (SDZ) was purchased from Bayer-Health Care AG (Wuppertal, Germany). The specific radioactivity was 0.43 MBq mg⁻¹ and was labeled at the C-2 position. For preparation of the desired SDZ solution concentration, SDZ dissolved in the 1 mM KCl solution for the desired concentration.

3.3 Surfactants

Triton X-100 (TX100) and sodium dodecylbenzenesulfonate (SDBS) were purchased from Merck KGaA (Darmstadt, Germany) and Sigma-Aldrich Chemie GmbH (Munich, Germany), respectively. TX100 and SDBS stock solutions (100 mg L⁻¹) were prepared by adding 50 mg surfactant into 500 ml Milli-Q water. In order to prepare MWCNTs suspension that modified with surfactant, ¹⁴C-labeled MWCNTs stock suspension (100 mg L⁻¹, in Milli-Q water) was diluted under different surfactant concentrations (SDBS and TX100, 0, 10, and 50 mg L⁻¹) at the desired ionic strength (1 mM KCl). These suspensions were labeled as surfactant-free MWCNTs (without surfactant), SDBS-MWCNTs (MWCNTs modified by SDBS), and TX100-MWCNTs (MWCNTs modified by TX100). Then, the mixture was ultrasonicated for 15 min at 65 W, and then ultrasonicated again for 10 min before injection, leading to better-dispersed MWCNTs during the experiments. The concentrations of TX100, SDBS, TX100-MWCNTs, and SDBS-MWCNTs were determined by UV-Vis spectrometer (Beckman DU-640, USA) as the wavelength of 274 (TX100 and TX100-MWCNTs) or 230 nm (SDBS and SDBS-MWCNTs). Obviously, both MWCNTs and TX100 or SDBS have the absorbance at the wavelengths of 274 or 230 nm. The calibrations curves of absorbance and concentrations of MWCNTs, TX100, SDBS, TX100-MWCNT and SDBS-MWCNTs are therefore determined at the different wavelengths and shown in Figure 3.2. Figure 3.2a and 3.2b shows the high correlation ($R^2 \geq 0.999$) between concentration and absorbance of TX100, MWCNT and TX100-MWCNT, and SDBS, MWCNT and SDBS-MWCNT, respectively. Both of them have two y-axes. The left one presented the concentration for MWCNT. The right one was for TX100 or SDBS. Figure 3.2 c shows the correlation between measured absorbance (TX100-MWCNT or SDBS-MWCNT) and calculated absorbance by the individual absorbance of MWCNTs, TX100, and SDBS, which demonstrated that the additivity of individual absorbance of MWCNTs, TX100, SDBS, TX100-MWCNT and SDBS-MWCNTs can be applied to quantitative analysis the concentrations of TX100 and SDBS in the effluent from column experiments.

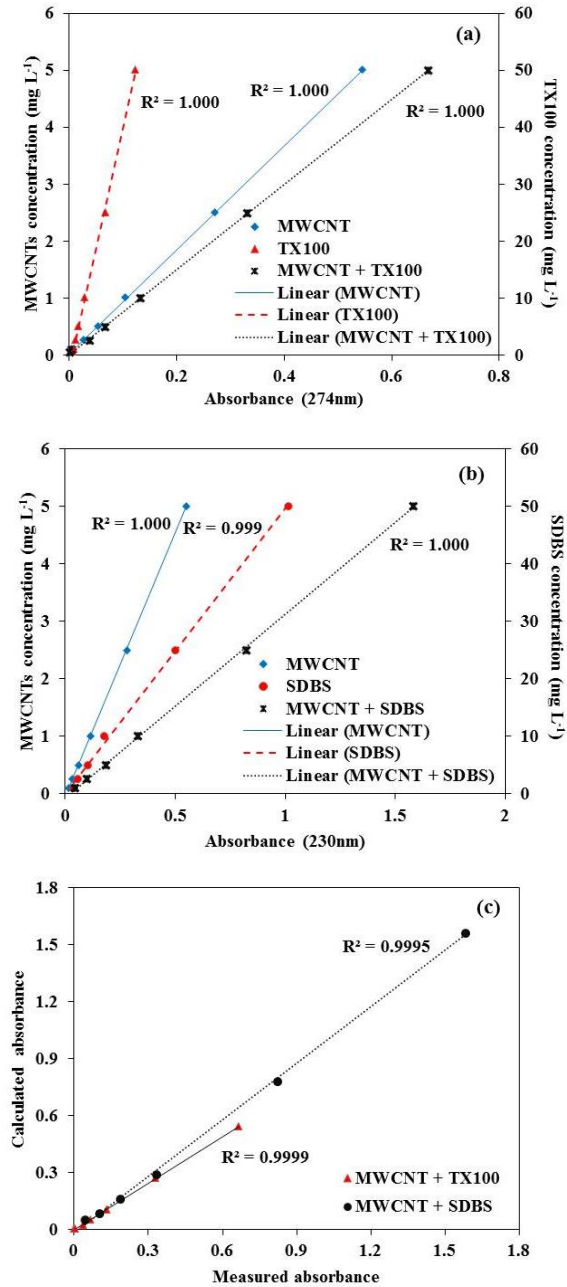


Figure 3.2 (a) Correlation between concentration and absorbance of TX100, MWCNT and TX100-MWCNT; (b) Correlation between concentration and absorbance of SDBS, MWCNT and SDBS-MWCNT; (c) Correlation between measured absorbance and calculated absorbance.

3.4 Quartz sand and goethite coated quartz sand

Three median grain sizes (240, 350, and 607 μm) of QS were used in experiments (Quarzwerke GmbH, Frechen, Germany for 240 and 350 μm ; Teco-Sil[®], C-E Minerals, King of Prussia, PA, USA for 607 μm). These QS were purified following protocols in the literature (Kasel et al. 2013a). In brief, QS was immersed in Milli-Q water for 24 h and boiled in additional fresh Milli-Q water for 2 h at 100 °C. After that, the sand was boiled with 65% HNO_3 for 2 h. After the sand was cooled down and removed the acid by Milli-Q water until the pH was around 5. Then, the sand was boiled with 10% H_2O_2 for additional 2 h and washed again by Milli-Q water. Finally, the sand was dried in an oven at 50 °C.

GQS was prepared using the similar procedure of Scheidegger et al. (1993). In brief, 42 g of goethite (Fluka, Sigma-Aldrich Chemie GmbH, Germany) were mixed with 140 ml of 0.01M NaNO_3 in a 500 ml glass bottle and the pH -value was adjusted to 2.5 by incrementally adding HNO_3 (1M and 0.01M). This mixture was then shaken at room temperature for 24h at 150 rpm min^{-1} . After shaking, 250 g of purified QS was added to the goethite solution at pH 2.5 and shaken for 24h at 150 rpm min^{-1} . After that, the sand-goethite mixture was sequentially washed with 1M NaNO_3 and deionized water to remove unattached goethite particles. Finally, the GQS was dried in an oven at 50 °C.

The specific surface areas of QS and GQS were determined by the Brunauer–Emmett–Teller (BET) method (Brunauer et al. 1938). Krypton adsorption was used for the low BET surface area determination of QS and GQS. The iron concentration of QS and GQS after digesting by aqua regia was measured by inductively coupled optical emission spectrometry (ICP-OES). The chemically heterogeneous porous medium was prepared by combining various amounts of QS with a known mass fraction of GQS (λ , mass ratio of GQS in the mixing porous media). The zeta potential for QS and goethite particles with desired electrolyte solutions was measured using a Zetasizer Nano (Malvern Instruments GmbH, Herrenberg, Germany).

3.5 Soil

Soil samples (loamy sand soil) were from the upper 30 cm of an agricultural field site in Germany (Kaldenkirchen-Hülst, Germany), which were sieved to a

fraction < 2 mm and air dried (d_{50} = 120 μm). This soil had a total organic carbon of 1.1 %mass, a cationic exchange capacity of 7.8 $\text{cmol}_\text{c} \text{ kg}^{-1}$, and pH value of 5.9 (Kasel et al. 2013b). The soil was composed of 4.9 % clay (<2 μm), 26.7% silt (2-63 μm), and 68.5 % sand (>2 μm). The surface charge characteristics of the soil were determined by Zetasizer Nano (Malvern Instruments GmbH, U.S.A) when it had been homogenized and sonicated in a selected electrolyte solution.

3.6 Batch and dialysis adsorption experiments

Batch experiments was based on Organisation for Economic Cooperation and Development (OECD) -guideline 106 (OECD 2000).

For the adsorption isotherms of MWCNTs on QS and GQS, experiments were carried out under quasi-equilibrium conditions by adding 20 ml of ^{14}C -labeled functionalized MWCNT suspensions of different concentrations (0-1 mg L^{-1} , in 1 mM KCl) to 1 g of QS or GQS with two different sizes (350 and 607 μm) in a centrifuge tube. The tubes were continuously mixed using an over-head shaker for 24 h. Preliminary experiments revealed that this duration was sufficient for sorption equilibrium. After removing the suspension of MWCNT, the sorbents (QS or GQS) were dried in an oven at 50 $^{\circ}\text{C}$ and combusted by using a biological oxidizer (OX 500, R.J. Harvey Instrumentation Corporation, Tappan, USA) at 900 $^{\circ}\text{C}$. The emerging $^{14}\text{CO}_2$ was dissolved in vials filled with scintillation cocktail (Oxisolv, MERCK KGAA, Darmstadt, Germany) and the ^{14}C concentration of MWCNTS adsorbed to the sorbents was determined using liquid scintillation counter (LSC, Perkin Elmer, Rodgau, U.S.A). The concentration of ^{14}C -labeled MWCNTs in the supernatant before and after the sorption experiments was measured using LSC by adding scintillation cocktail (Insta-Gel Plus) into liquid samples.

The adsorption kinetics and the adsorption isotherms of CLD on the loamy sand soil and on MWCNTs were determined in batch trials and by using the dialysis technique (Höllrigl-Rosta et al. 2003), respectively. The soil adsorption isotherms were measured using mixtures of 10 ml ^{14}C -labeled CLD solutions of different concentrations and 1 g soil (in 1 mM KCL), which were equilibrated for 24 h in an overhead shaker. After centrifugation, the supernatant was taken and measured by LSC. The dialysis technique (Höllrigl-Rosta et al. 2003) was applied to determine the adsorption of CLD and SDZ on MWCNTs because it was not sufficient to separate

the functionalized MWCNTs from the suspension by centrifugation. Two dialysis half-cells were therefore separated by a 1 kDa cut-off cellulose membrane (VWR International GmbH, Langenfeld, Germany) and inserted into a special frame. Then, one half-cell was filled with approximately 5 ml MWCNT suspension (10 mg L^{-1}), the other with approximately 5 ml CLD or SDZ solution of different concentrations. The special frame was inserted into a rotator and rotated at 10 rpm for 48 h. Afterwards, the solution concentration of ^{14}C -labeled CLD or SDZ was measured by LSC.

For determination of CLD sorption kinetics, 10 ml ^{14}C -labeled CLD solution at $10 \mu\text{g g}^{-1}$ was added to 10 mg MWCNTs. The mixtures were shaken, samples taken at defined interval time, and measured by LSC. The kinetic analysis of the batch experimental data was carried out using the following equation (Schijven and Hassanizadeh 2000):

$$\frac{C_c}{C_0} = \frac{k_{dmM} + k_{amM} \exp[-(k_{amM} + k_{dmM})t]}{k_{amM} + k_{dmM}} \quad (3.1)$$

where C_c is the contaminant concentration in the liquid phase [ML^{-3}]; C_0 is the initial contaminant concentration in the liquid phase [ML^{-3}]; k_{amM} and k_{dmM} are the CLD adsorption and desorption rate coefficients to the mobile MWCNTs [T^{-1}], respectively.

The adsorption isotherms of surfactants (TX100 and SDBS) on QS (240 μm), and GQS (240 μm , $\lambda = 0.1$ or 0.3) were determined in batch trials, and on MWCNTs (5 mg L^{-1} , 1 mM KCl) by using the dialysis technique (Höllrigl-Rosta et al. 2003), respectively. 20 ml of surfactants (TX100 and SDBS) of different concentrations (in 1mM KCl) were added to 2 g of QS or GQS ($\lambda = 0.1$ or 0.3) in a centrifuge tube. Preliminary experiments revealed that 24 h was sufficient for sorption equilibrium. Thus, the tubes were continuously mixed and equilibrated for 24 h at 220 rpm. After 15 min centrifugation at $2525 \times g$ (4000 rpm), the supernatants of TX100 and SDBS were filtered through 0.2 μm polypropylene filters (Minisart® syringe filters, Sartorius Stedim Biotech GmbH, Germany) and measured by UV- Vis spectrometer (Beckman DU-640, USA) at the wavelength of 274 and 230 nm, respectively. The dialysis technique was applied to determine the adsorption of surfactants on MWCNTs. One half-cell was filled with approximately 5 ml unlabeled functionalized MWCNT suspension (5 mg L^{-1} , 1 mM KCl), the other with approximately 5 ml TX100 or SDBS solution of different concentrations (0-80 mg L^{-1} , 1 mM KCl). Then, these cells

rotated at 10 rpm for 48 h. Afterwards, the solution concentration of TX100 or SDBS from the half-cell was measured by UV-Vis spectrometer.

All the batch experiments were performed in triplicate. Blank experiments in all batch experiments were conducted to verify that minimal sorption of MWCNTs, CLD, SDZ, and surfactants occurred to the wall of the centrifuge tube and half-cell.

3.7 Water-saturated column setup

The stainless steel columns (3 cm in inner diameter and 12 cm in length) equipped with a stainless steel plate (1 mm openings) and a PTFE mesh (200 mm openings) at the column bottom to support the porous media. The column was connected to a pump (MCP V 5.10, Ismatec SA, Glattbrugg, Switzerland) on the inlet side with the flow direction from the bottom to the top of the column. The schematic image and photograph of column setup are shown in Figure 3.3a and 3.3b, respectively.

MWCNTs transport in GQS

Chemically heterogeneous porous media (QS and GQS mixtures, Chapter 4.1) were incrementally wet (Milli-Q water). The Darcy velocity is 0.72-0.75 cm min⁻¹. Approximately 50 pore volumes (PVs) of background electrolyte solution (1mM KCl) were passed through the column before conducting the transport experiments. A non-reactive tracer (1mM KBr) pulse (approximately 90 ml, 2.5 PVs) was injected into the column to characterize the hydraulic conditions (porosity and dispersivity). The schematic process for effluent and solid samples determination is shown in Figure 3.3c. Effluent solutions of bromide were collected using a fraction collector (FoxyJr.®, Teledyne Isco Inc., Lincoln, USA) every 30 s (e.g., approximately 2.5 mL per vial) and measured using a high performance liquid chromatography (HPLC, STH 585, Dionex, Sunnyvale, CA, USA) equipped with a UV-detector (UV2075, Jasco, Essex, UK). The same procedure was repeated when MWCNT suspensions (1 mg L⁻¹, 1 mM KCl) were applied.



Figure 3.3 The schematic image of column setup under water saturated condition. (a) The schematic running process of column experiments. (b) The photograph of the column setup. (c) The schematic process for effluent and solid samples determination.

MWCNTs transport in soil

MWCNT transport experiments in saturated soil column (soil and Milli-Q water were alternately and incrementally filled into the columns, Chapter 4.2) were conducted at different IS (1, 4, and 10 mM KCl) and different cation type at the same IS (1 mM KCl and CaCl_2 , molar concentration $0.33 \text{ mM L}^{-1} \text{ CaCl}_2$). The soil in the column was equilibrated before initiating the transport experiment by injecting approximately 30 PVs of a selected background electrolyte solution at a slow, constant Darcy velocity of 0.18 cm min^{-1} . Conservative tracer (KBr) and MWCNT transport experiments were then conducted sequentially at the same IS and cation type as the equilibrium phase, but at a higher, constant Darcy velocity of $0.71\text{-}0.73 \text{ cm min}^{-1}$. The conservative tracer experiment was performed first. Transport experiments for MWCNTs (input concentration, 1 mg L^{-1}) were conducted in a similar manner as

the conservative tracer; e.g., injection of a 2.1 PVs pulse of MWCNT suspension (approximately 90 mL), followed by elution with the same particle-free electrolyte solution for another 5.5 PVs. Additional experiments were performed to study the release behavior of MWCNTs with IS reduction and cation exchange at a constant Darcy velocity of 0.71-0.73 cm min⁻¹. The initial deposition phase (step A) was conducted using MWCNTs (1 mg L⁻¹) in 10 mM KCl (experiment I), 1 mM CaCl₂ (experiment II), and 10 mM CaCl₂ (experiment III) solutions in an analogous fashion to MWCNTs transport experiments discussed above. Release experiments II and III were then initiated by changing the eluting solution chemistry in the following sequence: Milli-Q water (step B); KCl at the same IS as in step A (step C); Milli-Q water (step D); 100 mM KCl (step E); and Milli-Q water (step F). Each solution chemistry step was conducted for 7.6 PVs. Experiment I consisted of only steps A and B. The ¹⁴C-labeled effluent and soil concentrations of MWCNT were measured. Cation exchange and soil colloids were quantified during the release experiments by measuring the effluent concentrations of K, Ca, Fe, and Al using ICP- OES. Because radioactive samples (¹⁴C) are not allowed for ICP-OES measurement, the release experiments were repeated using unlabeled functionalized MWCNTs for this analysis.

Co-transport of CLD and SDZ by MWCNTs in soil

Saturated soil columns were conducted (Chapter 4.3). Tracer experiments (1 mM KBr) were conducted first. The same procedure was repeated when CLD, SDZ, and MWCNTs were applied. The single-species transport of CLD (experiment I), SDZ (experiment II and III), or MWCNTs (experiment IV) in the saturated soil columns were investigated first. Based on information collected during this first step, the second set of column experiments was designed to investigate the effect of MWCNTs on the transport of CLD and SDZ. During the CLD co-transport experiment, a pulse (around 2.1 PVs) of CLD was injected first, followed by a MWCNT suspension pulse (around 2.1 PVs) applied at the same IS and flow velocity (experiment V and VI). In contrast, during the SDZ co-transport experiment, the MWCNT suspension (around 2.1 PVs) was injected first, followed by an injection of SDZ (around 2.1 PVs, experiments VII and VIII). For both CLD and SDZ co-transport experiments, the non-¹⁴C-labeled MWCNTs, prepared in the same way as the ¹⁴C-labeled MWCNTs, were applied. We assumed that the non-¹⁴C-labeled

MWCNTs in the co-transport experiments showed the same transport behavior as the ^{14}C -labeled MWCNTs in the single-species transport experiments.

MWCNTs transport in the presence of surfactant

The transport experiments with the same MWCNTs concentration (5 mg L^{-1} , 1 mM KCl) were conducted at different surfactant concentrations (0 , 10 , and 50 mg L^{-1}) in QS and at the same surfactant concentration (10 mg L^{-1} , $\lambda = 0.1$ and 0.3) in GQS (Chapter 4.4). Approximately 30 PVs of background electrolyte solution (1 mM KCl) were applied to the column before the transport experiments were carried out. A non-reactive tracer was injected into the column at a steady-state flow rate with Darcy velocity of $0.71\text{--}0.73\text{ cm min}^{-1}$. Then, the same procedure as tracer was repeated when different MWCNTs suspension applied. The ^{14}C -labeled effluent concentrations of MWCNT were determined using LSC. The effluent concentrations of TX100-MWCNTs or SDBS-MWCNTs were determined by UV-Vis spectrometer as the same wavelength as mentioned in Chapter 3.3. Then, the concentrations of TX100 and SDBS were calculated as mentioned in Chapter 3.3.

Similar to the batch experiments, the effluent concentrations of ^{14}C -labeled MWCNTs/CLD/SDZ in all column experiments were measured by LSC to determine BTCs. At the end of the transport experiments, the sands or soil in the packed column were excavated in approximately $0.5\text{--}1\text{ cm}$ thick increments, dried and then homogenized using a mill. Then, the sands or soil were weighted three 0.5 g replicates in a container, combusted by using a biological oxidizer at $900\text{ }^{\circ}\text{C}$ as batch experiments, and measured by using LSC to determine the MWCNTs retained (retention profiles, RPs) in the column packing (Figure 3.3c). The total mass balance of MWCNT in the effluent and retained in the solid phase was determined from this information. All column experiments were replicated and exhibited good reproducibility.

3.8 Soil fractionation

Soil fractionation experiments were conducted to further elucidate the interactions between ^{14}C -labeled functionalized MWCNTs and the soil. The initial deposition phase was conducted similar to the MWCNT transport experiments discussed above (Chapter 3.7) at the same IS (1 mM KCl or CaCl_2). After recovery of

the MWCNT breakthrough curve, all the soil was excavated from the column, dried, and then the soil particle-size was fractionated following the method of Séquaris and Lewandowski (2003). In brief, 100 g of dried soil was added to a 1 L Duran bottle (Schott, Mainz, Germany) containing 200 mL the same electrolyte solution as the transport experiments (1 mM KCl or CaCl₂) and horizontally shaken at 150 rpm for 6 h. An additional 600 mL of the same electrolyte solution (1 mM KCl or CaCl₂) solution was then added to this bottle and mixed before sedimentation. The pipette method was then used to separate the soil into three size classes based on their sedimentation time according to Stoke's law (a particle density of 2.65 g cm⁻³ was assumed): (i) > 20 µm (sand size) after 6 min; (ii) 2- 20 µm (silt size) after 12 h; and (iii) < 2 µm (water-dispersible colloids, WDCs) after 12 h. Triplicate 50 ml samples of the WDC suspension were further fractionated by centrifuging at 2525 × g for 4 min. Stoke's Law calculations indicated that the resulting supernatant consisted of electrolyte solution and the WDC fraction that was < 0.45 µm, whereas the pellet was the WDC fraction that was 0.45–2 µm. Concentrations of MWCNTs that were associated with the sand, silt, 0.45–2 µm, and < 0.45 µm fractions were determined by LSC in a similar manner to the transport experiments. Concentrations of MWCNTs in the column effluent and residual soil samples from columns that were not used for soil fractionation were measured to ensure mass balance. All the experiments were replicated and exhibited similar results.

3.9 Numerical modeling

In order to describe all the transport and co-transport mechanisms that mentioned in Chapter 2, the HYDRUS-1D and C-Ride code (Šimůnek et al. 2016, Šimůnek et al. 2012) was used to simulate the one-dimensional transport of MWCNTs, CLD or SDZ. The saturated column was discretized into 101 nodes with an observation node at the outlet. The conservative tracer was simulated using an equilibrium model based on ADE to determine the hydrodynamic parameters of the column.

MWCNT transport in GQS (Chapter 4.1) was described using the ADE with two kinetic retention sites (Schijven and Šimůnek 2002, Wang et al. 2011b):

$$\theta \frac{\partial C}{\partial t} + \rho \frac{\partial S_1}{\partial t} + \rho \frac{\partial S_2}{\partial t} = \theta D \frac{\partial^2 C}{\partial x^2} - q \frac{\partial C}{\partial x} \quad (3.2)$$

where S_1 and S_2 [NM^{-1}] are the solid phase concentrations of MWCNTs on retention sites 1 and 2, respectively. The solid phase mass balance on sites 1 and 2 are given as:

$$\rho \frac{\partial S_1}{\partial t} = \theta \psi_1 k_{sw1} C - \rho k_{rs1} S_1 \quad (3.3)$$

$$\rho \frac{\partial S_2}{\partial t} = \theta \psi_2 k_{sw2} C - \rho k_{rs2} S_2 \quad (3.4)$$

where subscripts 1 and 2 on parameters denote the site, k_{sw1} and k_{sw2} [T^{-1}] are the first-order retention rate coefficients, k_{rs1} and k_{rs2} [T^{-1}] are the first-order release rate coefficients, and ψ_1 and ψ_2 [-] are dimensionless functions that account for time or depth-dependent retention. The total solid phase concentration (S ; NM^{-1}) is equal to the sum of S_1 and S_2 .

Three model formulations for MWCNT retention were considered in this work. The first model (M1) considers retention only on Site 1 ($k_{sw2} = 0$), and time-dependent Langmuirian blocking by setting ψ_1 equal to:

$$\psi_1 = 1 - \frac{S_1}{S_{max1}} \quad (3.5)$$

where S_{max1} [NM^{-1}] is the maximum solid phase concentration on Site 1. This model accounts for retention of MWCNTs on both QS and GQS using a single retention site. The percentage of the solid surface area that is favorable for MWCNT retention (S_f) can be determined from S_{max1} as (Jaisi and Elimelech 2009):

$$S_f = 100 * \frac{A_c \rho S_{max1}}{(1-\gamma)A_s} \quad (3.6)$$

where γ [-] is the porosity of a monolayer packing of MWCNTs on the solid surface, A_c [L^2N^{-1}] is the effective cross section area per MWCNT, and A_s [L^{-1}] is the solid surface area per unit volume. In this work, we assume a value of $\gamma = 0.5$ based on literature information (Johnson and Elimelech 1995). The value of A_c was taken to be equal to product of the width and length of a representative MWCNT that is equal to 15 and 1000 nm, respectively (Kasel et al. 2013a, Kasel et al. 2013b). Two values of

A_s were considered in this work: (i) geometric estimates determined as $6 * (1 - \theta)/d_{50}$ (where d_{50} [L] is the median grain size of the porous media); (ii) BET measurements (Chapter 3.4 and 4.1).

The M2 model separately accounts for retention and blocking of MWCNTs on QS (Site 1) and GQS (Site 2) sites using Equation (3.3) and (3.4), respectively, by defining ψ_2 in an analogous fashion to ψ_1 (e.g., S_1 and S_{max1} in Equation (3.5) are replaced with S_2 and S_{max2} , respectively). The M3 model considers retention and time-dependent blocking on Site 1 using Equation (3.3) and (3.5), and depth-dependent retention on Site 2 using Equation (2.6).

We set the value of $\beta = 0.765$ based on reported results for MWCNTs in all the column experiments (Kasel et al. 2013a, Kasel et al. 2013b).

MWCNT transport in soil (Chapter 4.2) was described using the ADE with one site kinetic retention based on Equation (2.1) and (2.4). The time- and depth-dependent blocking by setting ψ of Equation (2.4) is give as,

$$\psi = \left(1 - \frac{S}{S_{max}}\right) \left(\frac{d_{50} + x}{d_{50}}\right)^{-\beta} \quad (3.7)$$

Co-transport of MWCNTs and CLD or SDZ in soil (Chapter 4.3) was described using ADE with one site kinetic retention based on Equation (2.1) and (2.4) for the interaction between MWCNTs and soil, with two-site adsorption-desorption model based on Equation (2.7) through (2.10) for the interaction between the contaminant and soil, and with the C-Ride module of HYDRUS-1D based on Equation (2.11) through (2.13) for the interaction between the contaminant and MWCNTs. The diffusion coefficients of CLD and SDZ are from Pritchard et al. (1986) and Chen et al. (2013), respectively. Due to the short duration of the experiments, degradation and transformation of contaminants can be neglected.

4. Results and discussion⁴

4.1 Transport and retention of carbon nanotubes in goethite coated quartz sand

4.1.1 Characterization of goethite coated sand

The average zeta potential of MWCNTs, crushed quartz sand, and goethite particles in 1 mM KCl solution was measured to be -40.6, -63.6 and 10.2 mV, respectively. Consequently, the electrostatic interaction between the MWCNTs and quartz is unfavorable, whereas that between MWCNTs and goethite is favorable. The BET and iron concentration of QS and GQS are shown in Table 4.1, indicating an increasing trend after goethite coating for both BET and iron concentration.

Table 4.1 Characteristics of porous media

λ	d_{50}	BET	Geometric	BET	Fe
			A_s	A_s	Conc.
	[μm]	[$\text{cm}^2 \text{g}^{-1}$]	[cm^{-1}]	[cm^{-1}]	[$\mu\text{g g}^{-1}$]
0	240	880	NC	NC	22.8
0	350	380	101.14	642.20	6.4
0	607	50	NC	NC	1.8
1	240	1470	NC	NC	644.0
1	350	550	NC	NC	527.0
1	607	130	NC	NC	455.0
0.1	240	939 [†]	142.50	1530.57	84.9 [†]
0.1	350	397 [†]	102.86	674.90	58.5 [†]
0.1	607	58 [†]	52.39	74.82	47.1 [†]
0.3	350	431 [†]	97.71	737.01	162.6 [†]

⁴ Contains parts from “Resubmitted to Environmental Pollution, Miaoyue Zhang, Irina Engelhardt, Jirka Šimůnek, Scott A. Bradford, Daniela Kasel, Anne E. Berns, Harry Vereecken, Erwin Klumpp, Co-transport of chlordecone and sulfadiazine in the presence of functionalized multi-walled carbon nanotubes in soils, 2016”, “In press in Environmental Science & Technology, Miaoyue Zhang, Scott A. Bradford, Jirka Šimůnek, Harry Vereecken, and Erwin Klumpp, Do Goethite Surfaces Really Control the Transport and Retention of Multi-Walled Carbon Nanotubes in Chemically Heterogeneous Porous Media?, 2016”, and “Under revision in Water Research, Miaoyue Zhang, Scott A. Bradford, Jirka Šimůnek, Harry Vereecken and Erwin Klumpp, Roles of Cation Valance and Exchange on the Retention and Colloid-Facilitated Transport of Functionalized Multi-walled Carbon Nanotubes in a Natural Soil, 2016 ”.

λ [-] is the mass ratio of GQS in the mixing porous media; A_s [L^{-1}] is the solid surface area per unit volume; NC- not calculated; *Fe Conc.* - Fe concentration of the samples.

[†]- BET and Fe concentrations are determined in a similar way to effective values of K_D in the sand mixtures discussed in Chapter 4.1.3 by assuming a linear combination of individual components.

4.1.2 Batch results

Batch experiments were conducted to quantify the sorption behavior of MWCNTs onto two grain sizes (350 and 607 μm) of QS and GQS. Replicate batch experiments exhibited good reproducibility and mass balance. Figure 4.1 shows the sorption isotherms. The linear equilibrium sorption model ($S=K_D C$; where K_D [$L^3 M^{-1}$] is the equilibrium partition coefficient for MWCNT) provided an excellent description of all of isotherm datasets, with the coefficient of linear regression (R^2) always greater than 0.97. The sorption behavior over this concentration range was therefore completely characterized by values of K_D ; i.e., the slope of the linear isotherm. Values of K_D depended on both the surface chemistry and the size of the sand. In particular, values of K_D were much larger on GQS ($K_D=9.5$ and $3.6 \text{ cm}^3 \text{ g}^{-1}$ on 350 and 607 μm sand, respectively) than QS ($K_D=0.3$ and $0.6 \text{ cm}^3 \text{ g}^{-1}$ on 350 and 607 μm sand, respectively). This result is expected because the electrostatic interaction between the negatively charged MWCNTs (i.e., carboxylate groups, $-\text{COO}^-$) and the positively charged GQS (Fe-OH^{2+}) is attractive, whereas it is repulsive for the negatively charged QS (Hofmann and Liang 2007, Wang et al. 2013). The value of K_D also dramatically increased with a decrease in the grain size of the GQS because of a corresponding increase in the specific surface area. This grain size effect was not observed for QS because it had much lower K_D values.

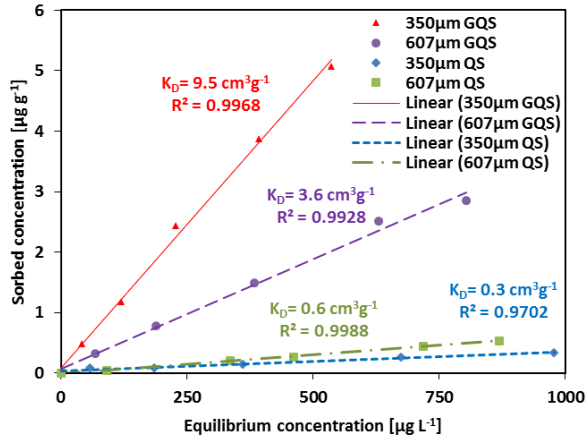


Figure 4.1 Linear sorption isotherms for MWCNTs on QS or GQS having grain sizes of 350 and 607 μm. The electrolyte solution was 1 mM KCl.

4.1.3 Effect of mass ratio of goethite in porous media

Figures 4.2a and 4.2b present BTCs and RPs, respectively, for MWCNTs in various mass ratios of uncoated and goethite-coated quartz sand ($\lambda = 0, 0.1$ and 0.3). The BTCs are plotted as the normalized effluent concentration (C/C_o ; where C_o is the influent suspension concentration of MWCNTs) of MWCNTs versus pore volumes. The RPs are given as normalized solid-phase concentration (S/C_o) against column depth. The experimental conditions and mass balance information are presented in Table 4.2. The total mass balance (M_{total}) for MWCNTs in these experiments was very good ($>90.7\%$). The MWCNT effluent mass balance (M_{eff}) strongly decreased from 79.6% to 9.7 % (Table 4.2) as λ increased from 0 to 0.3. Similarly, the MWCNT solid phase mass balance (M_{solid}) increased from 16.3% to 82.8% as λ increased from 0 to 0.3. As expected from batch experiments, these observations reflect the increasing amounts of favorable electrostatic interactions between negatively charged MWCNTs and positively charged goethite as λ increases.

Table 4.2 Experimental conditions, hydraulic parameters and mass balance information for all column experiments. IS was 1mM KCl. The input concentration of MWCNT was 1mg L⁻¹.

λ	d_{50} [μm]	ρ [g cm ⁻³]	q [cm min ⁻¹]	$Disp.$ [cm]	$Porosity$	M_{eff} [%]	M_{solid} [%]	M_{total} [%]
0	350	1.69	0.73	0.025	0.41	79.6	16.3	95.9
0.1	350	1.7	0.72	0.033	0.4	60.6	30.1	90.7
0.3	350	1.71	0.75	0.036	0.43	9.7	82.8	92.5
0.1	240	1.63	0.75	0.036	0.43	2.4	94.2	96.6
0.1	350	1.7	0.72	0.033	0.4	60.6	30.1	90.7
0.1	607	1.29	0.73	0.033	0.47	76.0	17.7	93.7

ρ is the bulk density; $Disp.$ is the estimated longitudinal dispersivity;

M_{eff} is the effluent percentage of MWCNTs recovered from the column experiment;

M_{solid} is the retained percentage of MWCNTs recovered from the column experiment;

M_{total} is the total percentage of MWCNTs recovered from the column experiment.

Mathematical model studies were conducted to investigate the relationship between column retention and batch sorption parameters for MWCNTs. The M1 model was initially employed to describe the BTCs shown in Figure 4.2a for the various sand mixtures. Table 4.3 provides a summary of fitted M1 model parameters (k_{sw1} , k_{rs1} , and S_{max1}) and separate R^2 values for BTCs and RPs. Simulations for the M1 model are shown in Figure 4.2, and R^2 values for BTCs were always very good ($R^2 > 0.96$). Fitted M1 model values of k_{sw1} and k_{rs1} were subsequently employed to determine column values of $K_D = \frac{\theta k_{sw1}}{\rho k_{rs1}}$ (Jaisi and Elimelech 2009, Schijven and Hassanizadeh 2000). Batch K_D values for these same sand mixtures were determined as a linear combination of components equal to $(1 - \lambda) K_{QS} + \lambda K_{GQS}$; where K_{QS} and K_{GQS} are batch K_D values for QS and GQS (cf. Figure 4.1), respectively. Column and batch values of K_D are given in Table 4.3. Note that column values of K_D were always much larger than batch values, and this difference increased with λ (nearly two orders of magnitude higher when $\lambda=0.3$). Clearly, the batch results had little relevance in predicting column scale retention despite the electrostatically favorable conditions. Others have observed a similar inconsistency between batch and column retention parameters (Jin et al. 1997, Praetorius et al. 2014, Torkzaban and Bradford 2016,

Treumann et al. 2014). Torkzaban and Bradford (2016) provided a detailed explanation for differences in colloid retention parameters in batch and column studies. In brief, the torque balance between applied hydrodynamic (T_H) and resisting adhesive (T_A) torques is not continuously satisfied in a well-mixed batch system because the lever arms are changing. Conversely, colloid immobilization by surface straining can occur in column systems because the torque balance is constantly satisfied ($T_H \leq T_A$) at microscopic roughness locations and grain-grain contacts that reduce the lever arm for T_H and increase the lever arm for T_A .

Fitted values of k_{swl} showed a nonlinear dependency on λ . In particular, k_{swl} slightly increased as λ increased from 0 to 0.1, but dramatically increased when λ increased from 0.1 to 0.3. This result is consistent with bacteria transport studies in various fractions of iron oxide coated sands (Foppen and Schijven 2005, Kim et al. 2008), but a linear increase in k_{swl} with λ has been reported for nanoparticles (Elimelech et al. 2000, Wang et al. 2012a). This discrepancy is likely related to differences in the size of the electrostatic zone of influence, which is proportional to the colloid size (Duffadar and Davis 2008). In particular, the influence of nanoscale chemical heterogeneity is less pronounced for larger colloids because these effects are averaged over a larger zone of influence (Bendersky and Davis 2011, Bradford and Torkzaban 2012).

MWCNT BTCs shown in Figure 4.2a exhibited time-dependent blocking behavior (increasing breakthrough concentrations with injection) as retention locations filled over time. Fitted values of S_{maxl} increased with λ (Table 4.3) because of the presence of more electrostatically favorable goethite coated retention locations. Time dependent blocking behavior therefore became less apparent as λ increased (Figure 4.2a), and the fitted value of S_{maxl} therefore exhibited a greater standard error when $\lambda=0.3$.

Table 4.3 shows the 95% confidence interval when using fitted values of S_{maxl} and its standard error, and geometric estimates and BET measurements for A_s to calculate S_f . Calculated values of S_f were very small. For example, when $\lambda=0.1$ the 95% confidence interval for S_f was always $<1.6\%$ even when goethite coated 10% of the sand surface. Furthermore, this calculated value of S_f was around one order of magnitude smaller when using BET measurement than geometric estimates of A_s . These low S_f values suggested that highly unfavorable attachment conditions occurred even on goethite coated surfaces that are electrostatically favorable for attachment. An

explanation for this observation is due to nanoscale roughness. The combined influence of nanoscale roughness and Born repulsion produces shallow primary minima (Bradford and Torkzaban 2013), and colloids that interact in these minima are susceptible to diffusive or hydrodynamic removal (Bradford and Torkzaban 2015, Torkzaban and Bradford 2016).

The M2 model may be used to separately quantify the transport and retention of MWCNTs on QS and GQS sites. In this case, fitted values of k_{swl} and S_{maxl} from the M1 model were used to predict QS and GQS parameters for the M2 model by assuming a linear dependence on λ (Table 4.3). A summary of these calculated M2 model parameters is given in Table 4.3, as well as the R^2 values between observed and predicted BTCs and RPs. Predicted BTCs and RPs for the M2 model provided a much poorer description of the data than the fitted M1 model. This occurs because fitted M1 model parameters exhibited a nonlinear dependence on λ (Table 4.3). Consequently, information on the transport and retention parameters for the individual components is not sufficient to predict behavior of the sand mixture. However, M2 model parameters may still be fitted to BTCs for MWCNTs to give an equal or superior description of this data than the M1 model.

Although the M1 model always described the BTCs very well, the RPs were poorly described when $\lambda=0$ or 0.1 (cf., Figure 4.2b and Table 4.3). In these cases, the RPs exhibited a hyper-exponential shape, with MWCNT mass removal under predicted near the column inlet and over estimated at the column outlet. Interestingly, the BTC and RP were both well described when $\lambda=0.3$. A number of potential explanations for hyper-exponential RPs have been provided in the literature, including: straining (Bradford et al. 2003); chemical and/or size heterogeneity of the colloid suspension (Tong and Johnson 2007, Tufenkji and Elimelech 2005b); and the pore-scale fluid distribution (Bradford et al. 2009, Wang et al. 2011b). The relative importance of all of these factors on MWCNT retention cannot be conclusively deduced from the collected information. However, dramatic differences in batch and column scale retention indicate that surface straining played an important role in retention. In addition, surface straining processes also have been demonstrated to be more important under highly unfavorable attachment conditions (Bradford and Torkzaban 2015), which is consistent with observed changes in the RP shape with λ .

Table 4.3 Fitted model parameters using different model formulations.

Model	λ	d_{50} [μm]	k_{sw1} [min^{-1}]	k_{rs1} [min^{-1}]	S_{max1}/C_o [$\text{cm}^3 \text{g}^{-1}$]	S.E. S_{max}/C_o	Column K_D [$\text{cm}^3 \text{g}^{-1}$]	Batch K_D [$\text{cm}^3 \text{g}^{-1}$]	Geometric S_f [%]	BET S_f [%]	R^2 R^2_{BTC}	R^2_{RP}
M1	0	350	0.053	3E-03	0.186	6.10E-02	4.29	0.3	0.32 \pm 0.21	0.05 \pm 0.03	0.968	0.621
M1	0.1	350	0.079	1E-03	0.634	0.13	18.59	1.22	1.08 \pm 0.46	0.17 \pm 0.07	0.991	0.732
M1	0.3	350	0.34	4E-04	12.17	1.93	213.74	3.06	22.03 \pm 7.07	2.92 \pm 0.94	0.993	0.985
M1	0.1	240	0.551	3E-04	4.342	0.46	NF	NF	5.14 \pm 1.09	0.48 \pm 0.10	0.976	0.994
M1	0.1	607	0.059	5E-03	0.289	4.20E-02	NF	NF	0.74 \pm 0.21	0.52 \pm 0.15	0.987	0.726
Model	λ	d_{50} [μm]	k_{sw1} [min^{-1}]	S_{max1}/C_o [$\text{cm}^3 \text{g}^{-1}$]	k_{QS} [min^{-1}]	S_{maxQS}/C_o [$\text{cm}^3 \text{g}^{-1}$]	k_{sw2} [min^{-1}]	S_{max2}/C_o [$\text{cm}^3 \text{g}^{-1}$]	k_{GQS} [min^{-1}]	S_{maxGQS}/C_o [$\text{cm}^3 \text{g}^{-1}$]	R^2_{BTC+RP}	
M2	0	350	0.053	0.186	0.053	0.186	0	0	0.32	4.67	0.917	
M2	0.1	350	0.047	0.167	0.053	0.186	0.032	0.47	0.32	4.67	0.867	
M2	0.3	350	0.037	0.13	0.053	0.186	0.096	1.40	0.32	4.67	0.466	
Model	λ	d_{50} [μm]	k_{sw1} [min^{-1}]	k_{rs1} [min^{-1}]	S_{max1}/C_o [$\text{cm}^3 \text{g}^{-1}$]	k_{sw2} [min^{-1}]	β		R^2_{BTC}		R^2_{RP}	
M3	0	350	0.059	NF	0.039	0.491	NF	0.765	0.971		0.986	
M3	0.1	350	0.061	NF	0.151	0.817	NF	0.765	0.99		0.906	
M3	0.3	350	0.309	NF	3.862	1.066	NF	0.765	0.991		0.958	
M3	0.1	240	0.513	NF	4.665	0.907	NF	0.765	0.974		0.999	
M3	0.1	607	0.032	NF	0.044	0.516	NF	0.765	0.987		0.995	

R^2_{BTC} , R^2_{RP} and R^2_{BTC+RP} reflect the correlation of observed and fitted data for BTC, RP and total (BTC+RP), respectively.

R^2_{BTC} , R^2_{RP} and R^2_{BTC+RP} reflect the correlation of observed and fitted data for BTC, RP and total (BTC+RP), respectively;

NF - denotes not fitted.

In M2 model, $k_{rs1} = k_{rs2} = 1\text{E}^{-5} \text{ min}^{-1}$; $k_{sw1} = (1-\lambda) k_{QS}$, $k_{sw2} = \lambda k_{GQS}$, $S_{max1} = (1-\lambda) S_{maxQS}$, $S_{max2} = \lambda S_{maxGQS}$, where k_{QS} and k_{GQS} are k_{sw} values for QS and GQS, respectively; S_{maxQS} and S_{maxGQS} are S_{max} values for QS and GQS, respectively;

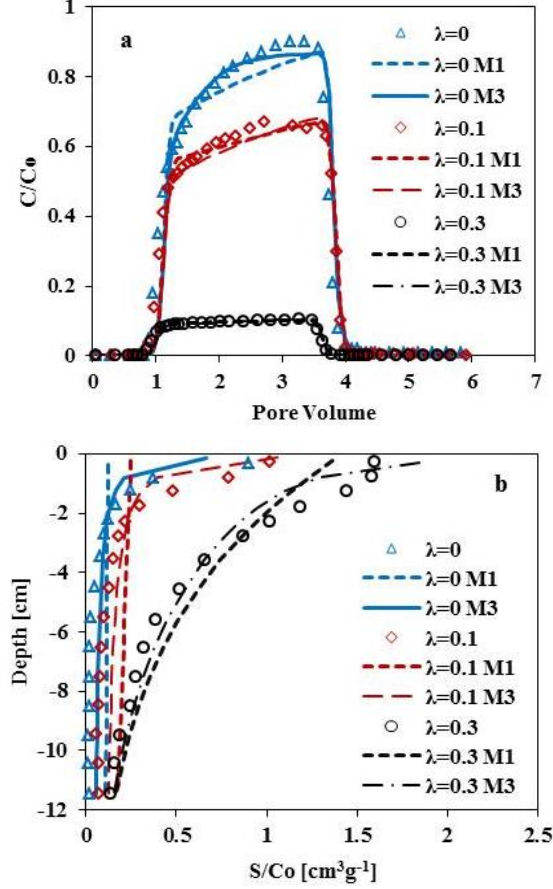


Figure 4.2 Experimental and estimated breakthrough curves (a) and retention profiles (b) for MWCNTs under different mixing mass ratios (λ). The Darcy velocity was $0.72\text{-}0.75 \text{ cm min}^{-1}$. The grain size of the sand was $350\mu\text{m}$.

Additional terms need to be considered in the model to account for the observed depth dependent retention shown in Figure 4.2b. In particular, we employed a two-site retention model with time-dependent blocking on Site 1 and depth-dependent retention on Site 2 (M3 model). Simulated BTCs and RPs for the M3 model are also shown in Figure 4.2, and provided an excellent description of BTCs and RPs. The fitted model parameters and R^2 values are given in Table 4.3. As expected, the values of k_{sw1} , k_{sw2} , and S_{max1} increased with increasing λ . It should be mentioned that the relative importance of Sites 1 and 2 cannot be determined by comparison of the values of k_{sw1} and k_{sw2} because of the depth-dependency on Site 2.

4.1.4 Effect of grain size

Additional column experiments were conducted to investigate the transport and retention behavior of MWCNTs in porous media having the same value of $\lambda=0.1$ but different grain sizes (240, 350 and 607 μm). Figures 4.3a and 4.3b show the observed and simulated BTCs and RPs, respectively. The experimental conditions and mass balance information are summarized in Table 4.2. Fitted M1 and M3 model parameters and R^2 values for BTCs and RPs are shown in Table 4.3. The M_{total} was always greater than 90.7%. Values of M_{eff} and M_{solid} increased (2.4 to 76.0 %) and decreased (94.2 to 17.7%), respectively, as the grain size increased from 240 to 607 μm . Similarly, fitted values of k_{sw1} when using the one site retention and blocking model (M1) increase in a nonlinear fashion with decreasing grain size. Colloid filtration theory predicts that this trend of increasing k_{sw1} and M_{solid} with decreasing grain size occurs because of an increasing rate of mass transfer to the solid surface (Jaisi and Elimelech 2009, Kasel et al. 2013a, Liang et al. 2013b). Direct comparison of fitted and filtration theory predictions for k_{sw1} are hampered by the needle like shape of the MWCNTs and the need to independently estimate the sticking efficiency.

Fitted values of S_{max1} from the M1 model also increased with decreasing grain size. This trend is expected because the surface area of the sand increases with decreasing grain size, and this produces more electrostatically favorable sites for retention on the goethite coated sand. The MWCNT BTCs exhibited some time dependent blocking behavior in Figure 4.3. These blocking effects were more pronounced for increasing collector grain size because of smaller values of S_{max1} . As explained previously, corresponding values of S_f values were very small; e.g., the 95% confidence interval on S_f was always less than 6.3% and 0.68% (Table 4.3) when using geometric estimates and BET measurement for A_s , respectively. This observation further supports the conclusion that only a small portion of the goethite coatings on the sand surface were favorable for retention.

The RPs shown in Figure 4.3b again exhibited a hyper-exponential distribution with depth that was not well described using the one-site retention and blocking model (M1). The two-site model with time- (Site 1) and depth- (Site 2) dependent retention (M3) was used to simulate this behavior. Simulation results are shown in Figure 4.3, and fitted model parameters are given in Table 4.3. Values of k_{sw1} , k_{sw2} , and S_{max1} increased with decreasing grain size. The value of k_{sw1} was more sensitive to grain size than k_{sw2} , especially when the grain size decreased from 350 to 240 μm . In

general, the value of k_{sw2} was relatively insensitive to λ , because this parameter was mainly controlled by system hydrodynamics such as flow velocity and grain size distribution (Wang et al. 2012c).

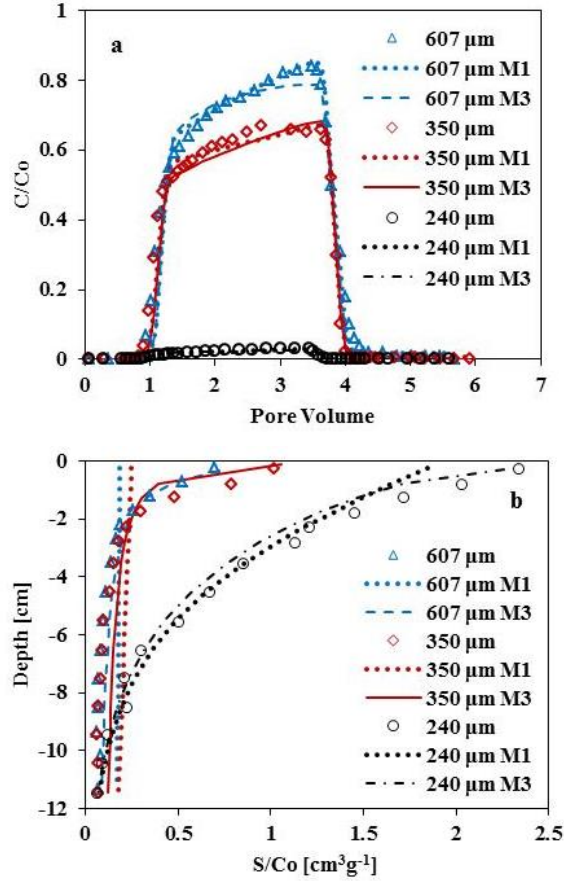


Figure 4.3 Observed and simulated breakthrough curves (a) and retention profiles (b) for MWCNTs in goethite-coated quartz sand with three different grain sizes (240, 350 and 607 μm) but the same λ (0.1). The Darcy velocity was 0.72- 0.75 cm min^{-1} .

4.2 Transport and retention of carbon nanotubes in soil

4.2.1 MWCNT suspension stability

The hydrodynamic radius of MWCNTs in KCl and CaCl₂ solutions at an IS=10 mM was measured 0, 1, and 4 h after suspension preparation by DLS. The hydrodynamic radius was always within the measurement error, and did not show a systematic trend with the cation type or time. The MWCNT suspensions were therefore considered to be stable during the injection phase (approximately 18 min) of all transport and release experiments discussed below.

4.2.2 Zeta potential

Figure 4.4 presents plots of measured zeta potential for MWCNTs and soil as a function of IS and cation valence (K⁺ and Ca²⁺). Both MWCNTs and soil exhibited a net negative charge for the considered solution chemistry conditions. This result indicates that net electrostatic interactions between the MWCNTs and soil were repulsive. The zeta potential was generally similar in magnitude for MWCNTs and soil under the same solution chemistry condition. Furthermore, increasing the solution IS and cation valence tended to decrease the magnitude of both zeta potentials. These trends are consistent with published literature (Elimelech et al. 2013, Israelachvili 2011, Khilar and Fogler 1998).

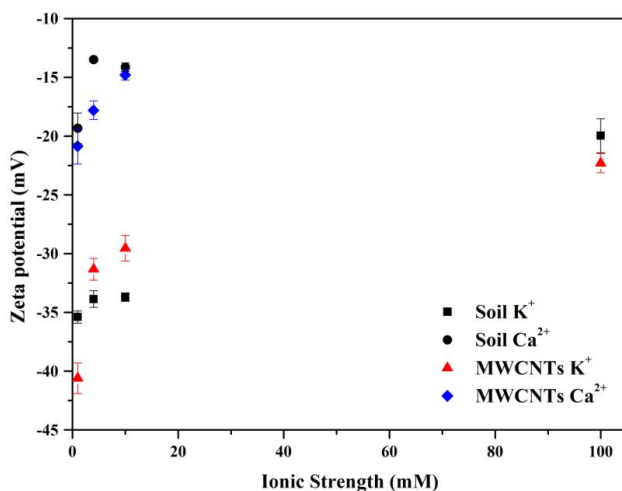


Figure 4.4 Zeta potentials of MWCNTs and soil as a function of the ionic strength in electrolyte solutions (KCl and CaCl₂).

4.2.3 Transport and Retention of MWCNTs

Figure 4.5 presents observed and simulated BTCs and RPs for functionalized MWCNTs when the IS=1, 4, and 10 mM KCl. The BTCs (Figure 4.5a) are plotted as the normalized effluent concentration (C/C_o ; where C_o is the influent suspension concentration of MWCNTs) versus pore volumes, whereas the RPs are plotted as normalized solid phase concentration (S/C_o) as a function of distance from the column inlet. The experimental conditions, hydraulic parameters, and mass balance information for these experiments are presented in Table 4.4. Simulations provided an excellent description of BTCs and RPs with a Pearson's correlation coefficient (R^2) > 0.95. Table 4.5 provides a summary of fitted retention model parameters.

The total mass balance (M_{total}) for data shown in Figure 4.5 was very good (> 91%, Table 4.4). The mass percentage recovered from the effluent (M_{eff}) strongly decreased from 45.8% to 4.0% as the IS increased from 1 to 10 mM (KCl), resulting in a corresponding increase in the solid phase mass percentage (M_{solid}) from 48.8% to 90.3%. Fitted values of k_{sw} and S_{max}/C_o also increased with IS, whereas k_{rs} decreased with IS. These trends are attributable to an increase in the adhesive force for MWCNTs on soil with IS due to compression of the double layer thickness and a decrease in the magnitude of the zeta potential (Figure 4.4), and is consistent with other studies (Jaisi et al. 2008, Tian et al. 2012c, Yang et al. 2013). It should also be mentioned that the influence of nanoscale heterogeneities on colloid retention increases with an increase in IS (Bradford and Torkzaban 2013).

BTCs for MWCNTs (Figure 4.5a) exhibited increasing breakthrough concentrations over time due to blocking; e.g., filling of a limited number of retention sites with continued MWCNT injection. The breakthrough time for MWCNTs was also delayed in comparison with the tracer (data not shown). This occurs because k_{sw} was sufficiently high to produce complete retention until available retention sites fill enough to induce breakthrough (e.g., Leij et al. 2015). This delay in breakthrough increases with IS because a larger value of S_{max}/C_o takes longer to fill. Other studies that have investigated the effect of IS on CNTs transport in clean sands or glass beads have not observed this result (Jaisi et al. 2008, Tian et al. 2012c, Yang et al. 2013), but it has been previously demonstrated for other nanoparticles (e.g., Sasidharan et al. 2014). This apparent discrepancy is due to the strong dependency of blocking on k_{sw} , S_{max} , C_o , and the input pulse duration (Leij et al. 2015). In particular, delay in the

breakthrough will not occur if k_{sw} , C_o , and the input pulse duration is too low, or if S_{max} is too high.

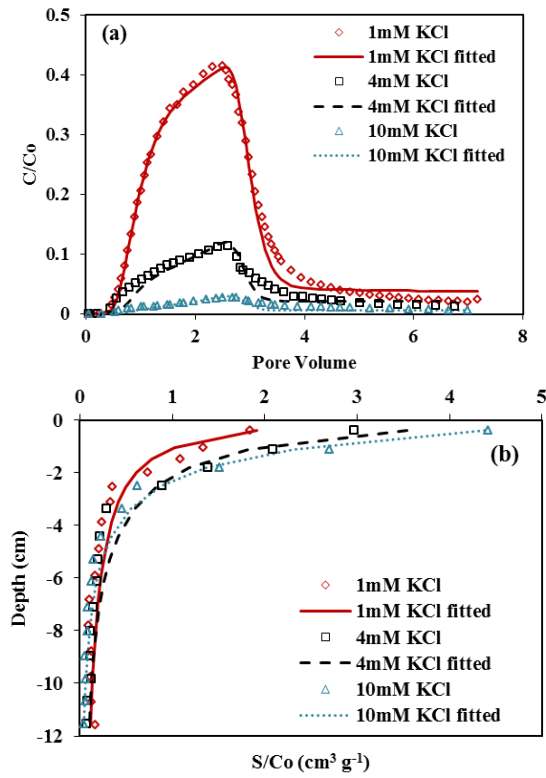


Figure 4.5 Effect of ionic strength on the transport and retention of MWCNTs in soil: observed and fitted breakthrough curves (a) and retention profiles (b) of MWCNTs under 1, 4, and 10 mM KCl, respectively.

Table 4.4 Experimental conditions, hydraulic parameters and mass balance information for all column experiments.

	IS [mM]	C_o [mg L ⁻¹]	q [cm min ⁻¹]	$Disp.$ [cm]	ϕ	M_{eff} [%]	M_{solid} [%]	M_{total} [%]
Figure 4.5	1, K ⁺	1	0.72	0.604	0.5	45.8	48.8	94.6
	4, K ⁺	1	0.72	0.364	0.51	13.8	77.2	91.0
	10, K ⁺	1	0.71	0.417	0.5	4	90.3	94.3
Figure 4.6	1, K ⁺	1	0.72	0.604	0.5	45.8	48.8	94.6
	1, Ca ²⁺	1	0.72	0.711	0.5	4	91.8	95.8

	q [cm min ⁻¹]	ϕ	IS_A [mM]	M_A [%]	M_B H ₂ O [%]	IS_C [mM]	M_C [%]	M_D H ₂ O [%]	IS_E [mM]	M_E [%]	M_F H ₂ O [%]	M_{solid} [%]	M_{total} [%]
Figure 4.7	I, 0.71	0.47	10, K ⁺	4.6	42.2							45.1	91.9
	II, 0.72	0.49	1, Ca ²⁺	4.2	7.7	1, K ⁺	0.6	5.3	100, K ⁺	0.4	21.7	50.6	90.5
	III, 0.73	0.48	10, Ca ²⁺	0.03	0.3	10, K ⁺	0.02	11	100, K ⁺	0.6	11.6	64.8	88.4

Figure 4.5: ionic strength effect; Figure 4.6: cation type effect; Figure 4.7: release of MWCNT by ionic strength reduction and cation exchange; C_o , MWCNT input concentration; q , Darcy velocity; IS , ionic strength; ϕ , porosity; $Disp.$ is the estimated longitudinal dispersivity;

M_{eff} , M_{solid} , and M_{total} are mass percentages recovered from effluent, solid phase (soil), and total, respectively; M_A – M_F are the mass percentages recovered from effluent (Steps A–F) in release experiments.

Table 4.5 Fitted model parameters.

	IS	β	S_{max}/C_o	S.E.	k_{sw}	S.E.	k_{rs}	S.E.	R^2
	[mM]		[cm ³ g ⁻¹]	S_{max}/C_o	[min ⁻¹]	k_{sw}	[min ⁻¹]	k_{rs}	
Figure 4.5	1, K ⁺	0.765	5.45	1.51	10.30	5.89E-01	6.80E-03	5.00E-04	0.975
	4, K ⁺	0.765	5.98	NF	28.22	6.88E-01	5.70E-03	4.59E-04	0.958
	10, K ⁺	0.765	6.10	4.65E-01	49.69	1.17E+00	4.56E-03	1.30E-03	0.991
Figure 4.6	1, K ⁺	0.765	5.45	1.51	10.30	5.89E-01	6.80E-03	5.00E-04	0.975
	1, Ca ²⁺	0.765	9.33	NF	44.54	1.39E+00	3.31E-03	1.34E-03	0.971

Figure 4.5 ionic strength effect; Figure 4.6: cation type effect; R^2 reflects the correlation of observed and fitted data; NF - denotes not fitted. k_{sw} , the first-order retention rate coefficient; k_{rs} , the first-order release rate coefficient; S_{max}/C_o , normalized maximum solid phase concentration of deposited MWCNTs; S.E. – standard error.

The RPs for MWCNTs (Figure 4.5b) exhibited a hyper-exponential shape that was well described using the model with a depth-dependent retention function (Equation 3.7). This indicates that a greater retention rate occurred near the column inlet than the outlet. Hyper-exponential RPs have previously been observed for MWCNTs (Bradford and Bettahar 2006, Kasel et al. 2013a, Kasel et al. 2013b). A variety of potential explanations for hyper-exponential RPs have been identified in the literature, including: straining (Bradford et al. 2003, Bradford et al. 2002), colloid aggregation (Chen and Elimelech 2006, 2007), chemical heterogeneity on the soil and colloid (Tong and Johnson 2007, Tufenkji and Elimelech 2005b), and system hydrodynamic factors (Bradford et al. 2009, Li et al. 2005). It is difficult to ascertain the potential contribution of each factor to the observed RP. However, MWCNTs retention still resulted in a hyper-exponential shape even under low IS conditions (1 mM KCl) that should minimize the contribution of colloid aggregation and chemical heterogeneity. Results for theoretical calculations that consider forces and torques that act on colloids near heterogeneous surfaces, and comparison of retention in batch and column studies indicate that retention of MWCNTs is controlled by surface straining locations near macroscopic roughness locations and grain-grain contacts under low IS conditions (Bradford and Torkzaban 2015). Similarly, other studies have concluded that straining played a dominant role in the retention of MWCNTs (Jaisi et al. 2008, Kasel et al. 2013a, Kasel et al. 2013b, Wang et al. 2012d).

The effect of cation type on the transport and retention of MWCNTs in soil is presented in Figure 4.6. In this case, MWCNTs were deposited and eluted at the same IS=1 mM in the presence of monovalent K^+ or divalent Ca^{2+} cations. Figure 4.6 presents observed and simulated BTCs and RPs. Table 4.5 summarizes the fitted retention model parameters that provided an excellent description of this data ($R^2 > 0.97$). Retention of MWCNTs (Table 4.4) and fitted values of k_{sw} and S_{max}/C_o (Table 4.5) were much higher in the presence of Ca^{2+} than K^+ at the same IS. In comparison to K^+ , Ca^{2+} produces a stronger adhesive force due to the smaller magnitude of the zeta potential (Figure 4.4), localized neutralization and/or reversal of surface charge (Grosberg et al. 2002), and cation bridging (Torkzaban et al. 2012) that all enhances retention of MWCNTs. Fitted values of S_{max}/C_o clearly indicate that many more retention sites were available in the presence of Ca^{2+} than K^+ (an increase of 171%). This larger increase in the value of S_{max}/C_o in the presence Ca^{2+} also

influenced the blocking behavior in the MWCNT BTC. In particular, a greater delay in the breakthrough time and a slower rate of increase in the BTC with time was observed (Figure 4.5b). Similar to RPs in the presence of K^+ (Figure 4.6b), the RP in the presence of Ca^{2+} also exhibited a hyper-exponential shape. This observation suggests that similar retention mechanisms were operative in the presence of both monovalent and divalent cations.

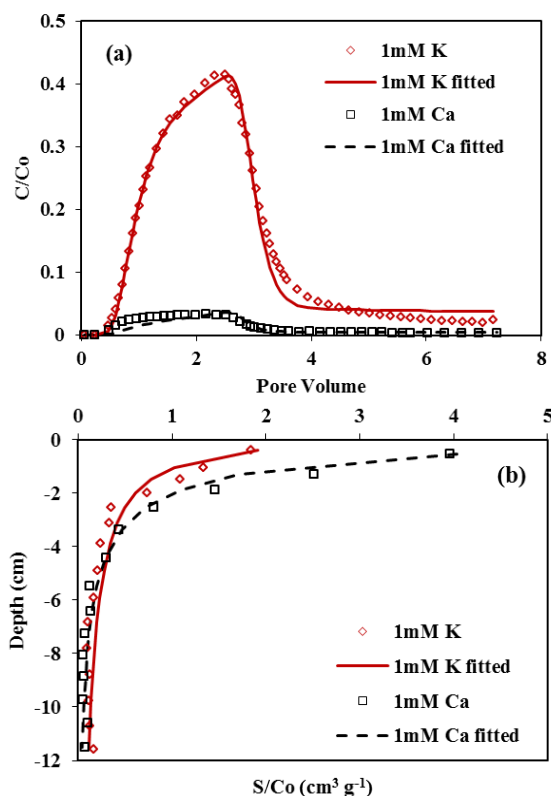


Figure 4.6 Effect of cation type on the transport and retention of MWCNTs in soil: observed and fitted breakthrough curves (a) and retention profiles (b) of MWCNTs under 1 mM KCl and $CaCl_2$, respectively.

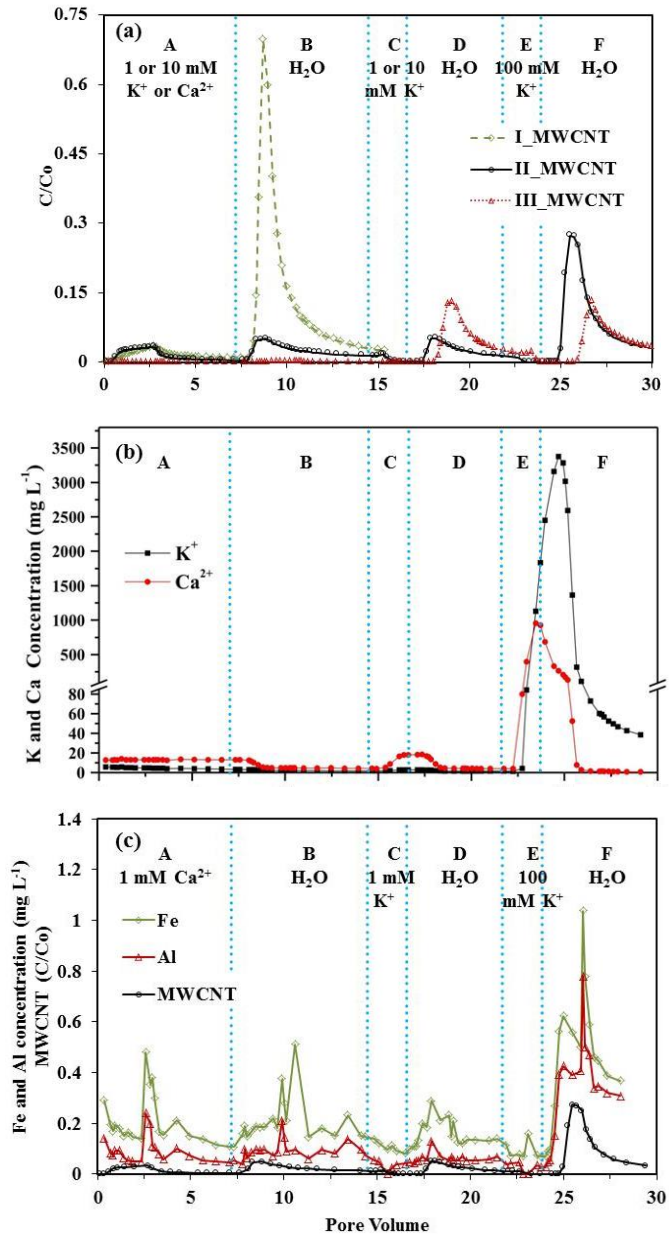
4.2.4 Release of MWCNTs

Very little release of MWCNTs was observed under steady-state solution chemistry conditions (Figure 4.5 and 4.6, and Table 4.4). Conversely, significant amounts of colloid and nanoparticle release have been reported when transient

solution chemistry conditions reduce the adhesive force (e.g., Liang et al. 2013a). Additional experiments were therefore conducted to better understand the effect of IS reduction and cation exchange on the release of MWCNTs in soil. Step A of Figure 4.7 presents BTCs when MWCNTs were retained and eluted in the presence of IS=10 mM KCl (experiment I), and CaCl₂ solution at IS=1 mM (experiment III) and IS=10 mM (experiment III). Transport of MWCNTs was limited in Step A for all of these conditions. Indeed, effluent mass balance during step A (M_A) only equaled 4.6, 4.2, and 0.03% for experiments I, II, and III, respectively.

Step B in Figure 4.7a presents the subsequent release curves when retained MWCNTs were eluted by Milli-Q water. Release was much more pronounced when the MWCNTs were retained (step A) in the presence of monovalent K⁺ (42.2%) than divalent Ca²⁺ (<7.7%) cation. This result indicates that the adhesive interaction was stronger and less reversible in the presence of Ca²⁺ than K⁺. Furthermore, release of MWCNTs was less pronounced when they were retained in IS=10 mM CaCl₂ (0.3%) than IS=1 mM CaCl₂ (7.7%) solution, respectively. This implies that a stronger adhesive force continued to act on the MWCNTs when they were initially retained in the presence of a higher concentration of Ca²⁺. A potential explanation for these observations is due to localized charge neutralization/reversal or cation bridging by Ca²⁺ which creates strong interactions with MWCNTs (Jaisi et al. 2008, Liang et al. 2013a).

Experiments II and III were continued to further study the release of MWCNTs that were retained in the presence of Ca²⁺ using the following elution sequence: KCl at the same IS as in step A (step C); Milli-Q water (step D); 100 mM KCl (step E); and Milli-Q water (step F). The effluent concentrations of MWCNTs during each of these steps are shown in Figure 4.7a, with corresponding mass balance information given in Table 4.4 (denoted as M_C-M_F). Effluent concentrations of K⁺ and Ca²⁺, and Al and Fe in a replicate release experiment for MWCNT in IS=1 mM CaCl₂ solution during step A are shown in Figure 4.7b and 4.7c, respectively. The RPs for MWCNTs following completion of transient release experiments I, II, and III are shown in Figure 4.7d.



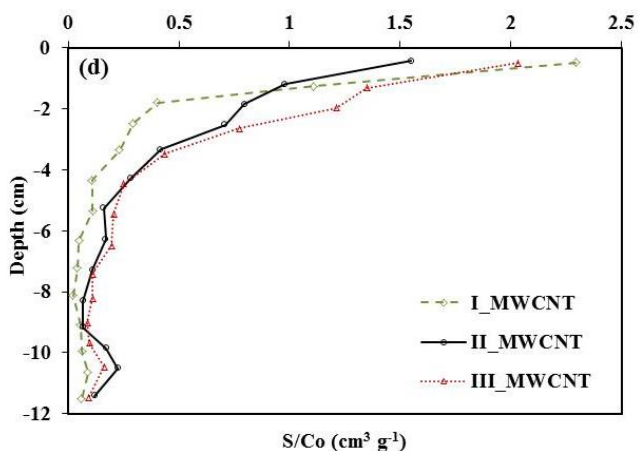


Figure 4.7 (a) Breakthrough and release behavior, and retention profiles (d) of MWCNTs in soil. Deposition (step A) occurred at an IS = 10 mM using KCl for experiment I, and an IS = 1 and 10 mM using CaCl_2 for experiment II and III, respectively, whereas release was initiated by ionic strength reduction (steps B, D, and F, Milli-Q water) and cation exchange (steps C and E) as summarized in Table 4.4. (b) Effluent concentrations of K and Ca during steps A–F in experiment II. (c) Release of MWCNTs and naturally occurring minerals due to ionic strength reduction (steps B, D, and F, Milli-Q water) and cation exchange (steps C and E) in soil in experiment II. For experiment III, the range of step A–F is not shown as the blue dotted line due to the different experimental conditions compared with experiment II. The injection procedure in experiment II is step A (0–7.61 pore volumes (PVs)), step B (7.61–15.23 PVs), step C (15.23–17.51 PVs), step D (17.51–22.85 PVs), step E (22.85–25.13 PVs), and step F (25.13–30.47 PVs).

MWCNT release always occurred when Milli-Q water was injected into the column during steps B, D, and F, but gradually ceased when KCl was injected during steps C and E (Figure 4.7a). The amount of MWCNTs that was released with Milli-Q water strongly depended on the concentrations of injected Ca^{2+} during step A and K^+ during steps C and E. Release of MWCNTs that occurred with IS reduction during steps D and F were also influenced by the amount of cation exchange that occurred during steps C and E. Specifically, greater amounts of Ca^{2+} ions were exchanged back into the aqueous phase when a higher concentration of K^+ was injected (Figure 4.7b). This exchange process reduced the strength of the adhesive interaction, such that

greater amounts of MWCNTs were released with a subsequent reduction in solution IS. Consequently, M_D was less when the IS equaled 1 mM ($M_D=5.3\%$) than 10 mM ($M_D=11\%$) KCl during step C. The value of M_F was influenced by: (i) the initial concentration of Ca^{2+} during deposition (step A); (ii) the amount of cation exchange (steps C and E); and (iii) the previous amounts of MWCNT that were released (steps B and D). In this case, the value of M_F equaled 21.1 and 11.6% when the IS equaled 1 and 10 mM CaCl_2 , respectively, during step A. A similar trend was observed for the total recovered mass of MWCNTs during steps A-F, and this indicates that increased strength of the adhesive force at a higher Ca^{2+} concentration (step A) was the dominant consideration.

Figure 4.7d presents the RPs for MWCNTs following completion of the release experiments. Similar to Figure 4.5 and 4.6, RPs were still hyper-exponential in shape. However, close inspection of Figure 4.5b, 4.6b, and 4.7b reveals that retained MWCNTs in release experiments were shifted from the top into deeper layers. This observation supports the potential for continued slow remobilization of MWCNTs in the subsurface due to the effects of IS reduction and cation exchange.

Bradford and Kim (2010) examined the release behavior of in situ kaolinite clay from sand due to cation exchange and IS reduction, and observed similar trends as seen for the MWCNTs in Figure 4.7. This observation suggests the potential for colloid-facilitated transport of MWCNTs in this study. Indeed, effluent samples exhibited differences in sample turbidity due to release of soil colloids. To better understand the potential association of released MWCNTs and soil colloids, Figure 4.7c presents plots of effluent concentrations of Al, Fe, and MWCNTs during the release experiment. Note that release behavior of Fe, Al, and MWCNTs closely follow each other with IS reduction and cation exchange. Liang et al. (2013a) also observed this same phenomenon for silver nanoparticles with Al and Fe. All of these observations strongly support the potential for colloid-facilitated transport of MWCNTs during the release experiments.

4.2.5 Soil size fractionation

Soil fractionation was conducted following completion of MWCNT transport experiments at IS=1 mM in KCl and CaCl_2 solutions to further investigate the association between MWCNTs and soil colloids in the presence of different cation types. Figure 4.8a shows a plot of the soil mass percentage of the different size

fractions. Results indicate that the soil was composed of 2.38% WDCs (1.51% in the range of 0.45-2 μm and 0.87% less than 0.45 μm), 11.5% silt (2-20 μm), and 86.2% sand (20-2000 μm). This size fractionation is comparable to that obtained by (Kasel et al. 2013b), with small variations likely due to the use of different soil fractionation methods.

Figure 4.8b presents a plot of the recovered mass percentages of MWCNTs in the various soil size fractions when the IS=1 mM KCl and CaCl₂. The total mass recovery was calculated to be more than 85%. Mass percentages of MWCNTs in the sand and silt fractions were only 9.5 and 17.2%, respectively, even though they accounted for 97.7% of the soil mass. Mass percentage of MWCNTs in the 0.45-2 μm WDC fraction that accounted for 1.51% of the soil mass was 23.6%. The mass percentage of MWCNTs in the <0.45 μm WDC fraction and the so-called electrolyte phase (Jiang et al. 2014) was 49.7%. This fraction included MWCNTs associated with very fine soil colloids and those released during the fractionation procedure.

Figure 4.8c presents the retained concentration (S/C_o) of MWCNTs in different soil fractions in the presence of KCl or CaCl₂ when the IS=1 mM. The retained concentration of MWCNTs in each soil fraction was more pronounced in the presence of Ca²⁺ than K⁺, especially in the WDC fraction. This observation can be explained by charge reversal/neutralization (Grosberg et al., 2002) and/or bridging complexation between soil grains and functionalized MWCNTs in the presence of Ca²⁺ (Torkzaban et al., 2012). Similar to experimental observations, bridging complexation is expected to be more pronounced with the WDC fraction (Torkzaban et al., 2012).

The above information indicates that the WDC fractions were enriched in MWCNTs in comparison with the sand and silt fractions, and that the association between WDCs and MWCNTs was related to the cation valance. This strong association between WDCs and MWCNTs provides further evidence for colloid-facilitated transport of MWCNTs during the release experiments.

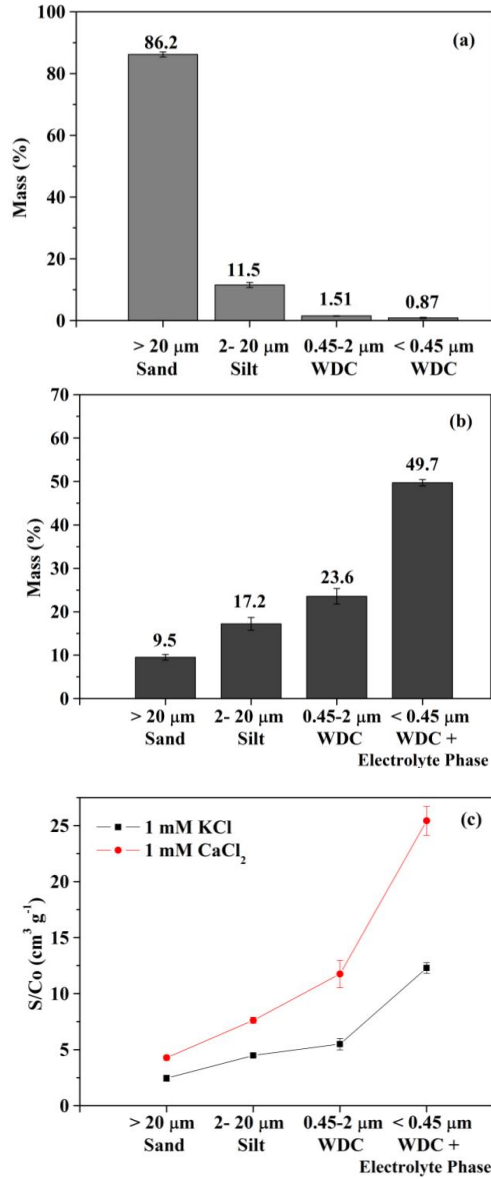


Figure 4.8 (a) Mass percentage of each soil sized fraction: sand, silt, 0.45-2 μm WDCs and < 0.45 μm WDCs; (b) Mass percentage of MWCNTs in sand, silt and 0.45-2 μm WDCs of soil. The < 0.45 μm WDCs also contained the MWCNTs in the so-called electrolyte phase (1 mM KCl and CaCl_2); (c) Retention amount of MWCNTs in sand, silt, 0.45-2 μm WDCs and < 0.45 μm WDCs including electrolyte phase under different cation type.

4.3 Co-transport of chlordecone and sulfadiazine in the presence of carbon nanotubes in soils

4.3.1 Sorption results

All the optimized results from batch experiments are summarized in Table 4.6. A linear adsorption isotherm provided a good description of CLD adsorption on the soil ($R^2 = 0.99$, Table 4.6, Figure 4.9a). The sorption coefficient (K_d) equaled $56 \text{ cm}^3 \text{ g}^{-1}$. This value of K_d can be used in conjunction with the soil organic carbon fraction ($f_{oc}=0.011 \text{ g g}^{-1}$) (Kasel et al. 2013b) to calculate the octanol-water partition coefficient ($K_{oc}=K_d/f_{oc}$) (OECD. 2000) that is equal to $5090 \text{ cm}^3 \text{ g}^{-1}$. This K_{oc} value is consistent with the reported range in the literature of 2500 to 20,000 $\text{cm}^3 \text{ g}^{-1}$ (Woignier et al. 2012) and indicates that the hydrophobic adsorption is controlled by the interaction between CLD and the soil organic carbon (Cabidoche et al. 2009, Levillain et al. 2012, Li et al. 2012), which produces a limited mobility of CLD in soils (Fernandez-Bayo et al. 2013a, Fernandez-Bayo et al. 2013b). The adsorption of SDZ in the same (Kaldenkirchen-Hülst) soil was described in an earlier study (Zarfl 2008). Reported values of $K_d=0.56 \text{ cm}^3 \text{ g}^{-1}$ and $K_{oc}=5.09 \text{ cm}^3 \text{ g}^{-1}$ indicate that organic carbon was also the main factor affecting the fate of SDZ in soils (Kasteel et al. 2010). However, SDZ has a much lower K_{oc} value than CLD; its mobility in soils is therefore expected to be much higher than that of CLD.

Table 4.6 Optimized results from batch experiments.

Chemicals	Absorbents	k_{amM}	k_{dmM}	K_d	K_{oc}
		$[\text{min}^{-1}]$	$[\text{min}^{-1}]$	$[\text{cm}^3 \text{ g}^{-1}]$	$[\text{cm}^3 \text{ g}^{-1}]$
CLD	MWCNT	0.10	5.32E-03	60,000	NF
CLD	soil			56	5,090
SDZ	MWCNT			6,000	NF
SDZ*	soil			0.56	5.09

* The adsorption of SDZ in the soil was described by Zarfl (2008).

NF - not fitted.

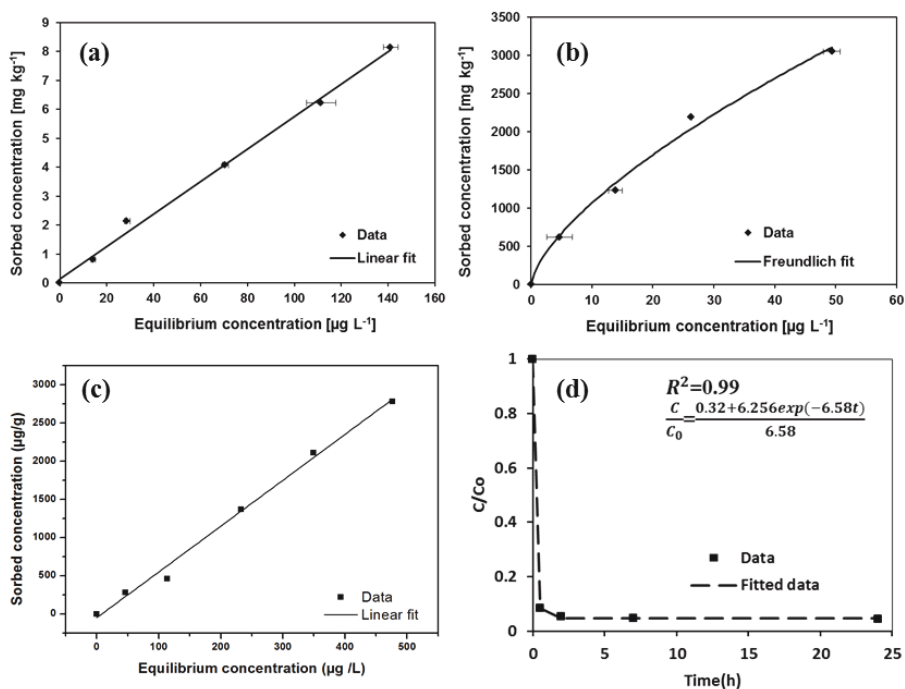


Figure 4.9 (a) Adsorption isotherm of CLD on soil. (b) Adsorption isotherm of CLD on MWCNTs. (c) Adsorption isotherm of SDZ on MWCNTs. (d) Kinetic sorption data for CLD on MWCNTs.

The Freundlich equation provided a good description of adsorption isotherms of CLD on MWCNTs ($R^2 = 0.95$), with the Freundlich coefficient (K_F) and exponent (n) equal to $229 \mu\text{g}^{(1-1/n)} \text{L}^{1/n} \text{g}^{-1}$ and 1.49, respectively (Figure 4.9b). The sorption coefficient K_d was calculated from a linear fit of the first part of the isotherm to be $60,000 \text{ cm}^3 \text{g}^{-1}$, which demonstrates strong adsorption. A linear adsorption isotherm provided a good description of SDZ adsorption on the MWCNTs ($R^2 = 0.99$, Figure 4.9c), with a sorption coefficient K_d of $6,000 \text{ cm}^3 \text{g}^{-1}$, which is in agreement with reported K_d values (10^3 - $10^4 \text{ cm}^3 \text{g}^{-1}$) (Ji et al. 2009). The K_d values of CLD and SDZ on MWCNTs were three and five orders of magnitude higher than on the loamy sand soil, respectively. This strong adsorption capacity of MWCNTs for CLD and SDZ is mainly attributed to their large specific surface area and surface heterogeneities (Liao et al. 2008, Upadhyayula et al. 2009). The presence of MWCNTs in soils is therefore expected to strongly influence the mobility of CLD and SDZ.

Equation (3.1) provided a good description for the adsorption kinetics of CLD on MWCNTs ($R^2 = 0.99$, Figure 4.9d). The adsorption (k_{amM}) and desorption (k_{dmM}) rates of CLD to/from the MWCNTs were determined to be 6.26 h^{-1} and 0.32 h^{-1} , respectively. The adsorption rate was much faster than the desorption rate.

4.3.2 Single-species transport in soil

The first three column experiments (I, II, and IV) were performed to improve our understanding of the single-species transport behavior of CLD, SDZ, and MWCNTs in soils. The experimental conditions are presented in Table 4.7 and optimized model parameters in Table 4.8. The BTCs (Figure 4.10a) are plotted as normalized effluent concentrations (C/C_o) versus pore volumes, where C_o is the influent concentration of MWCNT, CLD or SDZ. The RPs (Figure 4.10b) are plotted as normalized solid phase concentrations (S/C_o) versus column depth. The total mass percentage recovered from the effluent and retained in the column ranged from 95% to 105% (Table 4.7) for the three compounds. The retardation factors for CLD, SDZ, and MWCNTs that were calculated from respective BTCs relative to the conservative tracer transport (data not shown) (Ptak et al. 2004) indicated that CLD, SDZ, and MWCNTs reached the column outlet with only a slight retardation compared to the conservative tracer. Thus, pore size exclusion was not observed (Bradford et al. 2003).

About half of the injected mass of MWCNTs was retained in the soil column (Figure 4.10). Equations (2.1), (2.4), and (3.7) provided a good description of the BTC and RP ($R^2=0.975$). The fitted value of k_{sw} was considerably (several orders of magnitude) higher than the k_{rs} (Table 4.8), indicating only a slow rate of release. The BTC exhibited blocking behavior (a decreasing rate of retention with continued MWCNT injection). The fitted value of $S_{max}/C_o = 5.45 \text{ cm}^3 \text{ g}^{-1}$ was used to account for this blocking process, and its low value indicates that only a small fraction of the solid surface area contributed to MWCNT retention (Bradford et al. 2009, Kasel et al. 2013a). This result is expected because the soil and functionalized MWCNTs exhibit a net negative charge under low ionic strength conditions that produces an energy barrier to attachment (Bradford et al. 2009, Bradford et al. 2006a). The RP shape was hyper-exponential (e.g., a greater rate of retention near the column inlet than the outlet). A number of potential explanations for hyper-exponential RPs have appeared in the literature, including: straining (Bradford et al. 2003, Bradford et al. 2002), heterogeneity in colloid size and charge (Bolster et al. 1999, Tong and Johnson 2007,

Tufenkji and Elimelech 2005b), and system hydrodynamics (Bradford et al. 2009, Wang et al. 2011a). The exact reason of the hyper-exponential RP cannot be deduced from the experimental data, but other literature information for the retention of MWCNTs suggests that straining was the domain process under our experimental conditions (Jaisi et al. 2008, Kasel et al. 2013a, Wang et al. 2012d).

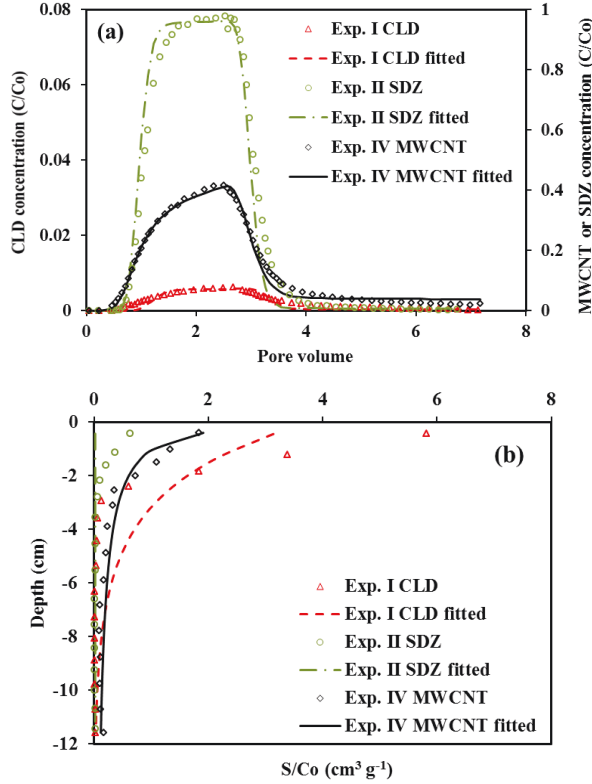


Figure 4.10 Observed and estimated BTCs (a) and RPs (b) for a single-species transport of CLD (experiment I), SDZ (experiment II), and MWCNTs (experiment IV) in saturated soil columns. The left figure (a) has two vertical axes. The left axis shows the relative CLD concentrations (C/C_0), while the right axis shows the relative SDZ and MWCNTs concentrations.

Table 4.7 Experimental conditions, hydraulic parameters and mass balance information for all column experiments. IS for all column experiments was 1 mM KCl and d_{50} of soil was 120 μm .

Single-species transport experiments							
Chemical	No.	C_o [mg L ⁻¹]	q [cm min ⁻¹]	Porosity	D/D_c [cm]	M_{eff} [%]	M_{total} [%]
CLD	I	1	0.71	0.5	0.16	0.7	100.2
SDZ	II	0.1	0.70	0.52	0.18	93.7	11.8
SDZ	III	1	0.72	0.49	0.31	98.1	3.0
MWCNTs	IV	1	0.72	0.50	0.60	45.8	48.8
Co-transport experiments							
Chemical	No.	C_o [mg L ⁻¹]	q [cm min ⁻¹]	Porosity	D/D_c [cm]	M_{eff} [%]	M_{total} [%]
		MWCNTs	CLD/SDZ				
CLD/MWCNTs	V	1	1	0.71	0.16	1.0	100.7
CLD/MWCNTs	VI	10	1	0.71	NF	1.0	99.7
MWCNTs/SDZ	VII	1	1	0.70	0.09	97.6	7.3
MWCNTs/SDZ	VIII	1	0.1	0.69	0.21	88.4	28.0

C_o is the input concentration; D/D_c is the hydrodynamic longitudinal dispersivity estimated from Br; M_{eff} is the mass percentages recovered from effluent of MWCNT, CLD, or SDZ; M_{solid} is mass percentages recovered from solid phase of MWCNT, CLD, or SDZ; M_{total} is total mass percentages recovered from the column experiment; NF - not fitted.

CLD and SDZ exhibited very different mobilities in the soil. Almost 100% of the CLD was retained in the soil, mostly in the shallow layers (0-2 cm). On the other hand, SDZ easily passed through the column and, only 12% was retained in the soil (Table 4.7). These results are consistent with the batch experiments, which found that the K_d value was much larger for CLD ($56 \text{ cm}^3\text{g}^{-1}$) than for SDZ ($0.56 \text{ cm}^3\text{g}^{-1}$). The two-site sorption model fitted well the observed BTCs for both CLD and SDZ (Table 4.8). Values of K_d that were fitted to the column experiments were not the same as those obtained in the batch experiments, especially for CLD, likely due to the differences in the hydrodynamic conditions (Torkzaban and Bradford 2016, Treumann et al. 2014). The fitted fraction of equilibrium exchange sites (f) was always very small (Table 4.8), indicating that sorption of both CLD and SDZ was mainly a kinetic process. Equilibrium sorption can be neglected for SDZ due to the small value of K_d ($0.17 \text{ cm}^3\text{g}^{-1}$). Therefore, only a one-site kinetic sorption process was considered in the model by setting $f = 0$. In contrast, equilibrium sorption cannot be neglected for CLD because of the large value of K_d ($282.6 \text{ cm}^3\text{g}^{-1}$) that provides retardation of about 1.5. Unold et al. (2009) and Wehrhan et al. (2007) came to a similar conclusion for CLD and SDZ, even though they employed different sorption models. Although the sorption model described experimental BTCs well, it was not able to correctly fit RPs with their hyper-exponential shapes (Figure 4.10b). The same problem was also encountered by Unold et al. (2009) and Wehrhan et al. (2007). The most plausible reason for the hyper-exponential RPs for CLD and SDZ is due to system hydrodynamics (Li et al. 2005) since straining (Bradford et al. 2004, Bradford et al. 2005, Bradford et al. 2003) and heterogeneity in colloid size and charge (Bolster et al. 1999, Tufenkji and Elimelech 2005b) are unlikely.

4.3.3 Co-transport

Different injection sequences were employed in the co-transport experiments for CLD and SDZ in the presence of MWCNTs. Since CLD has a limited mobility in soil (Figure 4.10), the CLD co-transport experiment was conducted by first injecting CLD into the soil column followed by a MWCNT suspension. This sequence was meant to simulate the process of using MWCNTs to remediate soil contaminated with CLD. On the other hand, MWCNTs retained in the soil influence the soil adsorption capacity and may thus affect the transport and sorption of highly mobile contaminants such as SDZ. The SDZ co-transport experiment was thus performed by injecting the

Results and discussion

MWCNT suspension first, followed by a SDZ pulse. This sequence was meant to simulate the process of using retained MWCNTs in the soil to slow down the spread of a contaminant, as is commonly done using reactive barriers.

Table 4.8 Parameters optimized by using different models for the CLD, SDZ, and MWCNT transport, co-transport and retention in soil.

Single-species transport experiments							
Experiment		MWCNT parameters			Contaminant (CLD or SDZ) parameters		
No.	R^2	S_{max}/C_0 [cm ³ g ⁻¹]	K_{sw} [min ⁻¹]	K_{rs} [min ⁻¹]	$Frac. (f)$	K_d [cm ³ g ⁻¹]	ω [min ⁻¹]
I	0.827				5.46E-04	282.60	8.28E-04
II	0.963				0	0.17	1.22E-02
III	0.997				0	0.17	2.42
IV	0.975	5.45	10.3	6.80E-03			
Co-transport experiments							
Experiment		Contaminant (CLD or SDZ) parameters					
No.	R^2	k_{aiM} [min ⁻¹]			k_{diM} [min ⁻¹]		
V	0.872	0.10 [†]			5.32E-03 [†]		
VII	0.982	1.31E-02			1.02E-02		
VIII	0.982	0.38			0.49		

R^2 correlation of observed and fitted data; [†] - obtained from the batch experiments.

The colloid-facilitated contaminant transport model in the C-Ride module of HYDRUS-1D was used to describe the interactions between CLD and SDZ with soil, and with mobile and retained MWCNTs in the four co-transport experiments (V, VI, VII and VIII, respectively). The interactions between CLD or SDZ (experiment I and II) and soil (ω , f , and K_d) were described using equations (2.7) through (2.10). The interactions between MWCNTs (experiment III) and soil (S_{max} , k_{sw} and k_{rs}) were described using equations (2.1), (2.4), and (3.7). The interactions between CLD and mobile or retained MWCNTs were described by parameters k_{amM} , k_{dmM} , k_{aiM} , and k_{diM} using equations (2.11) through (2.13). As discussed above, rate parameters k_{amM} (6.26

$h^{-1} = 0.10 \text{ min}^{-1}$) and $k_{dmM} (=0.32 \text{ h}^{-1} = 5.32\text{E-}3 \text{ min}^{-1})$ were estimated from the sorption kinetic experiment (equation 3.1, Figure 4.9d). We have assumed that adsorption or desorption rates of CLD to/from mobile and retained MWCNTs were the same and used these values ($k_{aiM} = k_{amM} = 0.10 \text{ min}^{-1}$ and $k_{diM} = k_{dmM} = 5.32\text{E-}3 \text{ min}^{-1}$).

Pulse of CLD Followed by Pulse of MWCNTs

In experiments I, V and VI the effect of co-transport of CLD with MWCNTs under saturated conditions was investigated (Figure 4.11). It is noteworthy that even though CLD's mobility is limited, it still appeared again in the outflow after the application of the MWCNTs suspension (Figure 4.11a). The concentrations of retained CLD decreased due to the MWCNT injection by approximately 11% in the first layer (point 1 and 1', Figure 4.11b) and nearly 8% in the fourth layer (point 4 and 4', Figure 4.11b). Overall, nearly 17% of the CLD mass was remobilized from the top layers and shifted into deeper layers after injection of the MWCNT suspension (experiment I and V). This shift demonstrated that transport of MWCNTs facilitated the remobilization of CLD due to its strong sorption capacity for CLD. A similar trend was observed when CLD was injected prior to being eluted with a MWCNTs suspension at a higher input concentration of 10 mg L^{-1} (Figure 4.11c and 4.11d).

Table 4.8 shows the optimized parameters of the CLD co-transport experiment. For both mobile and retained MWCNTs, the adsorption rate of CLD was much greater than desorption rate, which demonstrated that the sorption was a reversible process and MWCNTs had a strong adsorption capacity for CLD.

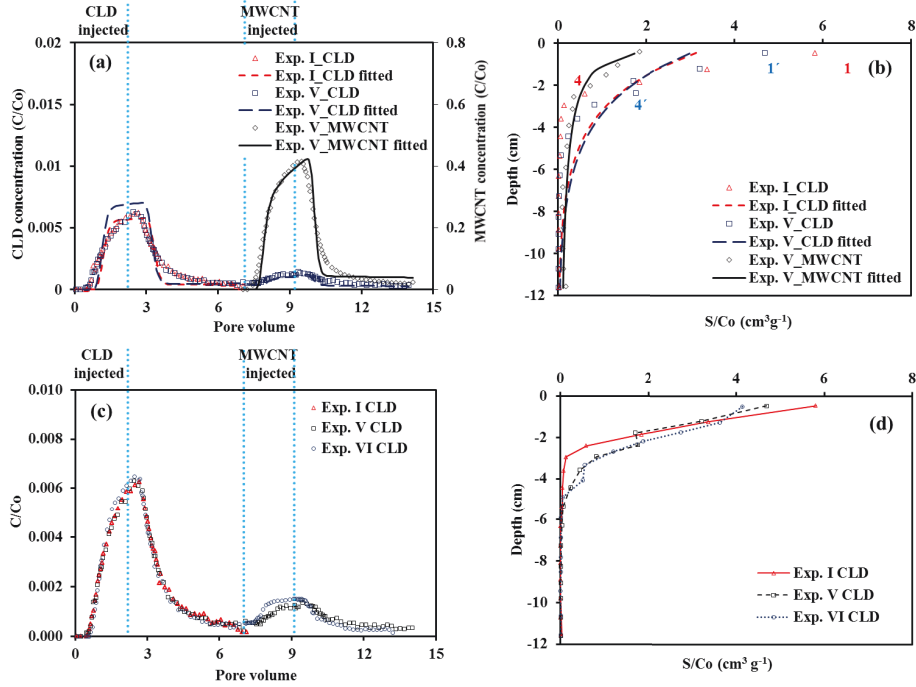


Figure 4.11 Observed and estimated BTCs (a and c) and RPs (b and d) for CLD in single-species (experiment I) and co-transport (experiment V and VI, respectively) experiments in saturated soil columns. The input concentration for CLD and MWCNTs was 1 mg L^{-1} . The left figure (a) has two vertical axes. The left axis shows the relative CLD concentrations, while the right axis shows the relative MWCNT concentrations. The vertical dotted lines indicate applications of CLD and MWCNTs.

Pulse of MWCNTs Followed by Pulse of SDZ

In experiments II, III, VII and VIII the influence of retained MWCNTs on SDZ transport and sorption was investigated (Figure 4.12). While SDZ has a high mobility in soil, it was retained to a greater extent in soil in the presence of immobilized MWCNTs. About 12% of the SDZ was retained in the soil column when it was applied without MWCNTs (experiment II), whereas about 28% of the SDZ was retained when it was applied after a MWCNT pulse (Figure 4.12a and 4.12b, Table 4.7). The peak effluent SDZ concentrations were reduced by about 5% due to a prior MWCNT application pulse and overall more SDZ was retained in the upper layer due to the prior MWCNT injection. These findings were further confirmed by conducting similar SDZ co-transport experiments (Figure 4.12c and 4.12d, experiments III and

VII) with a higher input concentration of SDZ ($C_0=1$ instead of 0.1 mg L^{-1}). Clearly, more SDZ was retained in the upper layer in the presence of MWCNTs (Figure 4c and 4d). However, it should be noted that the fraction of SDZ mass that was retained in the soil was greater when the experiment was conducted with a lower ($C_0=0.1 \text{ mg L}^{-1}$, experiment VIII) than higher ($C_0=1 \text{ mg L}^{-1}$; experiment VII) input concentration (Table 4.7, Figure 4.12). All these measures demonstrate that retained MWCNTs enhanced the sorption of SDZ in the soil column.

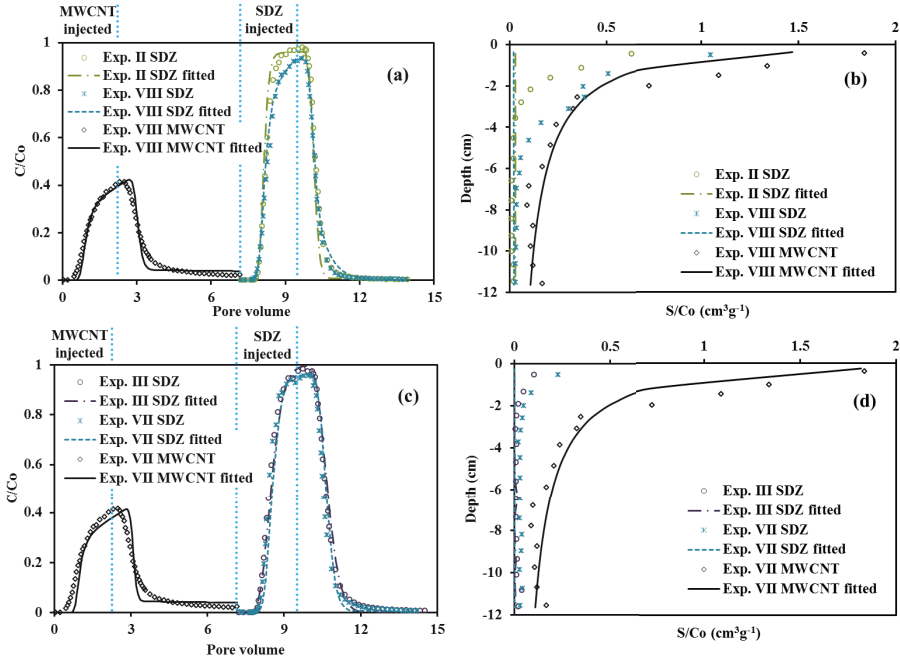


Figure 4.12 Observed and estimated BTCs (a and c) and RPs (b and d) for SDZ and MWCNTs of single-species (experiment II and III, respectively) or co-transport (experiment VIII and VII) experiments in saturated soil columns. The input concentration for SDZ and MWCNT was 0.1, 1 and 1 mg L^{-1} , respectively. The vertical dotted lines indicate applications of SDZ and MWCNTs.

Unlike the CLD co-transport experiment that had both mobile and retained MWCNTs, only the interactions between SDZ and retained MWCNTs was described by parameters k_{aiM} , and k_{diM} (Table 4.8). Estimated k_{aiM} , and k_{diM} in experiment VIII were about one order of magnitude higher than in experiment VII, which further

demonstrated that the retained MWCNTs strongly impacted the SDZ mobility. It should be noted that k_{aiM} was similar to k_{diM} , which demonstrated that sorption was a reversible process.

Mechanisms of Co-transport

Studies examining the facilitated contaminant transport by ENPs have typically been conducted by simultaneously injecting contaminants and ENPs (Hofmann and Von der Kammer 2009, Zhang et al. 2011). Results have demonstrated that a high sorption affinity of contaminants to the ENPs and a high concentration of ENPs are needed for facilitated contaminant transport. In our experiments MWCNTs and contaminants were injected at different times, which better reflects actual conditions for facilitated transport (i.e., a soil remediation scenario or an accidental release of ENPs and contaminants into the environment). Results indicated that CLD was remobilized and more SDZ was retained in the soil because of the impact of MWCNTs. Our experimental data and their numerical analysis provided an improved understanding of mechanisms and factors of that influence co-transport, including: (1) the interaction between contaminants and MWCNTs was a reversible kinetic sorption process; (2) both mobile and retained MWCNTs had a significant impact on CLD co-transport; and (3) the amount of retained MWCNTs had a strong influence on SDZ co-transport.

4.4 Outlook: Influence of surfactant on carbon nanotubes transport in porous media

4.4.1 Adsorption of surfactants on QS, GQS and MWCNTs

The results showed that the hydrodynamic radius was in the same range at 0 h and 1 h. It was assumed that all MWCNTs, SDBS-MWCNTs, and TX100-MWCNTs suspensions in the experiments were stable during the injection procedure (approximately 18 min).

The functionalization of MWCNTs produced an increased amount of groups containing oxygen in comparison to the pristine MWCNTs (Kasel et al. 2013a, Xia et al. 2007), resulting in its negative zeta potential in 1 mM KCl solution (Figure 4.13). Zeta potentials of MWCNTs, QS, and goethite decreased as added SDBS concentration increased, suggesting SDBS could further enhance the colloid stability of functionalized MWCNTs due to the increased electrostatic repulsion. TX100, as a nonionic surfactant, did not significantly change the zeta potentials of MWCNTs, QS and goethite, but it can maintain the stability of MWCNT suspension by steric stabilization (Moore et al. 2003). Similar to the zeta potential, the pH values of the MWCNTs and MWCNTs modified by TX100 (10 and 50 mg L⁻¹) suspension were the same. They were 5.28 and 5.23 for MWCNT and TX100-MWCNTs suspension, respectively. In contrast, the pH of the MWCNTs suspensions increased with the increasing SDBS concentration. It was 5.81 and 6.42 in the presence of 10 and 50 mg L⁻¹ SDBS, respectively.

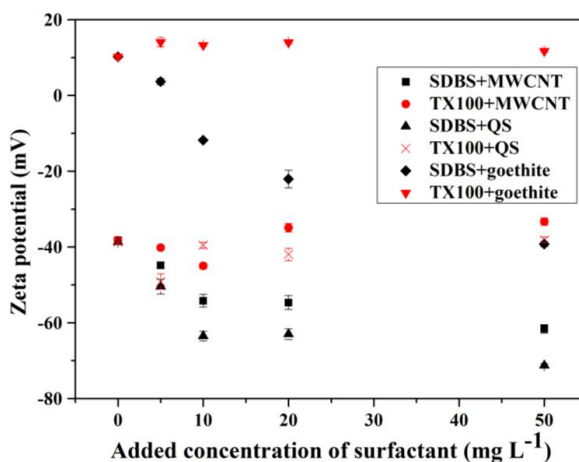


Figure 4.13 Zeta potentials of MWCNTs (5 mg L^{-1}), quartz sand (QS) and goethite at various added concentrations of TX100 and SDBS in $\text{IS} = 1 \text{ mM KCl}$. The zeta potential of MWCNTs (5 mg L^{-1} , 1 mM KCl) without surfactant was -38.2 mV . The zeta potential of quartz sand (QS, 1 mM KCl) without surfactant was -38.7 mV .

Adsorption isotherms of TX100 and SDBS on QS, GQS and MWCNTs are shown in Figure 4.14. Adsorption of TX100 and SDBS followed an order: $\text{MWCNTs} \gg \text{GQS} > \text{QS}$. It is worth noting that the adsorption affinity of SDBS on QS and MWCNTs were lower than TX100 due to the electrostatic repulsion between the negatively charged sorbents (QS and MWCNTs) and SDB^- anions. The adsorption of SDBS on GQS ($\lambda = 0.1$) was also lower than TX100, but the adsorption affinity increased as λ increased. That can be explained by the enhanced surface area and positive charges of goethite (see also the zeta potential results). The surfactant isotherms on QS and GQS were of L-type (Langmuir-type). Both TX100 and SDBS adsorption isotherms on MWCNTs were of H-type (High-affinity type). The adsorption increased sharply at the beginning part, then reached a plateau (at equilibrium surfactant concentration about 5 mg L^{-1}), which is similar to the trend of Han et al. (2008). The adsorption mechanism can be explained by hydrophobic interactions between the hydrophobic chains of surfactants and hydrophobic sites of the MWCNTs surface (Matarredona et al. 2003). It is worth noting that in the plateau region of the isotherms, a significant free concentration of surfactant existed in the

TX100-MWCNT or SDBS-MWCNT suspension. The SDB- adsorption on all sorbents resulted in a more negating zeta potential.

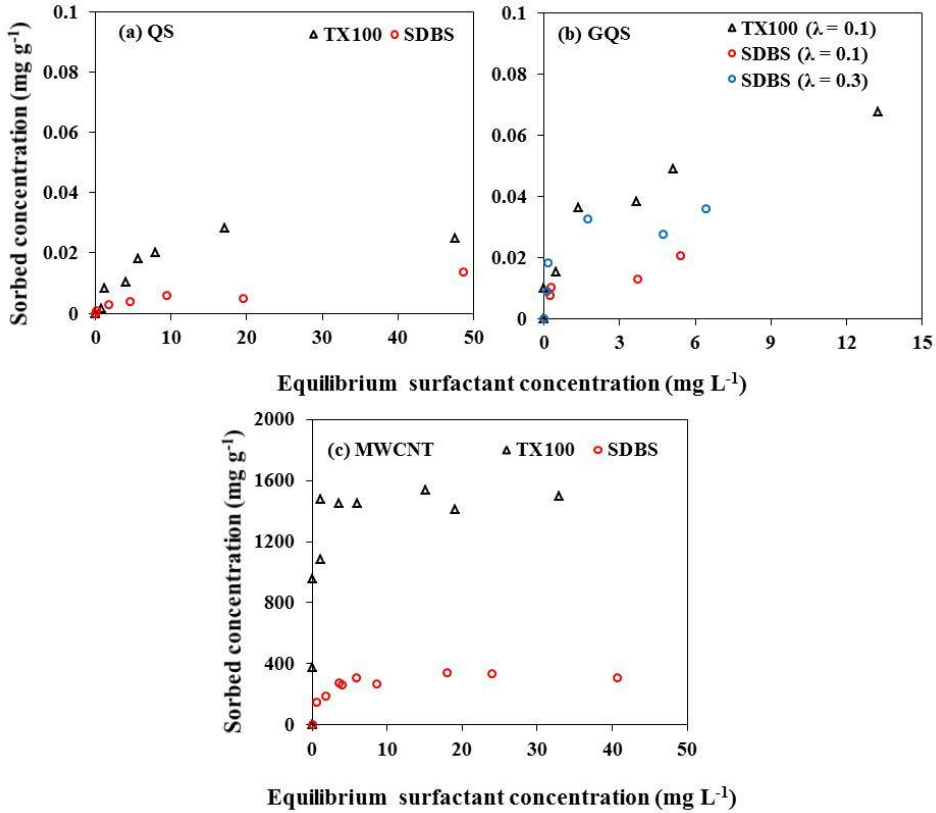


Figure 4.14 Adsorption isotherms of surfactant on different sorbents. (a) TX100 and SDBS on quartz sand; (b) TX100 and SDBS on goethite coated quartz sand at different λ (λ , the mass ratio of GQS in the mixing porous media); (c) TX100 and SDBS on MWCNT. The ionic strength was 1 mM KCl.

4.4.2 Transport of surfactant-MWCNTs in quartz sand

The effects of surfactant on MWCNTs transport in QS based on the observed BTCs are presented in Figure 4.15. The BTCs are plotted as the normalized effluent concentration (C/C_o ; where C_o is the influent concentration of MWCNT, TX100 or SDBS) versus pore volumes. The experimental information and mass recoveries from the effluent are presented in Table 4.9. The input concentration of MWCNTs in all transport experiments was 5 mg L⁻¹. The effluent mass percentage of MWCNTs (M_{eff} ,

Results and discussion

Figure 4.15c) strongly increased from 17.5 % to 90.5 % (Table 4.9) as input concentration of SDBS increased from 0 mg L⁻¹ to 50 mg L⁻¹ (experiment I, V and VI), with an increasing SDBS liquid phase mass recovery from 91.6 % to 95 % ($M_{eff_sur.}$, Figure 4.15d).

Table 4.9 Experimental conditions and mass recoveries from effluent for all column experiments. IS was 1mM KCl. $d_{50} = 240 \mu\text{m}$. Input concentration of MWCNTs was 5 mg L⁻¹.

No.	Surf.	Porous media	C_o (surfactant) [mg L ⁻¹]	q [cm min ⁻¹]	Porosity	$M_{eff_sur.}$ [%]	M_{eff} [%]
I	no	QS	0	0.71	0.43	no	17.5
II	no	GQS, $\lambda = 0.1$	0	0.73	0.44	no	2.4
III	TX100	QS	10	0.71	0.45	50.8	75.6
IV	TX100	QS	50	0.72	0.44	80.9	4.1
V	SDBS	QS	10	0.72	0.42	91.6	87.2
VI	SDBS	QS	50	0.72	0.45	95.0	90.5
VII	TX100	GQS, $\lambda = 0.1$	10	0.72	0.44	42.5	7.4
VIII	SDBS	GQS, $\lambda = 0.1$	10	0.73	0.41	86.4	64.2
IX	SDBS	GQS, $\lambda = 0.3$	10	0.73	0.42	84.4	0.32

M_{eff} is the effluent percentage of MWCNTs recovered from the column experiment; $M_{eff_sur.}$ is the effluent percentage of surfactant recovered from the column experiment; *Surf.* is the type of surfactant applied for the column experiments. C_o is the input concentration. QS- quartz sand, GQS- goethite coated quartz sand. λ , the mass ratio of GQS in the mixing porous media. q is the Darcy velocity.

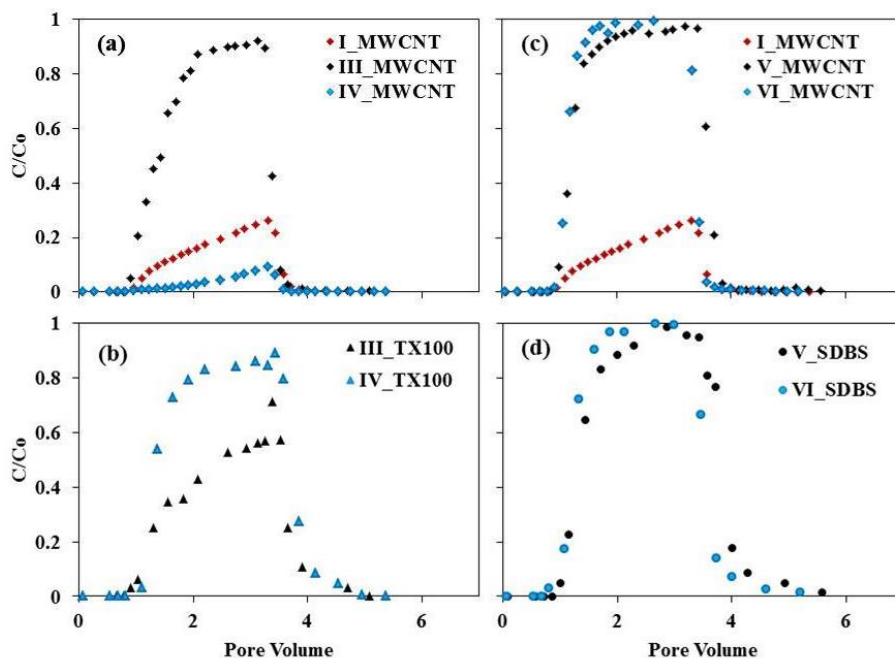


Figure 4.15 Observed breakthrough curves of MWCNTs, TX100 and SDBS in quartz sand. (a) BTCs of MWCNTs with adding 0 (I), 10(III), and 50(IV) mg L^{-1} TX100; (b) BTCs of TX 100 at the input concentration of 10 (III) and 50 (IV) mg L^{-1} ; (c) BTCs of MWCNTs with adding 0 (I), 10(V), and 50(VI) mg L^{-1} SDBS; (d) BTCs of SDBS at the input concentration of 10 (V) and 50 (VI) mg L^{-1} . The input concentration of MWCNTs was 5 mg L^{-1} . The ionic strength was 1 mM KCl . The Darcy velocity is $0.71\text{-}0.73 \text{ cm min}^{-1}$.

In case of SDBS, the breakthrough of MWCNTs was increased from 17.5 % (in absence of TX100 experiment I) to 75.6% (M_{eff} , Figure 4.15a) in the presence of 10 mg L^{-1} TX100 (experiment III), whereas, in contrast to SDBS, less MWCNTs broke through when the input concentration of TX100 was 50 mg L^{-1} (experiment IV) in comparison to without TX100 (M_{eff} decreased from 17.5 % to 4.1 %, Figure 4.15a). The breakthrough of TX100 increased from 50.8 % to 80.9 % (Figure 4.15b) as the input concentration of TX100 increased from 10 to 50 mg L^{-1} . These results suggested that attachment affinity of MWCNTs in quartz sand was related to the TX100 concentration. Lower amount of surfactant counterbalances the van der Waals attractions, whereas overcrowded surfactant micelles would deteriorate the dispersion

(Han et al. 2008, Jiang et al. 2003, Wang et al. 2004). In our case, the concentration of TX100 (50 mg L^{-1}) was lower than the critical micelle concentration (CMC) of TX100 ($142\text{--}155 \text{ mg L}^{-1}$), which should not deteriorate the MWCNT dispersion due to micelles effect in the TX100-MWCNTs suspension. Thus, the main reason why TX100 weakened MWCNTs transport in QS is still not clear in this study. Further investigations are therefore needed to better understand the interaction between TX100 and MWCNTs and the influence on MWCNTs transport in the presence of TX100.

Greater mobility of SDBS than TX100 in QS (Figure 4.15b and 4.15d) was observed, which was consistent with the adsorption isotherms and zeta potential. The breakthrough of TX100 (Figure 4.15b) indicated that only a small fraction of TX100 was adsorbed on MWCNTs surface and great amounts of TX100 were dissolved in the TX100-MWCNTs suspension. The BTCs of both TX100 and SDBS in QS was increased as their input concentration increased, suggesting a small fraction of SDBS or TX100 attached/ retained in QS surface.

4.4.3 Transport of surfactant-MWCNTs in goethite-coated quartz sand

The effect of goethite coating on surfactant-MWCNTs transport was conducted by 5 mg L^{-1} surfactant-free MWCNTs (experiment II) and 5 mg L^{-1} MWCNTs modified by 10 mg L^{-1} TX100 (experiment VII) or SDBS (experiment VIII and IX) in GQS ($\lambda = 0.1$, experiment II, VII and VIII, and $\lambda = 0.3$, experiment IX). Obviously, less MWCNTs of the surfactant-free MWCNTs suspension broke through in GQS (experiment II, Figure 4.16a and 4.16b) than in QS (experiment I, Figure 4.15a and 4.15d) due to the enhanced surface roughness and positively charged goethite that been explained by Chapter 4.1 Figure 4.16a shows the BTCs of MWCNTs and TX100 in GQS ($\lambda = 0.1$, experiment VII). The breakthrough of MWCNTs was only 5% more pronounced due to the TX100 effect in comparison to surfactant-free MWCNTs transport in GQS ($\lambda = 0.1$, experiment II), which was not as significant as in QS. The breakthrough of TX100 was approximately 8% less pronounced in the effluent in GQS than in QS (Table 4.9, Figure 4.15b and 4.16a), which was consistent with adsorption isotherms, suggesting that goethite influences the mobility of MWCNTs and TX100.

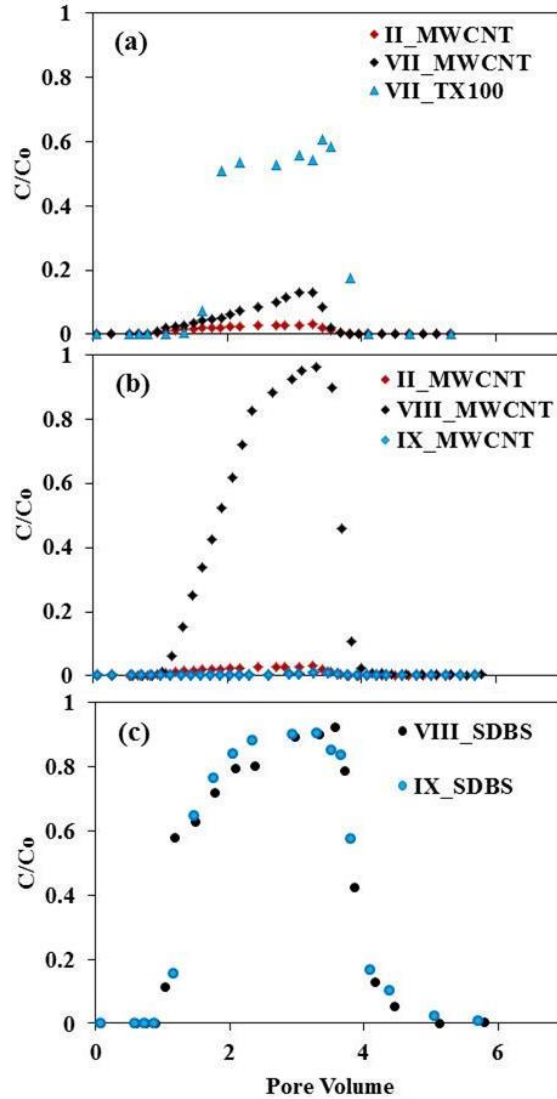


Figure 4.16 Observed breakthrough curves of MWCNTs, TX100 and SDBS with or without additional surfactant in goethite coated quartz sand different λ (λ , the mass ratio of GQS in the mixing porous media). (a) BTCs of MWCNTs with adding 0 (II) and 10 (VII) mg L⁻¹ TX100, and BTC of TX100 (10 mg L⁻¹, VII) at $\lambda = 0.1$; (b) BTCs of MWCNTs with adding 0 (II, $\lambda = 0.1$) and 10 mg L⁻¹ SDBS ($\lambda = 0.1$, VIII and 0.3, IX); (c) BTCs of SDBS (10 mg L⁻¹) at $\lambda = 0.1$ (VIII) and 0.3 (IX). The input concentration of MWCNTs was 5 mg L⁻¹. The ionic strength was 1 mM KCl. The Darcy velocity is 0.71-0.73 cm min⁻¹.

Figure 4.16b shows SDBS still significantly facilitate MWCNTs transport in GQS at $\lambda = 0.1$ (experiment VII) in comparison to surfactant-free MWCNTs system (experiment II). However, MWCNTs exhibited limited transport in GQS at $\lambda = 0.3$. SDBS still exhibited high mobility in GQS at $\lambda = 0.3$ and it slightly decreased as λ increased (Figure 4.16c, Table 4.9).

Similar to MWCNTs transport in QS, the breakthrough of MWCNTs was more pronounced in the presence of SDBS than in the presence of TX100 in GQS ($\lambda = 0.1$). And SDBS also exhibited more breakthrough than TX100 in GQS ($\lambda = 0.1$) as we expected from adsorption isotherms and zeta potential.

Following potential mechanisms may contribute to surfactant effect on MWCNTs stabilization and mobility (Han et al. 2008, Liang et al. 2013b): (1) releasing some ions from QS or GQS, (2) changing the pH values of the MWCNTs suspension, (3) adsorption of surfactant by QS and GQS from surfactant-MWCNTs, and (4) interaction between QS or GQS and MWCNTs through surfactant. Since all used QS and GQS has been washed by deionized water to remove potential soluble ion, and no released ions were observed in adsorption experiments after shaking 24 h in GQS system (data not shown) when the concentration of surfactant less than or equal to 10 mg L^{-1} . The release of ions could be eliminated by TX100 or SDBS effect in this study. The pH change of MWCNTs suspension after TX100 addition could be neglected. SDBS slightly altered the pH of MWCNTs suspension depending on the amounts of SDBS added. However, the pH of MWCNTs suspension in presence of 50 mg L^{-1} SDBS was 6.42, which was still lower than the zero point charge for Fe (pH = 7.5) (Bolster et al. 1999). Therefore, the second mechanism was not the dominant mechanism in this study. From the adsorption and transport results, the adsorption of the surfactants by QS or GQS can be assumed due to the free surfactants (previously exist or desorption from MWCNTs). Thus, the surfactant and MWCNT had a competition for the attachment sites of the porous media (Liang et al. 2013b). Thus, the third mechanism was likely to play an important role. In previous study, electrostatic interaction has been considered as the main mechanisms regulating the associations between MWCNTs and soil minerals. The cationic surfactant such as cetylpyridinium chloride and cetyltrimethylammonium could enhance MWCNTs deposition or precipitation due to the positively charged hydrophilic head attracted to the negatively charged sand surface (Han et al. 2008, Lu et al. 2013, Zhang et al. 2012). Also in the present study, the hydrophobic interaction between the

hydrophobic chains of SDBS or TX100 and MWCNTs could weaken the associations between MWCNTs and solid surface (4.th mechanism), resulting in a facilitated MWCNTs transport in porous media. It is noted that the interaction between solid surface and MWCNTs through surfactant depended on: (1) the type of surfactant, (2) the input concentration of surfactant, and (3) the type of porous media.

5. Summary and conclusions

Better understanding the transport, co-transport, retention, and remobilization of functionalized MWCNTs and contaminant in subsurface environment is essential for environmental protection and risk assessment. Batch and saturated column experiments in different porous media (quartz sand (QS), goethite coated quartz sand (GQS), and soil) were therefore performed under various physiochemical conditions. The aims of the work were to study i) the MWCNTs transport in chemically heterogeneous porous media, ii) the role of cation valance and exchange on the retention and colloid-facilitated transport of MWCNTs in soil, iii) the co-transport of chlordecone (CLD) and sulfadiazine (SDZ) in the presence of MWCNTs in soil, and iv) the role of surfactants (sodium dodecylbenzenesulfonate (SDBS) and Triton[®] X-100 (TX100)) for MWCNTs transport as a first approach for soil remediation. Both breakthrough curves (BTCs) and retention profiles (RPs) were determined and simulated.

Chemical heterogeneity of porous media surfaces is commonly assumed to control colloid transport and retention. This assumption was systematically investigated using low concentrations of functionalized MWCNTs and various mass fractions of QS and GQS in both batch and packed column studies. Although MWCNT retention increased with the increasing GQS fraction in batch and column investigations, results revealed that much greater retention occurred in column than batch systems because of surface straining processes that occurred at microscopic roughness locations and grain-grain contacts. Only a small fraction of the goethite surface was found to be favorable for MWCNT retention in column systems because nanoscale roughness and Born repulsion created shallow primary minimum interactions that were susceptible to removal by diffusion and hydrodynamic forces. These observations demonstrated that colloid retention on electrostatically favorable goethite surfaces was controlled mainly by roughness, but that the mass fraction and surface area (inversely related to the sand size) of chemical heterogeneity also played an important secondary role. Measured BTCs and RPs for MWCNTs were demonstrated to exhibit time- and depth-dependent retention behavior even in the presence of significant fractions of GQS. This implied that simple, irreversible retention models to describe colloid retention in chemically heterogeneous soils may frequently be inadequate and that transport of colloids may be greater than expected.

Since the detachment or release of retained engineered nanoparticles (ENPs) like CNTs from the solid phase is important for predicting the ultimate fate and transport of ENPs in the subsurface, the roles of solution ionic strength (IS), cation valance, and soil colloids on the transport, retention, and remobilization of MWCNTs in soils were investigated. Experimental and modeling results indicated that the mobility of MWCNTs was highly sensitive to the IS and cation valence, with greater amounts of retention occurring at high IS and with divalent cations. BTCs for MWCNTs exhibited a delay in breakthrough that increased with solution IS and cation valence due to blocking. RPs for MWCNTs showed a hyper-exponential shape likely due to surface straining processes. Significant amounts of MWCNTs could be released by perturbations in solution chemistry that reduced the adhesive force (e.g., IS reduction and cation exchange). This release behavior was demonstrated to depend on the concentration of Ca^{2+} during MWCNT deposition and the release of soil colloids with a high association for MWCNTs. These results suggested the potential for soil colloids to facilitate the transport of MWCNTs in the subsurface environment, and thereby pose a potential risk of groundwater pollution, especially during rainfall or irrigation events that alter the solution chemistry.

Co-transport study provided new information about the effects of MWCNTs on the transport behavior of CLD and SDZ in soils. Both BTCs and RPs of MWCNT, CLD, and SDZ were considered. In addition, MWCNTs and contaminants were injected at different times, which better reflects actual conditions for facilitated transport (i.e., a soil remediation scenario or an accidental release of ENPs and contaminants into the environment). MWCNTs due to their large sorption capacity and mobility could facilitate the remobilization of hydrophobic organic contaminants, such as CLD, that showed only a limited mobility in soils. In contrast, for strongly mobile contaminants such as SDZ, MWCNTs can enhance the SDZ deposition in the topsoil layers due to the large sorption affinity and higher input concentrations of MWCNTs in comparison to SDZ. Thus, immobilized MWCNTs could act as a barrier that reduces the fraction of the contaminant mass migrating easily through the topsoil and thus can prevent groundwater pollution. It is worth noting that it is likely that different environmental factors such as IS, flow velocity, and soil types may also significantly affect the mobility of MWCNTs and contaminants. Undoubtedly, more research is needed to further understand the mechanisms and factors that influence co-transport.

An outlook study investigated the effect of surfactant (SDBS and TX100) on the transport of MWCNTs in porous media. Experimental results indicated that the mobility of MWCNTs was highly sensitive to the type of surfactant, the input concentration of surfactant, and the properties of porous media. Significant amounts of MWCNTs could be released in the presence of SDBS due to the electrostatic repulsion between negatively charged sand surface and SDB⁻ anions. TX100 also could facilitate MWCNTs transport but it depended on the input concentration. These results suggested the potential for surfactants to facilitate the transport of MWCNTs in the subsurface environment.

References

- Åkerman, M.E., Chan, W.C., Laakkonen, P., Bhatia, S.N. and Ruoslahti, E. (2002) Nanocrystal Targeting in Vivo. *Proceedings of the National Academy of Sciences* 99(20), 12617-12621.
- Alvarez-Silva, M., Uribe-Salas, A., Mirnezami, M. and Finch, J.A. (2010) The Point of Zero Charge of Phyllosilicate Minerals Using the Mular–Roberts Titration Technique. *Minerals Engineering* 23(5), 383-389.
- Bendersky, M. and Davis, J.M. (2011) DLVO Interaction of Colloidal Particles with Topographically and Chemically Heterogeneous Surfaces. *Journal of Colloid and Interface Science* 353(1), 87-97.
- Bolster, C.H., Mills, A., Hornberger, G. and Herman, J. (1999) Spatial Distribution of Deposited Bacteria Following Miscible Displacement Experiments in Intact Cores. *Water Researchources Research* 35(6), 1797-1807.
- Boxall, A.B., Tiede, K. and Chaudhry, Q. (2007) Engineered Nanomaterials in Soils and Water: How Do They Behave and Could They Pose a Risk to Human Health?
- Bradford, S. and Bettahar, M. (2005) Straining, Attachment, and Detachment of Oocysts in Saturated Porous Media. *Journal of Environmental Quality* 34(2), 469-478.
- Bradford, S.A. and Bettahar, M. (2006) Concentration Dependent Transport of Colloids in Saturated Porous Media. *Journal of Contaminant Hydrology* 82(1), 99-117.
- Bradford, S.A., Bettahar, M., Šimůnek, J. and van Genuchten, M.T. (2004) Straining and Attachment of Colloids in Physically Heterogeneous Porous Media. *Vadose Zone Journal* 3(2), 384-394.
- Bradford, S.A. and Kim, H. (2010) Implications of Cation Exchange on Clay Release and Colloid-Facilitated Transport in Porous Media. *Journal of Environment Quality* 39(6), 2040.
- Bradford, S.A., Kim, H.N., Haznedaroglu, B.Z., Torkzaban, S. and Walker, S.L. (2009) Coupled Factors Influencing Concentration-Dependent Colloid Transport and Retention in Saturated Porous Media. *Environmental Science & Technology* 43(18), 6996-7002.
- Bradford, S.A., Šimůnek, J., Bettahar, M., Tadassa, Y.F., van Genuchten, M.T. and Yates, S.R. (2005) Straining of Colloids at Textural Interfaces. *Water Researchources Research* 41(10).
- Bradford, S.A., Šimůnek, J., Bettahar, M., Van Genuchten, M.T. and Yates, S. (2006a) Significance of Straining in Colloid Deposition: Evidence and Implications. *Water Researchources Research* 42(12).

- Bradford, S.A., Šimůnek, J., Bettahar, M., van Genuchten, M.T. and Yates, S.R. (2003) Modeling Colloid Attachment, Straining, and Exclusion in Saturated Porous Media. *Environmental Science & Technology* 37(10), 2242-2250.
- Bradford, S.A., Šimůnek, J. and Walker, S.L. (2006b) Transport and Straining of *E. Coli* O157: H7 in Saturated Porous Media. *Water Research* 42(12).
- Bradford, S.A. and Torkzaban, S. (2012) Colloid Adhesive Parameters for Chemically Heterogeneous Porous Media. *Langmuir* 28(38), 13643-13651.
- Bradford, S.A. and Torkzaban, S. (2013) Colloid Interaction Energies for Physically and Chemically Heterogeneous Porous Media. *Langmuir* 29(11), 3668-3676.
- Bradford, S.A. and Torkzaban, S. (2015) Determining Parameters and Mechanisms of Colloid Retention and Release in Porous Media. *Langmuir* 31(44), 12096-12105.
- Bradford, S.A., Torkzaban, S., Leij, F. and Šimůnek, J. (2015) Equilibrium and Kinetic Models for Colloid Release under Transient Solution Chemistry Conditions. *Journal of Contaminant Hydrology* 181, 141-152.
- Bradford, S.A., Torkzaban, S. and Šimůnek, J. (2011a) Modeling Colloid Transport and Retention in Saturated Porous Media under Unfavorable Attachment Conditions. *Water Research* 47(10).
- Bradford, S.A., Torkzaban, S. and Wiegmann, A. (2011b) Pore-Scale Simulations to Determine the Applied Hydrodynamic Torque and Colloid Immobilization. *Vadose Zone Journal* 10(1), 252-261.
- Bradford, S.A., Yates, S.R., Bettahar, M. and Šimůnek, J. (2002) Physical Factors Affecting the Transport and Fate of Colloids in Saturated Porous Media. *Water Research* 38(12), 63-61-63-12.
- Brunauer, S., Emmett, P.H. and Teller, E. (1938) Adsorption of Gases in Multimolecular Layers. *Journal of the American Chemical Society* 60(2), 309-319.
- Cabidoche, Y. and Lesueur-Jannoyer, M. (2012) Contamination of Harvested Organs in Root Crops Grown on Chlordecone-Polluted Soils. *Pedosphere* 22(4), 562-571.
- Cabidoche, Y.M., Achard, R., Cattani, P., Clermont-Dauphin, C., Massat, F. and Sansoulet, J. (2009) Long-Term Pollution by Chlordecone of Tropical Volcanic Soils in the French West Indies: A Simple Leaching Model Accounts for Current Residue. *Environmental Pollution* 157(5), 1697-1705.
- Cai, L., Tong, M., Wang, X. and Kim, H. (2014) Influence of Clay Particles on the Transport and Retention of Titanium Dioxide Nanoparticles in Quartz Sand. *Environmental Science & Technology* 48(13), 7323-7332.

- Camilli, L., Pisani, C., Gautron, E., Scarselli, M., Castrucci, P., D'Orazio, F., Passacantando, M., Moscone, D. and De Crescenzi, M. (2014) A Three-Dimensional Carbon Nanotube Network for Water Treatment. *Nanotechnology* 25(6), 065701.
- Chahine, N.O., Collette, N.M., Thomas, C.B., Genetos, D.C. and Loots, G.G. (2014) Nanocomposite Scaffold for Chondrocyte Growth and Cartilage Tissue Engineering: Effects of Carbon Nanotube Surface Functionalization. *Tissue Engineering Part A* 20(17-18), 2305-2315.
- Chen, C.-E., Zhang, H., Ying, G.-G. and Jones, K.C. (2013) Evidence and Recommendations to Support the Use of a Novel Passive Water Sampler to Quantify Antibiotics in Wastewaters. *Environmental Science & Technology* 47(23), 13587-13593.
- Chen, K.L. and Elimelech, M. (2006) Aggregation and Deposition Kinetics of Fullerene (C₆₀) Nanoparticles. *Langmuir* 22(26), 10994-11001.
- Chen, K.L. and Elimelech, M. (2007) Influence of Humic Acid on the Aggregation Kinetics of Fullerene (C₆₀) Nanoparticles in Monovalent and Divalent Electrolyte Solutions. *Journal of Colloid and Interface Science* 309(1), 126-134.
- Chen, Q., Saltiel, C., Manickavasagam, S., Schadler, L.S., Siegel, R.W. and Yang, H. (2004) Aggregation Behavior of Single-Walled Carbon Nanotubes in Dilute Aqueous Suspension. *Journal of Colloid and Interface Science* 280(1), 91-97.
- Cheng, J. and Cheng, S.H. (2012) Influence of Carbon Nanotube Length on Toxicity to Zebrafish Embryos. *International Journal of Nanomedicine* 7, 3731.
- Chi, M.-F., Wu, W.-L., Du, Y., Chin, C.-J.M. and Lin, C.-C. (2016) Inactivation of Escherichia Coli Planktonic Cells by Multi-Walled Carbon Nanotubes in Suspensions: Effect of Surface Functionalization Coupled with Medium Nutrition Level. *Journal of Hazardous Materials* 318, 507-514.
- Cho, H.-H., Smith, B.A., Wnuk, J.D., Fairbrother, D.H. and Ball, W.P. (2008) Influence of Surface Oxides on the Adsorption of Naphthalene onto Multiwalled Carbon Nanotubes. *Environmental Science & Technology* 42(8), 2899-2905.
- Cho, H.-H., Wepasnick, K., Smith, B.A., Bangash, F.K., Fairbrother, D.H. and Ball, W.P. (2010) Sorption of Aqueous Zn[II] and Cd[II] by Multiwall Carbon Nanotubes: The Relative Roles of Oxygen-Containing Functional Groups and Graphenic Carbon. *Langmuir* 26(2), 967-981.
- Corapcioglu, M.Y. and Jiang, S. (1993) Colloid-Facilitated Groundwater Contaminant Transport. *Water Research* 29(7), 2215-2226.

- Das, S. (2013) A Review on Carbon Nano-Tubes-a New Era of Nanotechnology. *International Journal of Emerging Technology and Advanced Engineering* 3(3), 774-783.
- de Jonge, L.W., Moldrup, P., Rubæk, G.H., Schelde, K. and Djurhuus, J. (2004) Particle Leaching and Particle-Facilitated Transport of Phosphorus at Field Scale. *Vadose Zone Journal* 3(2), 462-470.
- de las Casas, C. and Li, W. (2012) A Review of Application of Carbon Nanotubes for Lithium Ion Battery Anode Material. *Journal of Power Sources* 208, 74-85.
- Derjaguin, B.V.L., L. (1941) Theory of the Stability of Strongly Charged Lyophobic Sols and of the Adhesion of Strongly Charged Particles in Solutions of Electrolytes. *Acta Physicochim. URSS* 14.
- Dolliver, H., Kumar, K. and Gupta, S. (2007) Sulfamethazine Uptake by Plants from Manure-Amended Soil. *Journal of Environment Quality* 36(4), 1224.
- Duffadar, R.D. and Davis, J.M. (2008) Dynamic Adhesion Behavior of Micrometer-Scale Particles Flowing over Patchy Surfaces with Nanoscale Electrostatic Heterogeneity. *Journal of Colloid and Interface Science* 326(1), 18-27.
- Eatemadi, A., Daraee, H., Karimkhanloo, H., Kouhi, M., Zarghami, N., Akbarzadeh, A., Abasi, M., Hanifehpour, Y. and Joo, S.W. (2014) Carbon Nanotubes: Properties, Synthesis, Purification, and Medical Applications. *Nanoscale Research Letters* 9(1), 1-13.
- Elimelech, M., Gregory, J. and Jia, X. (2013) Particle Deposition and Aggregation: Measurement, Modelling and Simulation, Butterworth-Heinemann.
- Elimelech, M., Nagai, M., Ko, C.-H. and Ryan, J.N. (2000) Relative Insignificance of Mineral Grain Zeta Potential to Colloid Transport in Geochemically Heterogeneous Porous Media. *Environmental Science & Technology* 34(11), 2143-2148.
- Fang, J., Shan, X.-q., Wen, B. and Huang, R.-x. (2013) Mobility of Tx100 Suspended Multiwalled Carbon Nanotubes (MWCNTs) and the Facilitated Transport of Phenanthrene in Real Soil Columns. *Geoderma* 207-208, 1-7.
- Faraudo, J., Andreu, J.S. and Camacho, J. (2013) Understanding Diluted Dispersions of Superparamagnetic Particles under Strong Magnetic Fields: A Review of Concepts, Theory and Simulations. *Soft Matter* 9(29), 6654-6664.
- Farré, M., Gajda-Schranz, K., Kantiani, L. and Barceló, D. (2009) Ecotoxicity and Analysis of Nanomaterials in the Aquatic Environment. *Analytical and Bioanalytical Chemistry* 393(1), 81-95.
- Fernandez-Bayo, J.D., Saison, C., Geniez, C., Voltz, M., Vereecken, H. and Berns, A.E. (2013a) Sorption Characteristics of Chlordecone and Cadusafos in Tropical Agricultural Soils. *Current Organic Chemistry* 17(24), 2976-2984.

References

- Fernandez-Bayo, J.D., Saison, C., Voltz, M., Disko, U., Hofmann, D. and Berns, A.E. (2013b) Chlordecone Fate and Mineralisation in a Tropical Soil (Andosol) Microcosm under Aerobic Conditions. *Science of The Total Environment* 463-464, 395-403.
- Foppen, J.W.A. and Schijven, J.F. (2005) Transport of E. Coli in Columns of Geochemically Heterogeneous Sediment. *Water Research* 39(13), 3082-3088.
- Gannon, C.J., Cherukuri, P., Yakobson, B.I., Cognet, L., Kanzius, J.S., Kittrell, C., Weisman, R.B., Pasquali, M., Schmidt, H.K., Smalley, R.E. and Curley, S.A. (2007) Carbon Nanotube-Enhanced Thermal Destruction of Cancer Cells in a Noninvasive Radiofrequency Field. *Cancer* 110(12), 2654-2665.
- Gargiulo, G., Bradford, S., Šimůnek, J., Ustohal, P., Vereecken, H. and Klumpp, E. (2007) Bacteria Transport and Deposition under Unsaturated Conditions: The Role of the Matrix Grain Size and the Bacteria Surface Protein. *Journal of Contaminant Hydrology* 92(3-4), 255-273.
- Gohardani, O., Elola, M.C. and Elizetxea, C. (2014) Potential and Prospective Implementation of Carbon Nanotubes on Next Generation Aircraft and Space Vehicles: A Review of Current and Expected Applications in Aerospace Sciences. *Progress in Aerospace Sciences* 70, 42-68.
- Gottschalk, F., Sonderer, T., Scholz, R.W. and Nowack, B. (2009) Modeled Environmental Concentrations of Engineered Nanomaterials (TiO₂, ZnO, Ag, CNT, Fullerenes) for Different Regions. *Environmental Science & Technology* 43(24), 9216-9222.
- Grassian, V.H. (2008) *Nanoscience and Nanotechnology: Environmental and Health Impacts*, John Wiley & Sons.
- Grolimund, D., Borkovec, M., Barmettler, K. and Sticher, H. (1996) Colloid-Facilitated Transport of Strongly Sorbing Contaminants in Natural Porous Media: A Laboratory Column Study. *Environmental Science & Technology* 30(10), 3118-3123.
- Grosberg, A.Y., Nguyen, T. and Shklovskii, B. (2002) Colloquium: The Physics of Charge Inversion in Chemical and Biological Systems. *Reviews of modern physics* 74(2), 329.
- Grubek-Jaworska, H., Nejman, P., Czumińska, K., Przybyłowski, T., Huczko, A., Lange, H., Bystrzejewski, M., Baranowski, P. and Chazan, R. (2006) Preliminary Results on the Pathogenic Effects of Intratracheal Exposure to One-Dimensional Nanocarbons. *Carbon* 44(6), 1057-1063.
- Guldi, D.M., Rahman, G., Prato, M., Jux, N., Qin, S. and Ford, W. (2005) Single - Wall Carbon Nanotubes as Integrative Building Blocks for Solar - Energy Conversion. *Angewandte Chemie* 117(13), 2051-2054.

- Han, P., Wang, X., Cai, L., Tong, M. and Kim, H. (2014) Transport and Retention Behaviors of Titanium Dioxide Nanoparticles in Iron Oxide-Coated Quartz Sand: Effects of Ph, Ionic Strength, and Humic Acid. *Colloids and Surfaces A: Physicochemical and Engineering Aspects* 454, 119-127.
- Han, Z., Zhang, F., Lin, D. and Xing, B. (2008) Clay Minerals Affect the Stability of Surfactant-Facilitated Carbon Nanotube Suspensions. *Environmental Science & Technology* 42(18), 6869-6875.
- Harris, T.J., von Maltzahn, G., Derfus, A.M., Ruoslahti, E. and Bhatia, S.N. (2006) Proteolytic Actuation of Nanoparticle Self - Assembly. *Angewandte Chemie* 118(19), 3233-3237.
- Hassellöv, M., Readman, J.W., Ranville, J.F. and Tiede, K. (2008) Nanoparticle Analysis and Characterization Methodologies in Environmental Risk Assessment of Engineered Nanoparticles. *Ecotoxicology* 17(5), 344-361.
- Hofmann, A. and Liang, L. (2007) Mobilization of Colloidal Ferrihydrite Particles in Porous Media—an Inner-Sphere Complexation Approach. *Geochimica et Cosmochimica Acta* 71(24), 5847-5861.
- Hofmann, T. and Von der Kammer, F. (2009) Estimating the Relevance of Engineered Carbonaceous Nanoparticle Facilitated Transport of Hydrophobic Organic Contaminants in Porous Media. *Environmental Pollution* 157(4), 1117-1126.
- Höllrigl - Rosta, A., Vinken, R., Lenz, M. and Schäffer, A. (2003) Sorption and Dialysis Experiments to Assess the Binding of Phenolic Xenobiotics to Dissolved Organic Matter in Soil. *Environmental Toxicology and Chemistry* 22(4), 743-752.
- Iijima, S. (1991) Helical Microtubules of Graphitic Carbon. *Nature* 354(6348), 56-58.
- Israelachvili, J.N. (2011) *Intermolecular and Surface Forces: Revised Third Edition*, Academic press.
- Jaisi, D.P. and Elimelech, M. (2009) Single-Walled Carbon Nanotubes Exhibit Limited Transport in Soil Columns. *Environmental Science & Technology* 43(24), 9161-9166.
- Jaisi, D.P., Saleh, N.B., Blake, R.E. and Elimelech, M. (2008) Transport of Single-Walled Carbon Nanotubes in Porous Media: Filtration Mechanisms and Reversibility. *Environmental Science & Technology* 42(22), 8317-8323.
- Janas, D., Herman, A.P., Boncel, S. and Koziol, K.K. (2014) Iodine Monochloride as a Powerful Enhancer of Electrical Conductivity of Carbon Nanotube Wires. *Carbon* 73, 225-233.
- Ji, L., Chen, W., Zheng, S., Xu, Z. and Zhu, D. (2009) Adsorption of Sulfonamide Antibiotics to Multiwalled Carbon Nanotubes. *Langmuir* 25(19), 11608-11613.

- Jiang, C.-L., Séquaris, J.-M., Vereecken, H. and Klumpp, E. (2012) Effects of Inorganic and Organic Anions on the Stability of Illite and Quartz Soil Colloids in Na-, Ca-and Mixed Na–Ca Systems. *Colloids and Surfaces A: Physicochemical and Engineering Aspects* 415, 134-141.
- Jiang, C., Séquaris, J.-M., Wacha, A., Bóta, A., Vereecken, H. and Klumpp, E. (2014) Effect of Metal Oxide on Surface Area and Pore Size of Water-Dispersible Colloids from Three German Silt Loam Topsoils. *Geoderma* 235, 260-270.
- Jiang, L., Gao, L. and Sun, J. (2003) Production of Aqueous Colloidal Dispersions of Carbon Nanotubes. *Journal of Colloid and Interface Science* 260(1), 89-94.
- Jiang, S. and Corapcioglu, M.Y. (1993) A Hybrid Equilibrium Model of Solute Transport in Porous Media in the Presence of Colloids. *Colloids and Surfaces A: Physicochemical and Engineering Aspects* 73, 275-286.
- Jin, Y., Yates, M.V., Thompson, S.S. and Jury, W.A. (1997) Sorption of Viruses During Flow through Saturated Sand Columns. *Environmental Science & Technology* 31(2), 548-555.
- Johnson, P.R. and Elimelech, M. (1995) Dynamics of Colloid Deposition in Porous Media: Blocking Based on Random Sequential Adsorption. *Langmuir* 11(3), 801-812.
- Jones, A.D.K. and Bekkedahl, T. (1997) Storage of Hydrogen in Single-Walled Carbon Nanotubes. *Nature* 386, 377.
- Joško, I., Oleszczuk, P., Pranagal, J., Lehmann, J., Xing, B. and Cornelissen, G. (2013) Effect of Biochars, Activated Carbon and Multiwalled Carbon Nanotubes on Phytotoxicity of Sediment Contaminated by Inorganic and Organic Pollutants. *Ecological Engineering* 60, 50-59.
- Kam, N.W.S., Liu, Z. and Dai, H. (2006) Carbon Nanotubes as Intracellular Transporters for Proteins and DNA: An Investigation of the Uptake Mechanism and Pathway. *Angewandte Chemie* 118(4), 591-595.
- Kang, S., Herzberg, M., Rodrigues, D.F. and Elimelech, M. (2008) Antibacterial Effects of Carbon Nanotubes: Size Does Matter! *Langmuir* 24(13), 6409-6413.
- Kasel, D., Bradford, S.A., Šimůnek, J., Heggen, M., Vereecken, H. and Klumpp, E. (2013a) Transport and Retention of Multi-Walled Carbon Nanotubes in Saturated Porous Media: Effects of Input Concentration and Grain Size. *Water Research* 47(2), 933-944.
- Kasel, D., Bradford, S.A., Šimůnek, J., Pütz, T., Vereecken, H. and Klumpp, E. (2013b) Limited Transport of Functionalized Multi-Walled Carbon Nanotubes in Two Natural Soils. *Environmental Pollution* 180(0), 152-158.
- Kasteel, R., Mboh, C.M., Unold, M., Groeneweg, J., Vanderborght, J. and Vereecken, H. (2010) Transformation and Sorption of the Veterinary Antibiotic

- Sulfadiazine in Two Soils: A Short-Term Batch Study. *Environmental Science & Technology* 44(12), 4651-4657.
- Kemper, N. (2008) Veterinary Antibiotics in the Aquatic and Terrestrial Environment. *Ecological Indicators* 8(1), 1-13.
- Khilar, K.C. and Fogler, H.S. (1998) *Migrations of Fines in Porous Media*, Springer Science & Business Media.
- Kim, H., Hwang, Y.S. and Sharma, V.K. (2014) Adsorption of Antibiotics and Iopromide onto Single-Walled and Multi-Walled Carbon Nanotubes. *Chemical Engineering Journal* 255, 23-27.
- Kim, S.B., Park, S.J., Lee, C.G., Choi, N.C. and Kim, D.J. (2008) Bacteria Transport through Goethite-Coated Sand: Effects of Solution Ph and Coated Sand Content. *Colloids and Surfaces B: Biointerfaces* 63(2), 236-242.
- Lalwani, G., Henslee, A.M., Farshid, B., Lin, L., Kasper, F.K., Qin, Y.-X., Mikos, A.G. and Sitharaman, B. (2013) Two-Dimensional Nanostructure-Reinforced Biodegradable Polymeric Nanocomposites for Bone Tissue Engineering. *Biomacromolecules* 14(3), 900-909.
- Lam, C.-w., James, J.T., McCluskey, R., Arepalli, S. and Hunter, R.L. (2006) A Review of Carbon Nanotube Toxicity and Assessment of Potential Occupational and Environmental Health Risks. *Critical Reviews in Toxicology* 36(3), 189-217.
- Lam, C.-W., James, J.T., McCluskey, R. and Hunter, R.L. (2004) Pulmonary Toxicity of Single-Wall Carbon Nanotubes in Mice 7 and 90 Days after Intratracheal Instillation. *Toxicological Sciences* 77(1), 126-134.
- Leij, F.J., Bradford, S.A., Wang, Y. and Sciortino, A. (2015) Langmuirian Blocking of Irreversible Colloid Retention: Analytical Solution, Moments, and Setback Distance. *Journal of Environmental Quality* 44(5), 1473-1482.
- Levillain, J., Cattani, P., Colin, F., Voltz, M. and Cabidoche, Y.-M. (2012) Analysis of Environmental and Farming Factors of Soil Contamination by a Persistent Organic Pollutant, Chlordecone, in a Banana Production Area of French West Indies. *Agriculture, Ecosystems & Environment* 159(0), 123-132.
- Li, C., Ji, R., Schaffer, A., Sequaris, J.M., Amelung, W., Vereecken, H. and Klumpp, E. (2012) Sorption of a Branched Nonylphenol and Perfluorooctanoic Acid on Yangtze River Sediments and Their Model Components. *Journal of Environmental Monitoring* 14(10), 2653-2658.
- Li, X., Zhang, P., Lin, C. and Johnson, W.P. (2005) Role of Hydrodynamic Drag on Microsphere Deposition and Re-Entrainment in Porous Media under Unfavorable Conditions. *Environmental Science & Technology* 39(11), 4012-4020.

- Liang, Y., Bradford, S.A., Šimůnek, J., Heggen, M., Vereecken, H. and Klumpp, E. (2013a) Retention and Remobilization of Stabilized Silver Nanoparticles in an Undisturbed Loamy Sand Soil. *Environmental Science & Technology* 47(21), 12229-12237.
- Liang, Y., Bradford, S.A., Šimůnek, J., Vereecken, H. and Klumpp, E. (2013b) Sensitivity of the Transport and Retention of Stabilized Silver Nanoparticles to Physicochemical Factors. *Water Research* 47(7), 2572-2582.
- Liao, Q., Sun, J. and Gao, L. (2008) The Adsorption of Resorcinol from Water Using Multi-Walled Carbon Nanotubes. *Colloids and Surfaces A: Physicochemical and Engineering Aspects* 312(2), 160-165.
- Lin, D., Tian, X., Wu, F. and Xing, B. (2010) Fate and Transport of Engineered Nanomaterials in the Environment. *Journal of Environmental Quality* 39(6), 1896-1908.
- Lin, H., Zhu, H., Guo, H. and Yu, L. (2008) Microwave-Absorbing Properties of Co-Filled Carbon Nanotubes. *Materials Research Bulletin* 43(10), 2697-2702.
- Liu, P. (2005) Modifications of Carbon Nanotubes with Polymers. *European Polymer Journal* 41(11), 2693-2703.
- Liu, X., O'Carroll, D.M., Petersen, E.J., Huang, Q. and Anderson, C.L. (2009a) Mobility of Multiwalled Carbon Nanotubes in Porous Media. *Environmental Science & Technology* 43(21), 8153-8158.
- Liu, Z., Bai, G., Huang, Y., Li, F., Ma, Y., Guo, T., He, X., Lin, X., Gao, H. and Chen, Y. (2007) Microwave Absorption of Single-Walled Carbon Nanotubes/Soluble Cross-Linked Polyurethane Composites. *The Journal of Physical Chemistry C* 111(37), 13696-13700.
- Liu, Z., Tabakman, S., Welscher, K. and Dai, H. (2009b) Carbon Nanotubes in Biology and Medicine: In Vitro and in Vivo Detection, Imaging and Drug Delivery. *Nano research* 2(2), 85-120.
- Lowry, G. and Casman, E. (2009) *Nanomaterials: Risks and Benefits*, pp. 125-137, Springer.
- Lu, Y., Xu, X., Yang, K. and Lin, D. (2013) The Effects of Surfactants and Solution Chemistry on the Transport of Multiwalled Carbon Nanotubes in Quartz Sand-Packed Columns. *Environmental Pollution* 182, 269-277.
- Lu, Y., Yang, K. and Lin, D. (2014) Transport of Surfactant-Facilitated Multiwalled Carbon Nanotube Suspensions in Columns Packed with Sized Soil Particles. *Environmental Pollution* 192, 36-43.
- Luo, C., Wei, R., Guo, D., Zhang, S. and Yan, S. (2013) Adsorption Behavior of MnO₂ Functionalized Multi-Walled Carbon Nanotubes for the Removal of Cadmium from Aqueous Solutions. *Chemical Engineering Journal* 225, 406-415.

- Mansfeldt, T., Leyer, H., Barmettler, K. and Kretzschmar, R. (2004) Cyanide Leaching from Soil Developed from Coking Plant Purifier Waste as Influenced by Citrate. *Vadose Zone Journal* 3(2), 471-479.
- Matarredona, O., Rhoads, H., Li, Z., Harwell, J.H., Balzano, L. and Resasco, D.E. (2003) Dispersion of Single-Walled Carbon Nanotubes in Aqueous Solutions of the Anionic Surfactant Naddbs. *The Journal of Physical Chemistry B* 107(48), 13357-13367.
- Matthijs, E., Holt, M.S., Kiewiet, A. and Rijs, G.B. (1999) Environmental Monitoring for Linear Alkylbenzene Sulfonate, Alcohol Ethoxylate, Alcohol Ethoxy Sulfate, Alcohol Sulfate, and Soap. *Environmental Toxicology and Chemistry* 18(11), 2634-2644.
- Mattison, N.T., O'Carroll, D.M., Kerry Rowe, R. and Petersen, E.J. (2011) Impact of Porous Media Grain Size on the Transport of Multi-Walled Carbon Nanotubes. *Environmental Science & Technology* 45(22), 9765-9775.
- Mauter, M.S. and Elimelech, M. (2008) Environmental Applications of Carbon-Based Nanomaterials. *Environmental Science & Technology* 42(16), 5843-5859.
- Maynard, A.D. (2007) Nanotechnology: The Next Big Thing, or Much Ado About Nothing? *Annals of Occupational Hygiene* 51(1), 1-12.
- Metcalf, R.L. (2000) *Ullmann's Encyclopedia of Industrial Chemistry*, Wiley-VCH Verlag GmbH & Co. KGaA.
- Moore, V.C., Strano, M.S., Haroz, E.H., Hauge, R.H., Smalley, R.E., Schmidt, J. and Talmon, Y. (2003) Individually Suspended Single-Walled Carbon Nanotubes in Various Surfactants. *Nano letters* 3(10), 1379-1382.
- Mouchet, F., Gancet, C., Flahaut, E., Pinelli, E., Boutonnet, J.C. and Gauthier, L. (2016) International Standardized Procedures for in Vivo Evaluation of Multi-Walled Carbon Nanotube Toxicity in Water. *Toxicological & Environmental Chemistry* 98(8), 829-847.
- Newman, P., Minett, A., Ellis-Behnke, R. and Zreiqat, H. (2013) Carbon Nanotubes: Their Potential and Pitfalls for Bone Tissue Regeneration and Engineering. *Nanomedicine: Nanotechnology, Biology and Medicine* 9(8), 1139-1158.
- Nowack, B. and Bucheli, T.D. (2007) Occurrence, Behavior and Effects of Nanoparticles in the Environment. *Environmental Pollution* 150(1), 5-22.
- O'Carroll, D., Liu, X., Mattison, N. and Petersen, E. (2013) Impact of Diameter on Carbon Nanotube Transport in Sand. *Journal of Colloid and Interface Science* 390(1), 96-104.
- OECD (2000) Test No. 106: Adsorption -- Desorption Using a Batch Equilibrium Method, OECD Publishing.

- Pailler, J.Y., Krein, A., Pfister, L., Hoffmann, L. and Guignard, C. (2009) Solid Phase Extraction Coupled to Liquid Chromatography-Tandem Mass Spectrometry Analysis of Sulfonamides, Tetracyclines, Analgesics and Hormones in Surface Water and Wastewater in Luxembourg. *Science of The Total Environment* 407(16), 4736-4743.
- Pan, B. and Xing, B. (2012) Applications and Implications of Manufactured Nanoparticles in Soils: A Review. *European Journal of Soil Science* 63(4), 437-456.
- Pang, L. and Šimůnek, J. (2006) Evaluation of Bacteria-Facilitated Cadmium Transport in Gravel Columns Using the Hydrus Colloid-Facilitated Solute Transport Model. *Water Research* 42(12).
- Parks, G.A. (1965) The Isoelectric Points of Solid Oxides, Solid Hydroxides, and Aqueous Hydroxo Complex Systems. *Chemical Reviews* 65(2), 177-198.
- Pauluhn, J. (2010) Multi-Walled Carbon Nanotubes (Baytubes®): Approach for Derivation of Occupational Exposure Limit. *Regulatory Toxicology and Pharmacology* 57(1), 78-89.
- Pecora, R. (2000) Dynamic Light Scattering Measurement of Nanometer Particles in Liquids. *Journal of Nanoparticle Research* 2(2), 123-131.
- Peng, Y. and Liu, H. (2006) Effects of Oxidation by Hydrogen Peroxide on the Structures of Multiwalled Carbon Nanotubes. *Industrial & Engineering Chemistry Research* 45(19), 6483-6488.
- Penza, M., Cassano, G., Aversa, P., Antolini, F., Cusano, A., Cutolo, A., Giordano, M. and Nicolais, L. (2004) Alcohol Detection Using Carbon Nanotubes Acoustic and Optical Sensors. *Applied Physics Letters* 85(12), 2379-2381.
- Petosa, A.R., Jaisi, D.P., Quevedo, I.R., Elimelech, M. and Tufenkji, N. (2010) Aggregation and Deposition of Engineered Nanomaterials in Aquatic Environments: Role of Physicochemical Interactions. *Environmental Science & Technology* 44(17), 6532-6549.
- Postma, H.W.C., Teepen, T., Yao, Z., Grifoni, M. and Dekker, C. (2001) Carbon Nanotube Single-Electron Transistors at Room Temperature. *Science* 293(5527), 76-79.
- Praetorius, A., Tufenkji, N., Goss, K.-U., Scheringer, M., von der Kammer, F. and Elimelech, M. (2014) The Road to Nowhere: Equilibrium Partition Coefficients for Nanoparticles. *Environmental Science: Nano* 1(4), 317-323.
- Pritchard, P.H., Monti, C.A., O'Neill, E.J., Ahearn, D.G. and Connolly, J.P. (1986) Movement of Kepone®(Chlordecone) across an Undisturbed Sediment-Water Interface in Laboratory Systems. *Environmental Toxicology and Chemistry* 5(7), 647-657.

- Ptak, T., Piepenbrink, M. and Martac, E. (2004) Tracer Tests for the Investigation of Heterogeneous Porous Media and Stochastic Modelling of Flow and Transport-a Review of Some Recent Developments. *Journal of Hydrology* 294(1), 122-163.
- Ren, X., Chen, C., Nagatsu, M. and Wang, X. (2011) Carbon Nanotubes as Adsorbents in Environmental Pollution Management: A Review. *Chemical Engineering Journal* 170(2-3), 395-410.
- Saiers, J.E. and Hornberger, G.M. (1996) The Role of Colloidal Kaolinite in the Transport of Cesium through Laboratory Sand Columns. *Water Research* 32(1), 33-41.
- Salerno, M.B., Flamm, M., Logan, B.E. and Velegol, D. (2006) Transport of Rodlike Colloids through Packed Beds. *Environmental Science & Technology* 40(20), 6336-6340.
- Saltiel, C., Mengüç, M.P., Andrews, R. and Manickavasagam, S. (2005) Light-Scattering and Dispersion Behavior of Multiwalled Carbon Nanotubes. *JOSA A* 22(8), 1546-1554.
- Sasidharan, S., Torkzaban, S., Bradford, S.A., Dillon, P.J. and Cook, P.G. (2014) Coupled Effects of Hydrodynamic and Solution Chemistry on Long-Term Nanoparticle Transport and Deposition in Saturated Porous Media. *Colloids and Surfaces A: Physicochemical and Engineering Aspects* 457, 169-179.
- Saxena, R.K., Williams, W., Mcgee, J.K., Daniels, M.J., Boykin, E. and Ian Gilmour, M. (2007) Enhanced in Vitro and in Vivo Toxicity of Poly-Dispersed Acid-Functionalized Single-Wall Carbon Nanotubes. *Nanotoxicology* 1(4), 291-300.
- Scheidegger, A., Borkovec, M. and Sticher, H. (1993) Coating of Silica Sand with Goethite: Preparation and Analytical Identification. *Geoderma* 58(1), 43-65.
- Schijven, J.F. and Hassanizadeh, S.M. (2000) Removal of Viruses by Soil Passage: Overview of Modeling, Processes, and Parameters. *Critical Reviews in Environmental Science and Technology* 30(1), 49-127.
- Schijven, J.F. and Šimůnek, J. (2002) Kinetic Modeling of Virus Transport at the Field Scale. *Journal of Contaminant Hydrology* 55(1-2), 113-135.
- Schwab, F., Bucheli, T.D., Lukhele, L.P., Magrez, A., Nowack, B., Sigg, L. and Knauer, K. (2011) Are Carbon Nanotube Effects on Green Algae Caused by Shading and Agglomeration? *Environmental Science & Technology* 45(14), 6136-6144.
- Séquaris, J.-M. and Lewandowski, H. (2003) Physicochemical Characterization of Potential Colloids from Agricultural Topsoils. *Colloids and Surfaces A: Physicochemical and Engineering Aspects* 217(1), 93-99.

- Simon-Deckers, A., Loo, S., Mayne-L'hermite, M., Herlin-Boime, N., Menguy, N., Reynaud, C., Gouget, B. and Carrière, M. (2009) Size-, Composition-and Shape-Dependent Toxicological Impact of Metal Oxide Nanoparticles and Carbon Nanotubes toward Bacteria. *Environmental Science & Technology* 43(21), 8423-8429.
- Šimůnek, J., Genuchten, M.T.v. and Šejna, M. (2016) Recent Developments and Applications of the Hydrus Computer Software Packages. *Vadose Zone Journal*.
- Šimůnek, J., He, C., Pang, L. and Bradford, S.A. (2006) Colloid-Facilitated Solute Transport in Variably Saturated Porous Media. *Vadose Zone Journal* 5(3), 1035.
- Šimůnek, J., Šejna, M. and Genuchten, M.T.v. (2012) The C-Ride Module for Hydrus (2D/3D): Simulating Two-Dimensional Colloid-Facilitated Solute Transport in Variably-Saturated Porous Media. Version 1.0, PC Progress, Prague, Czech Republic, 45pp.
- Šimůnek, J., van Genuchten, M.T. and Šejna, M. (2008) Development and Applications of the Hydrus and Stanmod Software Packages and Related Codes. *Vadose Zone Journal* 7(2), 587-600.
- Sittig, S., Kasteel, R., Groeneweg, J., Hofmann, D., Thiele, B., Koppchen, S. and Vereecken, H. (2014) Dynamics of Transformation of the Veterinary Antibiotic Sulfadiazine in Two Soils. *Chemosphere* 95, 470-477.
- Smith, B., Wepasnick, K., Schrote, K.E., Cho, H.-H., Ball, W.P. and Fairbrother, D.H. (2009) Influence of Surface Oxides on the Colloidal Stability of Multi-Walled Carbon Nanotubes: A Structure-Property Relationship. *Langmuir* 25(17), 9767-9776.
- Smith, B., Yang, J., Bitter, J.L., Ball, W.P. and Fairbrother, D.H. (2012) Influence of Surface Oxygen on the Interactions of Carbon Nanotubes with Natural Organic Matter. *Environmental Science & Technology* 46(23), 12839-12847.
- Smith, C.J., Shaw, B.J. and Handy, R.D. (2007) Toxicity of Single Walled Carbon Nanotubes to Rainbow Trout, (*Oncorhynchus Mykiss*): Respiratory Toxicity, Organ Pathologies, and Other Physiological Effects. *Aquatic Toxicology* 82(2), 94-109.
- Sun, P., Huang, C.H. and Pavlostathis, S.G. (2014) Inhibition and Biotransformation Potential of Veterinary Ionophore Antibiotics under Different Redox Conditions. *Environmental Science & Technology* 48(22), 13146-13154.
- Sun, Y.-P., Fu, K., Lin, Y. and Huang, W. (2002) Functionalized Carbon Nanotubes: Properties and Applications. *Accounts of Chemical Research* 35(12), 1096-1104.

- Tamtam, F., Mercier, F., Le Bot, B., Eurin, J., Tuc Dinh, Q., Clément, M. and Chevreuil, M. (2008) Occurrence and Fate of Antibiotics in the Seine River in Various Hydrological Conditions. *Science of the Total Environment* 393(1), 84-95.
- Tan, A., Yildirimer, L., Rajadas, J., De La Peña, H., Pastorin, G. and Seifalian, A. (2011) Quantum Dots and Carbon Nanotubes in Oncology: A Review on Emerging Theranostic Applications in Nanomedicine. *Nanomedicine* 6(6), 1101-1114.
- Thiele - Bruhn, S. (2003) Pharmaceutical Antibiotic Compounds in Soils—a Review. *Journal of Plant Nutrition and Soil Science* 166(2), 145-167.
- Tian, Y., Gao, B., Morales, V.L., Wang, Y. and Wu, L. (2012a) Effect of Surface Modification on Single-Walled Carbon Nanotube Retention and Transport in Saturated and Unsaturated Porous Media. *Journal of Hazardous Materials* 239–240, 333-339.
- Tian, Y., Gao, B., Wang, Y., Morales, V.L., Carpena, R.M., Huang, Q. and Yang, L. (2012b) Deposition and Transport of Functionalized Carbon Nanotubes in Water-Saturated Sand Columns. *Journal of Hazardous Materials* 213-214, 265-272.
- Tian, Y., Gao, B., Wu, L., Munoz-Carpena, R. and Huang, Q. (2012c) Effect of Solution Chemistry on Multi-Walled Carbon Nanotube Deposition and Mobilization in Clean Porous Media. *Journal of Hazardous Materials* 231-232, 79-87.
- Tong, M. and Johnson, W.P. (2007) Colloid Population Heterogeneity Drives Hyperexponential Deviation from Classic Filtration Theory. *Environmental Science & Technology* 41(2), 493-499.
- Torkzaban, S. and Bradford, S.A. (2016) Critical Role of Surface Roughness on Colloid Retention and Release in Porous Media. *Water Research* 88, 274-284.
- Torkzaban, S., Wan, J., Tokunaga, T.K. and Bradford, S.A. (2012) Impacts of Bridging Complexation on the Transport of Surface-Modified Nanoparticles in Saturated Sand. *Journal of Contaminant Hydrology* 136, 86-95.
- Treumann, S., Torkzaban, S., Bradford, S.A., Visalakshan, R.M. and Page, D. (2014) An Explanation for Differences in the Process of Colloid Adsorption in Batch and Column Studies. *Journal of Contaminant Hydrology* 164, 219-229.
- Tufenkji, N. and Elimelech, M. (2004) Deviation from the Classical Colloid Filtration Theory in the Presence of Repulsive DLVO Interactions. *Langmuir* 20(25), 10818-10828.
- Tufenkji, N. and Elimelech, M. (2005a) Breakdown of Colloid Filtration Theory: Role of the Secondary Energy Minimum and Surface Charge Heterogeneities. *Langmuir* 21(3), 841-852.

- Tufenkji, N. and Elimelech, M. (2005b) Spatial Distributions of *Cryptosporidium* Oocysts in Porous Media: Evidence for Dual Mode Deposition. *Environmental Science & Technology* 39(10), 3620-3629.
- Tufenkji, N., Redman, J.A. and Elimelech, M. (2003) Interpreting Deposition Patterns of Microbial Particles in Laboratory-Scale Column Experiments. *Environmental Science & Technology* 37(3), 616-623.
- Unold, M., Kasteel, R., Groeneweg, J. and Vereecken, H. (2009) Transport and Transformation of Sulfadiazine in Soil Columns Packed with a Silty Loam and a Loamy Sand. *Journal of Contaminant Hydrology* 103(1-2), 38-47.
- Upadhyayula, V.K., Deng, S., Mitchell, M.C. and Smith, G.B. (2009) Application of Carbon Nanotube Technology for Removal of Contaminants in Drinking Water: A Review. *Science of the Total Environment* 408(1), 1-13.
- van de Weerd, H. and Leijnse, A. (1997) Assessment of the Effect of Kinetics on Colloid Facilitated Radionuclide Transport in Porous Media. *Journal of Contaminant Hydrology* 26(1), 245-256.
- van Genuchten, M.T. and Wagenet, R. (1989) Two-Site/Two-Region Models for Pesticide Transport and Degradation: Theoretical Development and Analytical Solutions. *Soil Science Society of America Journal* 53(5), 1303-1310.
- Von Gunten, H.R., Waber, U.E. and Krähenbühl, U. (1988) The Reactor Accident at Chernobyl: A Possibility to Test Colloid-Controlled Transport of Radionuclides in a Shallow Aquifer. *Journal of Contaminant Hydrology* 2(3), 237-247.
- Wang, D., Bradford, S.A., Harvey, R.W., Gao, B., Cang, L. and Zhou, D. (2012a) Humic Acid Facilitates the Transport of ARS-Labeled Hydroxyapatite Nanoparticles in Iron Oxyhydroxide-Coated Sand. *Environmental Science & Technology* 46(5), 2738-2745.
- Wang, D., Bradford, S.A., Harvey, R.W., Hao, X. and Zhou, D. (2012b) Transport of ARS-Labeled Hydroxyapatite Nanoparticles in Saturated Granular Media Is Influenced by Surface Charge Variability Even in the Presence of Humic Acid. *Journal of Hazardous Materials* 229-230, 170-176.
- Wang, D., Bradford, S.A., Paradelo, M., Peijnenburg, W.J. and Zhou, D. (2012c) Facilitated Transport of Copper with Hydroxyapatite Nanoparticles in Saturated Sand. *Soil Science Society of America Journal* 76(2), 375-388.
- Wang, D., Paradelo, M., Bradford, S.A., Peijnenburg, W.J., Chu, L. and Zhou, D. (2011a) Facilitated Transport of Cu with Hydroxyapatite Nanoparticles in Saturated Sand: Effects of Solution Ionic Strength and Composition. *Water Research* 45(18), 5905-5915.
- Wang, D., Paradelo, M., Bradford, S.A., Peijnenburg, W.J.G.M., Chu, L. and Zhou, D. (2011b) Facilitated Transport of Cu with Hydroxyapatite Nanoparticles in

- Saturated Sand: Effects of Solution Ionic Strength and Composition. *Water Research* 45(18), 5905-5915.
- Wang, D., Zhang, W. and Zhou, D. (2013) Antagonistic Effects of Humic Acid and Iron Oxyhydroxide Grain-Coating on Biochar Nanoparticle Transport in Saturated Sand. *Environmental Science & Technology* 47(10), 5154-5161.
- Wang, H., Zhou, W., Ho, D.L., Winey, K.I., Fischer, J.E., Glinka, C.J. and Hobbie, E.K. (2004) Dispersing Single-Walled Carbon Nanotubes with Surfactants: A Small Angle Neutron Scattering Study. *Nano Letters* 4(9), 1789-1793.
- Wang, P., Shi, Q., Liang, H., Steuerman, D.W., Stucky, G.D. and Keller, A.A. (2008) Enhanced Environmental Mobility of Carbon Nanotubes in the Presence of Humic Acid and Their Removal from Aqueous Solution. *Small* 4(12), 2166-2170.
- Wang, X., Li, Q., Xie, J., Jin, Z., Wang, J., Li, Y., Jiang, K. and Fan, S. (2009) Fabrication of Ultralong and Electrically Uniform Single-Walled Carbon Nanotubes on Clean Substrates. *Nano Letters* 9(9), 3137-3141.
- Wang, Y., Kim, J.H., Baek, J.B., Miller, G.W. and Pennell, K.D. (2012d) Transport Behavior of Functionalized Multi-Wall Carbon Nanotubes in Water-Saturated Quartz Sand as a Function of Tube Length. *Water Research* 46(14), 4521-4531.
- Wehrhan, A., Kasteel, R., Šimůnek, J., Groeneweg, J. and Vereecken, H. (2007) Transport of Sulfadiazine in Soil Columns: Experiments and Modelling Approaches. *Journal of Contaminant Hydrology* 89(1-2), 107-135.
- Wick, P., Manser, P., Limbach, L.K., Dettlaff-Weglikowska, U., Krumeich, F., Roth, S., Stark, W.J. and Bruinink, A. (2007) The Degree and Kind of Agglomeration Affect Carbon Nanotube Cytotoxicity. *Toxicology Letters* 168(2), 121-131.
- Woignier, T., Fernandes, P., Jannoyer-Lesueur, M. and Soler, A. (2012) Sequestration of Chlordecone in the Porous Structure of an Andosol and Effects of Added Organic Matter: An Alternative to Decontamination. *European Journal of Soil Science* 63(5), 717-723.
- Wu, L., Gao, B., Tian, Y., Muñoz-Carpena, R. and Zigler, K.J. (2013) DLVO Interactions of Carbon Nanotubes with Isotropic Planar Surfaces. *Langmuir* 29(12), 3976-3988.
- Xia, W., Wang, Y., Bergsträßer, R., Kundu, S. and Muhler, M. (2007) Surface Characterization of Oxygen-Functionalized Multi-Walled Carbon Nanotubes by High-Resolution X-Ray Photoelectron Spectroscopy and Temperature-Programmed Desorption. *Applied Surface Science* 254(1), 247-250.
- Xing, Y., Li, L., Chusuei, C.C. and Hull, R.V. (2005) Sonochemical Oxidation of Multiwalled Carbon Nanotubes. *Langmuir* 21(9), 4185-4190.

References

- Yang, J., Bitter, J.L., Smith, B.A., Fairbrother, D.H. and Ball, W.P. (2013) Transport of Oxidized Multi-Walled Carbon Nanotubes through Silica Based Porous Media: Influences of Aquatic Chemistry, Surface Chemistry, and Natural Organic Matter. *Environmental Science & Technology* 47(24), 14034-14043.
- Zarfl, C. (2008) Chemical Fate of Sulfadiazine in Soil: Mechanisms and Modelling Approaches, Shaker.
- Zhang, L., Petersen, E.J., Zhang, W., Chen, Y., Cabrera, M. and Huang, Q. (2012) Interactions of ¹⁴C-Labeled Multi-Walled Carbon Nanotubes with Soil Minerals in Water. *Environmental Pollution* 166, 75-81.
- Zhang, L., Wang, L., Zhang, P., Kan, A.T., Chen, W. and Tomson, M.B. (2011) Facilitated Transport of 2,2',5,5'-Polychlorinated Biphenyl and Phenanthrene by Fullerene Nanoparticles through Sandy Soil Columns. *Environmental Science & Technology* 45(4), 1341-1348.
- Zhang, S., Shao, T., Kose, H.S. and Karanfil, T. (2010) Adsorption of Aromatic Compounds by Carbonaceous Adsorbents: A Comparative Study on Granular Activated Carbon, Activated Carbon Fiber, and Carbon Nanotubes. *Environmental Science & Technology* 44(16), 6377-6383.

List of Figures

Figure 1.1 Schematic illustrations of a single-walled carbon nanotube (a) and a multi-walled carbon nanotube (b). Reprinted from Tan et al. (2011).	2
Figure 1.2 Oxidation of carbon nanotubes. Modified from Grassian (2008).	3
Figure 1.3 Structural formula of chlordecone.	10
Figure 1.4 Molecular structure of sulfadiazine. Reprinted from Wehrhan et al. (2007).	10
Figure 2.1 Schematic depiction of the classical DLVO theory. Adapted from Faraudo et al. (2013).	14
Figure 2.2 Schematic depictions of colloid/engineered nanoparticle (ENP) transport in porous media by Brownian diffusion (a), interception (b), gravitational sedimentation (c), straining (d), and blocking (e). The dotted lines and solid lines represent the fluid streamlines and colloid/ENP paths, respectively. Adapted from Lin et al. (2010) and Grassian (2008).	16
Figure 2.3 Schematic of colloids-facilitated solute transport in saturated porous media. Adapted from Šimůnek et al. (2012).	19
Figure 3.1 Transmission electron microscopy images of multi-walled carbon nanotubes at different magnifications: (a) 100 nm and (b) 5 nm. Reprinted from Kasel et al. (2013a).	22
Figure 3.2 (a) Correlation between concentration and absorbance of TX100, MWCNT and TX100-MWCNT; (b) Correlation between concentration and absorbance of SDBS, MWCNT and SDBS-MWCNT; (c) Correlation between measured absorbance and calculated absorbance.	24
Figure 3.3 The schematic image of column setup under water saturated condition. (a) The schematic running process of column experiments. (b) The photograph of the column setup. (c) The schematic process for effluent and solid samples determination.	29
Figure 4.1 Linear sorption isotherms for MWCNTs on QS or GQS having grain sizes of 350 and 607 μm . The electrolyte solution was 1 mM KCl.	37
Figure 4.2 Experimental and estimated breakthrough curves (a) and retention profiles (b) for MWCNTs under different mixing mass ratios (λ). The Darcy velocity was 0.72-0.75 cm min^{-1} . The grain size of the sand was 350 μm .	42
Figure 4.3 Observed and simulated breakthrough curves (a) and retention profiles (b) for MWCNTs in goethite-coated quartz sand with three different grain sizes (240, 350 and 607 μm) but the same λ (0.1). The Darcy velocity was 0.72- 0.75 cm min^{-1} .	44

Figure 4.4 Zeta potentials of MWCNTs and soil as a function of the ionic strength in electrolyte solutions (KCl and CaCl_2). 45

Figure 4.5 Effect of ionic strength on the transport and retention of MWCNTs in soil: observed and fitted breakthrough curves (a) and retention profiles (b) of MWCNTs under 1, 4, and 10 mM KCl, respectively. 47

Figure 4.6 Effect of cation type on the transport and retention of MWCNTs in soil: observed and fitted breakthrough curves (a) and retention profiles (b) of MWCNTs under 1 mM KCl and CaCl_2 , respectively. 51

Figure 4.7 (a) Breakthrough and release behavior, and retention profiles (d) of MWCNTs in soil. Deposition (step A) occurred at an IS = 10 mM using KCl for experiment I, and an IS = 1 and 10 mM using CaCl_2 for experiment II and III, respectively, whereas release was initiated by ionic strength reduction (steps B, D, and F, Milli-Q water) and cation exchange (steps C and E) as summarized in Table 4.4. (b) Effluent concentrations of K and Ca during steps A–F in experiment II. (c) Release of MWCNTs and naturally occurring minerals due to ionic strength reduction (steps B, D, and F, Milli-Q water) and cation exchange (steps C and E) in soil in experiment II. For experiment III, the range of step A–F is not shown as the blue dotted line due to the different experimental conditions compared with experiment II. The injection procedure in experiment II is step A (0–7.61 pore volumes (PVs)), step B (7.61–15.23 PVs), step C (15.23–17.51 PVs), step D (17.51–22.85 PVs), step E (22.85–25.13 PVs), and step F (25.13–30.47 PVs). 54

Figure 4.8 (a) Mass percentage of each soil sized fraction: sand, silt, 0.45–2 μm WDCs and < 0.45 μm WDCs; (b) Mass percentage of MWCNTs in sand, silt and 0.45–2 μm WDCs of soil. The < 0.45 μm WDCs also contained the MWCNTs in the so-called electrolyte phase (1 mM KCl and CaCl_2); (c) Retention amount of MWCNTs in sand, silt, 0.45–2 μm WDCs and < 0.45 μm WDCs including electrolyte phase under different cation type. 57

Figure 4.9 (a) Adsorption isotherm of CLD on soil. (b) Adsorption isotherm of CLD on MWCNTs. (c) Adsorption isotherm of SDZ on MWCNTs. (d) Kinetic sorption data for CLD on MWCNTs. 59

Figure 4.10 Observed and estimated BTCs (a) and RPs (b) for a single-species transport of CLD (experiment I), SDZ (experiment II), and MWCNTs (experiment IV) in saturated soil columns. The left figure (a) has two vertical axes. The left axis shows the relative CLD concentrations (C/C_0), while the right axis shows the relative SDZ and MWCNTs concentrations. 61

Figure 4.11 Observed and estimated BTCs (a and c) and RPs (b and d) for CLD in single-species (experiment I) and co-transport (experiment V and VI, respectively) experiments in saturated soil columns. The input concentration for CLD and MWCNTs was 1 mg L^{-1} . The left figure (a) has two vertical axes. The left axis shows the relative CLD concentrations, while the right axis shows the relative MWCNT concentrations. The vertical dotted lines indicate applications of CLD and MWCNTs. 66

Figure 4.12 Observed and estimated BTCs (a and c) and RPs (b and d) for SDZ and MWCNTs of single-species (experiment II and III, respectively) or co-transport (experiment VIII and VII) experiments in saturated soil columns. The input concentration for SDZ and MWCNT was 0.1, 1 and 1mg L⁻¹, respectively. The vertical dotted lines indicate applications of SDZ and MWCNTs. _____ 67

Figure 4.13 Zeta potentials of MWCNTs (5 mg L⁻¹), quartz sand (QS) and goethite at various added concentrations of TX100 and SDBS in IS = 1 mM KCl. The zeta potential of MWCNTs (5 mg L⁻¹, 1 mM KCl) without surfactant was -38.2 mV. The zeta potential of quartz sand (QS, 1 mM KCl) without surfactant was -38.7 mV. ____ 70

Figure 4.14 Adsorption isotherms of surfactant on different sorbents. (a) TX100 and SDBS on quartz sand; (b) TX100 and SDBS on goethite coated quartz sand at different λ (λ , the mass ratio of GQS in the mixing porous media); (c) TX100 and SDBS on MWCNT. The ionic strength was 1 mM KCl. _____ 71

Figure 4.15 Observed breakthrough curves of MWCNTs, TX100 and SDBS in quartz sand. (a) BTCs of MWCNTs with adding 0 (I), 10(III), and 50(IV) mg L⁻¹ TX100; (b) BTCs of TX 100 at the input concentration of 10 (III) and 50 (IV) mg L⁻¹; (c) BTCs of MWCNTs with adding 0 (I), 10(V), and 50(VI) mg L⁻¹ SDBS; (d) BTCs of SDBS at the input concentration of 10 (V) and 50 (VI) mg L⁻¹. The input concentration of MWCNTs was 5 mg L⁻¹. The ionic strength was 1 mM KCl. The Darcy velocity is 0.71-0.73 cm min⁻¹. _____ 73

Figure 4.16 Observed breakthrough curves of MWCNTs, TX100 and SDBS with or without additional surfactant in goethite coated quartz sand different λ (λ , the mass ratio of GQS in the mixing porous media). (a) BTCs of MWCNTs with adding 0 (II) and 10 (VII) mg L⁻¹ TX100, and BTC of TX100 (10 mg L⁻¹, VII) at $\lambda = 0.1$; (b) BTCs of MWCNTs with adding 0 (II, $\lambda = 0.1$) and 10 mg L⁻¹ SDBS ($\lambda = 0.1$, VIII and 0.3, IX); (c) BTCs of SDBS (10 mg L⁻¹) at $\lambda = 0.1$ (VIII) and 0.3 (IX). The input concentration of MWCNTs was 5 mg L⁻¹. The ionic strength was 1 mM KCl. The Darcy velocity is 0.71-0.73 cm min⁻¹. _____ 75

List of Tables

Table 4.1 Characteristics of porous media.	35
Table 4.2 Experimental conditions, hydraulic parameters and mass balance information for all column experiments. IS was 1mM KCl. The input concentration of MWCNT was 1mg L ⁻¹ .	38
Table 4.3 Fitted model parameters using different model formulations.	41
Table 4.4 Experimental conditions, hydraulic parameters and mass balance information for all column experiments.	48
Table 4.5 Fitted model parameters.	49
Table 4.6 Optimized results from batch experiments.	58
Table 4.7 Experimental conditions, hydraulic parameters and mass balance information for all column experiments. IS for all column experiments was 1 mM KCl and d_{50} of soil was 120 μm .	62
Table 4.8 Parameters optimized by using different models for the CLD, SDZ, and MWCNT transport, co-transport and retention in soil.	64
Table 4.9 Experimental conditions and mass recoveries from effluent for all column experiments. IS was 1mM KCl. $d_{50} = 240 \mu\text{m}$. Input concentration of MWCNTs was 5 mg L ⁻¹ .	72

List of Abbreviations

ADE	Advection-dispersion equation
Al	Aluminum
BET	Brunauer–Emmett–Teller
BTCs	Breakthrough curves
Ca	Calcium
CaCl ₂	Calcium chloride
¹⁴ C	Radioactive carbon isotope
¹⁴ CO ₂	Radioactively labeled carbon dioxide
Cd	Cadmium
CFT	Colloid filtration theory
CLD	Chlordecone
CMC	Critical micelle concentration
CNTs	Carbon nanotubes
Co-transport	Colloid-facilitated contaminant transport
CPC	Cetylpyridinium chloride
DDT	Dichlorodiphenyltrichloroethane
DLVO	Derjaguin-Landau-Verwey-Overbeek
DLS	Dynamic light scattering
ENPs	Engineered nanoparticles
Fe	Iron
Fe Conc.	Fe concentration of the samples
GQS	Goethite-coated quartz sand
HNO ₃	Nitric acid
H ₂ O ₂	Hydrogen peroxide
HPLC	High performance liquid chromatography
H ₂ SO ₄	Sulfuric acid
H-type	High-affinity type
ICP-OES	Inductively coupled optical emission spectrometry
IS	Ionic strength
K	Potassium
KBr	Potassium bromide

KCl	Potassium chloride
LSC	Liquid scintillation counter
L-type	Langmuir-type
M1	Attachment, detachment, and time-dependent Langmuirian blocking on Site 1
M2	Attachment, detachment, and time-dependent Langmuirian blocking on QS (Site 1) and GQS (Site 2) sites
M3	Attachment, detachment, and time-dependent Langmuirian blocking on Site 1 and depth-dependent retention on Site 2
MWCNTs	Multi-walled carbon nanotubes
NaCl	Sodium chloride
NC	Not calculated
NF	Not fitted
nTiO ₂	Titanium dioxide nanoparticles
OECD	Organisation for Economic Cooperation and Development
POP	Persistent organic pollutants
PTFE	Polytetrafluoroethylene
PVs	Pore volumes
QS	Quartz sand
RP _s	Retention profiles
SDBS	Sodium dodecylbenzenesulfonate
SDZ	Sulfadiazine
S.E.	Standard error
Surf.	Surfactant
SWCNTs	Single-walled carbon nanotubes
TEM	Transmission electron microscopy
TX100	Triton [®] X-100/ Octyl-phenolethoxylate
WDCs	Water-dispersible colloids

List of Symbols

A_s	Solid surface area per unit volume [L^{-1} , L denotes units of length]
C	Colloid/ENP concentration in liquid phase [ML^{-3} , M denotes units of mass]
C_c	Contaminant concentration in the liquid phase [ML^{-3}]
C_0	Influent concentration [ML^{-3}]
d_{50}	Median diameter of the porous media [L]
D	Hydrodynamic dispersion coefficient for colloids/ENPs [L^2T^{-1} , T denotes units of time]
D_c	Hydrodynamic dispersion coefficient for contaminant [L^2T^{-1}]
$Disp.$	Estimated longitudinal dispersivity
f	Fraction of exchange sites assumed to be in equilibrium with the solution phase [-]
f_{oc}	Soil organic carbon fraction [$M\ M^{-1}$]
k_{aiM}	Rate coefficients for contaminant sorption to immobile colloids/ENPs [T^{-1}]
k_{att}	First-order particle attachment rate coefficient [T^{-1}]
K_d	Partition coefficient of contaminant for linear adsorption [L^3M^{-1}]
k_{diM}	Rate coefficients for contaminant desorption from immobile colloids/ENPs [T^{-1}]
k_{rs1}	First-order release rate coefficients [T^{-1}] First-order release rate coefficients on Site 1 [T^{-1}]
k_{rs2}	First-order release rate coefficients on Site 2 [T^{-1}]
k_{sw}	First-order retention rate coefficients (including all the retention mechanism) [T^{-1}]
k_{sw1}	First-order retention rate coefficients on Site 1 [T^{-1}]
k_{sw2}	First-order retention rate coefficients on Site 2 [T^{-1}]
k_{QS}	k_{sw} value for QS [T^{-1}]
k_{GQS}	k_{sw} value for QS [T^{-1}]
K_D	Equilibrium partition coefficient for MWCNT [L^3M^{-1}]
K_F	Freundlich coefficient
K_{GQS}	Batch K_D values for GQS [L^3M^{-1}]

K_{oc}	Octanol-water partition coefficient [L^3M^{-1}]
K_{QS}	Batch K_D values for QS [L^3M^{-1}]
M_{eff}	Effluent percentage of MWCNTs recovered from the column experiment
M_{solid}	Retained percentage of MWCNTs recovered from the column experiment
M_{total}	Total percentage of MWCNTs recovered from the column experiment
n	Exponent
q	Darcy velocity [LT^{-1}]
R^2	Correlation coefficient
R^2_{BTC}	Correlation of observed and fitted data for BTC
R^2_{RP}	Correlation of observed and fitted data for RP
R^2_{BTC+RP}	Correlation of observed and fitted data for total (BTC+RP)
S	Total solid phase concentration (NM^{-1} , N denotes number)
S_1	Solid phase concentrations of MWCNTs on retention Site 1 [NM^{-1}]
S_2	Solid phase concentrations of MWCNTs on retention Site 2 [NM^{-1}]
S_c	Contaminant concentration sorbed to the solid phase [MM^{-1}]
S_e	Contaminant concentration on one fraction of the sorption sites (type-1 sites), on which sorption is assumed to be instantaneous [MM^{-1}]
S_{iM}	Contaminant concentration sorbed to immobile colloids/ENPs [MM^{-1}]
S_k	Contaminant concentration on the remaining sorption sites (type-2 sites), on which sorption is considered to be a first-order kinetic rate process [MM^{-1}]
S_{max}	Maximum solid phase concentration [NM^{-1}]
S_{max1}	Maximum solid phase concentration on Site 1 [NM^{-1}]
S_{maxQS}	S_{max} value for QS [NM^{-1}]
S_{maxGQS}	S_{max} value for GQS [NM^{-1}]

S_{mM}	Contaminant concentrations sorbed to mobile colloids/ENPs [MM ⁻¹]
t	Time [T]
T_H	Hydrodynamic adhesive
T_A	Resisting adhesive
W_{edl}	Electrical double layer repulsion energy
W_{ipe}	Total potential energy
W_{vdw}	Van der Waals attraction energy
x	Spatial coordinate [L]
α	Attachment or collision efficiency
β	Fitting parameter which controls the shape of the retention profile [-]
η	Single collector efficiency [-, porous medium]
η_0	Theoretical (maximum) collector efficiency
θ	Volumetric water content [L ³ L ⁻³]
λ	Mass ratio of GQS in the mixing porous media
ρ	Bulk density of the porous matrix [ML ⁻³]
φ	Porosity
ψ	Dimensionless functions that account for time or depth-dependent retention [-]
ψ_1	Dimensionless functions that account for time-dependent retention [-]
ψ_2	Dimensionless functions that account for depth-dependent retention [-]
ψ_m	Dimensionless variables that adjust the sorption rate to a number of mobile colloids/ENPs [-]
ψ_{im}	Dimensionless variables that adjust the sorption rate to a number of immobile colloids/ENPs [-]
ω	First-order rate constant [T ⁻¹]

Curriculum vitae

Miaoyue Zhang, M.Eng.

Ph.D. Student, Date of Birth: 12, Nov., 1987

Institute of Bio and Geosciences (IBG-3), Research Center Jülich - FZJ

D – 52425, Jülich, Germany

Tel: +49 (0)2461-61 3521; Fax: +49 (0)2461-61 2518

E-mail: m.zhang@fz-juelich.de
yue.zwz1987@hotmail.com

Education Background

2012/10-2016/10	PhD, in Environmental Science, Research Center Jülich – FZJ and RWTH Aachen University, Germany
2009/09-2012/06	Master, in Environmental Engineering, Chongqing University, P.R.China
2005/10-2009/07	Bachelor, in Environmental Engineering, Chongqing University, P.R.China

Working Experience

2016/03-2016/05	Visiting Scholar at Department of Environmental Sciences at University of California Riverside, USA, cooperation with Jirka Šimůnek and Scott A. Bradford on modeling of nanoparticle transport, co-transport and retention preparation.
2014/07-2014/08	Visiting Scholar at Department of Physical Chemistry and Materials Science at Budapest University of Technology and Economics, Hungary, cooperation with Prof. Krisztina László on methods of short multi-walled carbon nanotubes preparation.
2013/11-2013/12	Visiting Scholar at Department of Physical Chemistry and Materials Science at Budapest University of Technology and Economics, Hungary, cooperation with Prof. Krisztina László on methods of short multi-walled carbon nanotubes preparation.
2010/9-2011/3	Assistant tutor, Chongqing University, P.R. China

Academic Research Field

- Soil physico-chemistry: sorption & transport processes
- Colloids/nanoparticles/contaminants transport or facilitate transport in porous media
- Theory and technology of water pollution control

Research Projects

- 2012/10-2016/10 Transport or co-transport behavior of functionalized multi-walled carbon nanotubes in different porous media at vary physical-chemical conditions, Jülich, Germany
- 2010/09-2012/03 National special S&T project on treatment and control of water pollution, Chongqing, P.R. China
1. Research on control technology and ascending function on municipal wastewater treatment plant of oxidation ditch process
 2. Research on low cost upgrading technology research and comprehensive demonstration on municipal wastewater treatment plant of oxidation ditch process

Languages and Software

Chinese (native); English (fluent); German (basic)
Microsoft Office (daily use);
HYDRUS-1D with different codes (experienced);
Origin (daily use);
Computational Fluid Dynamics (CFD, basic)

Publications

Journal articles:

1. Miaoyue Zhang, Irina Engelhardt, Jirka Šimůnek, Scott A. Bradford, Daniela Kasel, Anne E. Berns, Harry Vereecken, Erwin Klumpp, (2016). Co-transport of chlordecone and sulfadiazine in the presence of functionalized multi-walled carbon nanotubes in soils, *Environmental Pollution*, resubmitted.
2. Miaoyue Zhang, Scott A. Bradford, Jirka Šimůnek, Harry Vereecken, and Erwin Klumpp, (2016). Do Goethite Surfaces Really Control the Transport and Retention of Multi-Walled Carbon Nanotubes in Chemically Heterogeneous Porous Media? *Environmental Science & Technology*, in press, DOI: 10.1021/acs.est.6b03285.
3. Miaoyue Zhang, Scott A. Bradford, Jirka Šimůnek, Harry Vereecken and Erwin Klumpp, (2016). Roles of Cation Valance and Exchange on the Retention and Colloid-Facilitated Transport of Functionalized Multi-walled Carbon Nanotubes in a Natural Soil , *Water Research*, under revision.

Conference contributions (oral):

1. Miaoyue Zhang, Irina Engelhardt, Erwin Klumpp, (2015). Co-transport of chlordecone(CLD) and sulfadiazine(SDZ) in the presence of functionalized multi-walled carbon nanotubes(MWCNT) in soils. International Soil Tillage Research Organization Conference, Nanjing, P.R. China, 2015/09/14-18.

Conference contributions (poster):

1. M., Zhang, S. A. Bradford, J. Šimůnek, H., Vereecken, E., Klumpp, (2016). Transport, retention and sorption interaction of functionalized multi-walled carbon nanotubes in goethite-coated quartz sand, *Interfaces Against Pollution Conference*, Lleida, Catalonia, Spain, 2016/09/04-07.
2. M., Zhang, I., Engelhardt, J. Šimůnek, S. A. Bradford, D. Kasel, A.E. Berns, H., Vereecken, E., Klumpp, (2015). Co-transport of chlordecone and sulfadiazine in an agriculture soil in the presence of functionalized multi-walled carbon nanotubes, *International Conference on the Environmental Effects of Nanoparticles and Nanomaterials*, Vienna, Austria, 2015/09/06-09.
3. Miaoyue Zhang, Daniela Kasel, Anne Berns, Harry Vereecken, Erwin Klump, (2014). Transport and retention of multi-walled carbon nanotubes in different porous

media. Interfaces in Water and Environmental Science, Leeuwarden, The Netherlands, 2014/05/25-28.

4. Miaoyue Zhang, Daniela Kasel, Anne Berns, Harry Vereecken, Erwin Klumpp, (2014). Transport and retention of multi-walled carbon nanotubes in different porous media and co-transport of Chlordecone. International workshop Nanoparticles in Soils and Waters: Fate, Transport and Effects, Landau, Germany. 2014/03/11-13.

Acknowledgements

First of all, I would like to thank the China Scholarship Council (CSC) for the financial support during my Ph.D. study.

I most sincerely appreciate to my doctoral advisor Prof. Dr. Erwin Klumpp for all his support. The excellent and useful suggestions, pathbreaking ideas, insightful comments and daily care helped me to overcome the difficulties during the past years in IBG-3. Thanks for everything.

Special thanks to Dr. Scott A. Bradford and Prof. Dr. Jirka Šimůnek in Riverside, California for the opportunity to visit UCR. Thanks to their professional support on numerical simulation, research discussion and paper revising for my research. Thanks to Jing Liang, Xiaolin Hu, and other colleagues and friends in Riverside, California for all of the enjoyable time in UCR.

I would also like to thank Prof. Dr. Andreas Schäffer in RWTH Aachen University for the support and discussion on my Ph.D. study.

Thanks to Prof. Dr. Harry Vereecken for the support to work and study in IBG-3. Thanks to the discussion, suggestions, and critical comments for presentations, reports, and paper revising during these four years.

Thanks to Prof. Dr. Irina Engelhardt in TU Freiberg for the support on numerical simulation and paper revising.

I would also like to thank Prof. Krisztina László, Nagy Balázs, Ábrahám Dániel, Bosznai György, Manek Enikő, and Tóth Ajna in Budapest University of Technology and Economics for the support the research on short carbon nanotubes preparation.

I would also like to thank Herbert Philipp, Claudia Walraf, Stephan Köppchen, Andrea Kubika, Martina Krause, Stephanie Stork, Dr. Wolfgang Tappe, Dipl.-Ing.

Ulrich Disko, Manana Megrelishvili in IBG-3, and Dr. Volker Nischwitz in ZEA-3 for all the support and help for my research.

Thanks to Prof. Wulf Amelung for the helpful discussion related to soil fractionation. Thanks to Dr. Anne Berns for helping with chlordecone preparation and experiments discussion. Thanks are also due to Dan Zhou for helping with the numerical investigations and discussion. Thanks to Markus Duschl for the suggestions on the method of goethite coating.

I would like to express my sincere appreciation to Xiaoqian Jiang, Xiao Liu, Lu Cao, Joanna Makselon, Anna Missong, Nina Gottselig, Shurong Liu, Yan Liang, Canlan Jiang, Daniela Kasel, Zhan Gao, Yi Wang, Yajie Sun, Ying Xing, Xi Yang, and other colleagues in IBG-3 and friends in Jülich for their help and company during my stay in Germany.

Finally, I would like to thank my family who always support me for everything I like and always take care of me. Thanks to my friends in China who always take care of me by phone or internet during these four years. I also would like to thank my boyfriend in Tokyo University, Japan who always support me, take care of me, bear me, and encourage me. Thanks for his four times visiting of this year just for looking at me even if it is a pretty long journey from Japan to Germany.

Band / Volume 339

Groundwater recharge in Slovenia

Results of a bilateral German-Slovenian Research project

Mišo Andjelov, Zlatko Mikulič, Björn Tetzlaff, Jože Uhan & Frank Wendland
(2016)

ISBN: 978-3-95806-177-4

Band / Volume 340

Atomic oxygen derived from SCIAMACHY O(¹S)

and OH airglow measurements in the Mesopause region

Y. Zhu (2016), 206 pp

ISBN: 978-3-95806-178-1

Band / Volume 341

**Diagnostic Mirror Concept Development for Use
in the Complex Environment of a Fusion Reactor**

A. Krimmer (2016), x, 123 pp

ISBN: 978-3-95806-180-4

Band / Volume 342

**Long-Term Measurements of the Radiation Exposure of the Inhabitants
of Radioactively Contaminated Regions of Belarus –
The Korma Report II (1998 – 2015)**

P. Zoriy, H. Dederichs, J. Pillath, B. Heuel-Fabianek, P. Hill, R. Lennartz
(2016), ca 105 pp

ISBN: 978-3-95806-181-1

Band / Volume 343

**Entwicklung und Charakterisierung von Nickel/Gadolinium-Ceroxid-
basierten Anoden für die metallgestützte Festoxid-Brennstoffzelle**

V. Rojek-Wöckner (2016), XVI, 136 pp

ISBN: 978-3-95806-182-8

Band / Volume 344

**Reaction-diffusion modelling of hydrogen retention
and release mechanisms in beryllium**

M. Wensing (2016), 100 pp

ISBN: 978-3-95806-184-2

Band / Volume 345

**Light Management by Intermediate Reflectors
in Silicon-based Tandem Solar Cells**

A. Hoffmann (2016), 199 pp

ISBN: 978-3-95806-186-6

Band / Volume 346

Design eines hocheffizienten Festoxid-Brennstoffzellensystems mit integrierter Schutzgaserzeugung

M. Engelbracht (2016), 190 pp

ISBN: 978-3-95806-189-7

Band / Volume 347

On model and measurement uncertainty in predicting land surface carbon fluxes

H. Post (2016), xviii, 135 pp

ISBN: 978-3-95806-190-3

Band / Volume 348

Bipolarplattenmaterialien für Polymer-Elektrolyt-Membran Elektrolyse

M. Langemann (2016), I-III, 189, IV-XVIII pp

ISBN: 978-3-95806-192-7

Band / Volume 349

Modellbasierte Ansteuerung räumlich ausgedehnter Aktuator- und Sensornetzwerke in der Strömungsregelung

M. Dück (2016), XIII, 153 pp

ISBN: 978-3-95806-193-4

Band / Volume 350

TRENDS 2015 – Transition to Renewable Energy Devices and Systems

ed. by D. Stolten and R. Peters (2016), 200 pp

ISBN: 978-3-95806-195-8

Band / Volume 351

Dual Phase Oxygen Transport Membrane for Efficient Oxyfuel Combustion

M. Ramasamy (2016), VIII, 136 pp

ISBN: 978-3-95806-196-5

Band / Volume 352

Transport, co-transport, and retention of functionalized multi-walled carbon nanotubes in porous media

M. Zhang (2016), VII, 112 pp

Energie & Umwelt /
Energy & Environment
Band / Volume 352
ISBN 978-3-95806-198-9

